Technical University of Denmark

DTU

Proton-Conducting Sulfonated Ionomers by Chemical Modification and Atom Transfer Radical Polymerization

Nielsen, Mads Møller; Hvilsted, Søren; Jankova Atanasova, Katja

Publication date:
2013

Document Version
Publisher's PDF, also known as Version of record

[Link back to DTU Orbit](#)

DTU Library
Technical Information Center of Denmark

Ph.D. Dissertation - February 2013

Proton-Conducting Sulfonated Ionomers
by Chemical Modification and
Atom Transfer Radical Polymerization

by **Mads Møller Nielsen**
DTU Chemical Engineering
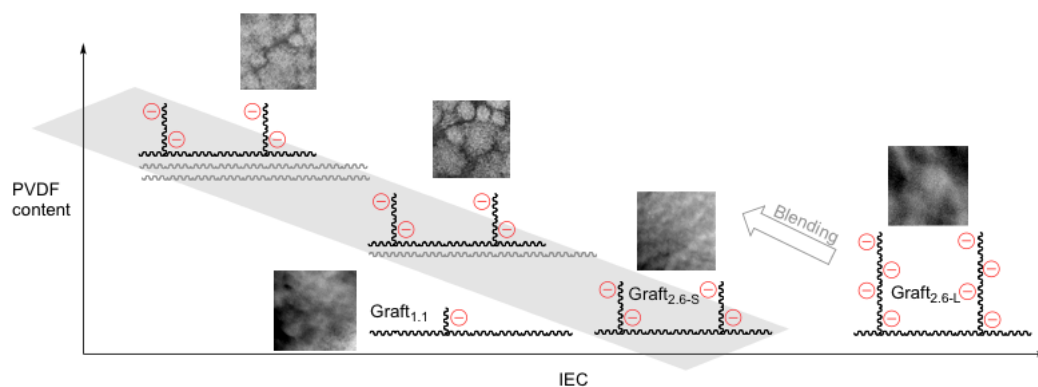
Supervisors:
Professor Søren Hvilsted, DTU Chemical Engineering
Associate Professor Katja Jankova, DTU Chemical Engineering

Til min familie

Om jag får 300 idéer på ett år och en är användbar, då är jag nöjd

If I have 300 ideas in a year and just one turns out to work I am satisfied

-Alfred Nobel, Swedish chemist, engineer and much more (1833-1896)

Preface

The work presented here is my contribution to the research project New Macromolecular Architectures and Functions for Proton Conducting Fuel Cell membranes (MAProCon), a collaboration between Technical University of Denmark (DTU), Lund University (LU), University of Southern Denmark and Danish Technological Institute (taken over from IRD Fuel Cell A/S at midway). The project is financed by the Danish Council for Strategic Research (project no. 09-065198). All work is carried out at DTU, at LU and during a five month research stay at Simon Fraser University (SFU) between March 1, 2010 and February 28, 2013.

There is a bunch of people whom I owe my gratitude:

My supervisors. *Søren Hvilsted*, for taking me on board, and for sharing your meticulous approach to research and how to present results. *Katja Jankova*, for your motivation throughout the years, and for always being available.

My external supervisor at SFU. *Steven Holdcroft*, for sharing your extensive expertise and for letting me become part of your group for five great months.

My project partners. *Patric Jannasch*, for shedding light on fuel cell issues in yielding conversations. *Shogo Takamuku* and *Ivaylo Dimitrov* for making the start-up phase proceed more smoothly and for sharing your valuable experiences with me. *Casper F. Nørgaard*, for the exciting collaboration on blend composites. *Peter Lund*, for your administrative role in the collaboration.

My DTU colleagues. *Irakli Javakhishvili* and *Anders E. Daugaard* for always taking the time to discuss synthesis and characterization related issues. *Lars Schulte*, for your work on the microtome and the TEM, and for your never failing helpfulness. *Kim C. Szabo*, for running TGA and DSC. *José R. Marin* and *Nicolas J. Alvarez*, for setting up the microindentation test stand. *Sarah Maria G. Frankær*, for LaTeX inputs.

My SFU colleagues - for the good times. *Ami C. C. Yang*, for good teamwork, and numerous rewarding conversations. *Rasoul Narimani*, for enlightening discussions on membrane morphology.

My family and friends. Most importantly, the people I love the most: *Pernille*, *Mor* and *Far*.

Resumé

Hensigten med de tre hovedarbejder som udgør grundstenene i denne PhD afhandling er at give et indblik i diversiteten af makromolekylære strukturer som er tilgængelige gennem brugen af en begrænset mængde kemiske redskaber. Hensigten er dels at bidrage til forståelsen af hvorledes man ved at dreje på udvalgte parametre kan finjustere den kemiske del af protonbytningsmembraner (PEM) og derved opnå forbedrede egenskaber på konkrete felter. Fra starten har det været af afgørende betydning at afprøve modelstrukturer som indgår i en større forskningsmæssig sammenhæng og visse steder at bevæge sig ud på områder som ikke hidtil har været videre belyst i litteraturen.

I designet af amfifile polymerer er der taget afsæt i en kommercielt tilgængelig polysulfon (PSU), Udel®, der besidder velegnede mekaniske og termiske egenskaber. Sulfonsyre-funktionaliserede, dendroniserede sidekæder er påsat vha. *click* kemi i et modelstudie for kulbrinte strukturer med øget fleksibilitet. Forskellige substitueringsgrader er benyttet i belysningen af ionbytningskapacitetens (IEC) betydning for vandoptag og protonledningsevne. Det har vist sig at der forekommer et snævert IEC-vindue hvori vandgennemsivningen øges fra at være meget lav til at forårsage kraftig kvældning og protonledningsevnen proportionalt hermed.

Et andet modelstudie af kulbrinte strukturer er foretaget på post-sulfoneret PSU med polystyren (PS) sidekæder, hvor IEC foruden gennem substitueringsgraden også varieres gennem kædelængden og sulfoneringsgraden. Atom transfer radikal polymerisering (ATRP) benyttes til kædeopbygningen.

I fremstillingen af et delvist fluoreret system, baseret på en lignende strategi, er PS kæderne på et primært poly(vinyliden fluorid) (PVDF)-holdigt *backbone* 100% sulfonerede. For at modvirke den dimensionsændring der følger ved kontakt med vand, blandes ionomeren med højmolekylær PVDF, der bidrager til bevarelse af den mekaniske stabilitet. Morfologien af disse *blends* påvirkes af PVDF-indholdet, hvor der ved 25 vol% ionomer indhold forekommer makrofaseseparation, mens der ved 40 vol% ionomer desuden forekommer gentagende mønstre af ion-holdige domæner i ellers primært PVDF-holdige områder. *Blends*'ene udviser høj afhængighed af den relative luftfugtighed, men skønt de giver lavere absolutte ledningsevner end Nafion® udviser de også en lavere sensitivitet overfor både luftfugtighed og temperatur. Når de er fuldt befugtede, præsterer *blends* desuden bedre end fuldt sulfonerede graft copolymer analoger.

Konstellationen af den høje grad af kontrol ved ATRP og *click* kemi muliggør fremstillingen af en bred vifte af polymerstrukturer hvor kontrolpanelet består af substitutions-, polymeriserings- og sulfoneringsgraden, og dertil *blending*.

Abstract

The cornerstone in this dissertation is made up by three individual assessments of the diversity in the macromolecular landscape that can be obtained by applying relatively few efficient chemical tools. The intention is to gain deeper knowledge on the chemical tuning of proton exchange membranes (PEM) and thereby optimizing their properties. Equally important has been the evolution of model systems that are part of a bigger research perspective as well as the application of unconventional strategies within the field.

In the design of amphiphilic polymers, a commercially available polysulfone (PSU), Udel$^{\circledR}$, is chosen as backbone due to its mechanical and thermal properties. Sulfonic acid functionalized, dendronised side chains are attached by click chemistry in the study of hydrocarbon structures with highly flexible spacers. Various degrees of sulfonation (DS) are used in the perspectivation of the influence of ion exchange capacity (IEC) on water sorption and proton conductivity. There appears to be a narrow IEC-window where the water percolation increases tremendously from being very low to where severe swelling occurs, and the proton conductivity proportionally with it.

In another model study of hydrocarbon macromolecular architectures, PSU with post-sulfonated polystyrene (PS) grafts are investigated. Here, IEC is controlled through the degree of substitution, the graft length and DS. The grafting is performed with atom transfer radical polymerization (ATRP).

The third assessment is dedicated to a partially fluorinated system that is based on a poly(vinylidene fluoride) (PVDF)-containing backbone with fully sulfonated PS grafts. To counteract the dimensional change upon water contact that is a result of the increased IEC, the ionomer is blended with a high molecular weight PVDF, which contributes to the conservation of mechanical stability. The morphology of these blends is affected by the PVDF content. At 25 vol% ionomer macro-phase-separation occurs, while a 40 vol% ionomer content on top of the macro-phase-separation develops a repetitive patten of ion-rich domains in primarily PVDF-containing areas. The blends are highly humidity sensitive, yet, despite lower absolute conductivities than Nafion$^{\circledR}$, they display a reduced dependence on both humidity and temperature. Under fully humidified conditions the blends perform superior to fully sulfonated graft copolymer analogues.

The combination of a high degree of control by ATRP and click chemistry enables a wide selection of polymer structures with the handles: degree of substitution (DS), polymerization and sulfonation, and blending.

Contents

Abbreviations and symbols

AGET	activators generated by electron transfer
A-PS	alkyne terminated polystyrene
ARGET	activators regenerated by electron transfer
ATRP	atom transfer radical polymerization
Bpy	2,2'-bipyridyl
b	block
co	copolymer
CTFE	chlorotrifluoroethylene
CuAAC	copper(I)-catalyzed azide-alkyne 1,3-cycloaddition
DCE	1,2-dichloroethane
DG	degree of grafting
DI	deionized
DMAc	*N,N*-dimethyl acetamide
DMF	*N,N*-dimethyl formamide
DMFC	direct methanol fuel cell
DP	degree of polymerization
DS	degree of sulfonation
DSC	differential scanning calorimetry
DVS	dynamic vapor sorption
EBiB	ethyl 2-bromoisobutyrate
EDX	energy-dispersive X-ray spectroscopy
EW	equivalent weight
EW^{-1}	inverse equivalent weight (= IEC)
FC	fuel cell
FCEV	fuel cell electric vehicle
g	graft
GDL	gas diffusion layer
HT-PEM	high temperature proton exchange membrane
HT-PEMFC	high temperature proton exchange membrane fuel cell
IEC	ion exchange capacity
LT-PEMFC	low temperature proton exchange membrane fuel cell
MEA	membrane-electrode assembly
MI	macroinitiator
N117	Nafion® 117
N212	Nafion® 212
PAE	poly(arylene ether)
PBI	polybenzimidazole

PDEVPh	poly(diethyl vinylphosphate)
PDI	polydispersity index
PEM	proton exchange membrane
PEMFC	proton exchange membrane fuel cell
PFSA	perfluorosulfonic acid
PMDETA	N,N,N',N'',N''-pentamethyldiethylenetriamine
PS	polystyrene
PSSS	poly(sodium styrene sulfonate)
PSU	polysulfone
PSU-Cl	(chloromethyl)benzoyl functionalized polysulfone
PSU-N	azide functionalized polysulfone
PSU-g-PS	polysulfone-$graft$-polystyrene
PSU-g-SPS	sulfonated polysulfone-$graft$-polystyrene
PTFE	polytrifluoroethylene
PVDF	poly(vinylidene fluoride)
P(VDF-co-CTFE)-g-SPS	sulfonated poly(vinylidene fluoride-co-chlorotrifluoroethylene)-g-polystyrene
PVDF-co-PSSS	polyvinylidene-co-poly(sodium styrene sulfonate)
RH	relative humidity
RT	room temperature
SEC	size exclusion chromatography
SSS	sodium styrene sulfonate
St	styrene
$T_{d\,10\%}$	decomposition temperature at 10% weight loss
TEM	transmission electron microscopy
T_{exo}	exothermal response temperature
T_g	glass transition temperature
TGA	thermogravimetric analysis
THF	tetrahydrofuran
TMSPrBr	trimethylsilyl protected propargyl bromide
TMS-PS	trimethylsilyl protected propargyl end-capped polystyrene
WU	water uptake
μ_{eff}	effective proton mobility
λ	hydration number or [H_2O/-SO_3H]
σ	proton conductivity

1

Objectives

From the start the intention has been to prepare new material for proton exchange membranes (PEM) and to evaluate their potential use in low temperature fuel cells (FC). Focus is thus on the most favourable protogenic group under aqueous conditions [1], meaning that only sulfonic acid functionalized membranes were to be targeted. The ideal candidate would address the limitations of current state-of-the-art membranes (as further described in next chapter) and provide new information on the influence of specific parameters. Therefore emphasis was set on ensuring a balance between new architectural discoveries, powerful chemical pathways and promising trends in FC performance.

When laying out the strategy in the pursuit of novel PEM's, two approaches were used. The first is a macromolecular re-thinking with the intention to create and dig into a new structural family with offset in a commercial backbone. The second is a continuation of an established system, where previously identified structure-property relationships are cornerstones. The following two chapters deal with the new architectures: A hydrocarbon family consisting of members having 1. short side chains introduced by click chemistry, and 2. medium to long side chains controlled by atom transfer radical polymerization. Then comes the introduction of a partially fluorinated blend graft copolymer system in a third chapter.

The main section of the dissertation is based on these three manuscripts, and the chapter that follows is dealing with alternative systems that for various reasons never made it far. The applied analytical techniques are summarized in Appendix I, and the original manuscripts are included as Appendix II - V, starting with the popular scientific paper in Danish and ending with the milestones of the thesis (*Manuscripts 1 - 3*). It should be noted that chemical details can be found in the manuscripts.

In part one a commercial polysulfone (PSU) known to have good film forming properties [2] is chosen as backbone for a family of hydrocarbon short side chain architectures. Click chemistry is used for the coupling reaction between sulfonic acid functionalized alkynes and azide functionalized PSU, which results in a triazole link - previous studies indicate that the pK_a could contribute with non-covalent bondings in order to improve the ionic domain

1

formation. Aiming at a high degree of flexibility to improve phase separation, an aliphatic dendronised structure is investigated and compared with linear side chains.

In part two the PSU family is extended with a hydrocarbon graft copolymer member. The backbone is modified to become an atom transfer radical polymerization (ATRP) macroinitiator from which styrene is grafted and subsequently sulfonated. Water sorption observations from analogue partially fluorinated and phosphonated structures that are prepared by clicking the side chains onto the backbone predict a high sensitivity towards swelling. Therefore, the family extension is performed from a predominantly chemical angle, where synthetical pathways are investigated, and the relatively short backbone serves as a model component.

In part three, fully sulfonated poly(vinylidene fluoride-*co*-chlorotrifluoroethylene)-*g*-polystyrene [P(VDF-*co*-CTFE)-*g*-SPS] is investigated. Previous discoveries from analogue partially sulfonated systems showed that graft structures provide superior mechanical integrity upon water sorption compared to diblock copolymers [3] and that the graft density should be low [4]. When increasing both graft length and degree of sulfonation, water swelling becomes excessive. Studies of partially fluorinated systems blended with low molecular weight poly(vinylidene fluoride) (PVDF) showed that graft copolymers are more morphologically tolerant to blending than diblocks [5], and in evaluating the effect of chain length and crystallinity of the graft copolymer systems, it was proven that high molecular weight PVDF improved the water sorption behavior through increased entanglement and crystallinity [6]. The presence of non-sulfonated polystyrene (PS) in the grafts has a restricting effect in the ionic domain size [4] so the next step - as taken here - was to first sulfonate graft copolymers with a low degree of grafting (DG) and then prepare blends with high molecular weight PVDF thereof. The influence of graft length, volumetric PVDF content and blending versus pure graft copolymers are evaluated in a structure-property relationship analysis.

Manuscripts

1 - *Appendix III*
M. M. Nielsen, I. Dimitrov, S. Takamuku, P. Jannasch, K. Jankova and S. Hvilsted. Dendronised Polymer Architectures for Fuel Cell Membranes. Submitted to *Fuel Cells*, October 2012.

2 - *Appendix IV*
M. M. Nielsen, K. Jankova and S. Hvilsted. Sulfonated Hydrocarbon Graft Architectures for Cation Exchange Membranes. Submitted to *European Polymer Journal*, February 2013.

3 - *Appendix V*
M. M. Nielsen, A. C. C. Yang, K. Jankova, S. Hvilsted and S. Holdcroft. Enhancing the Ionic Purity of Hydrophilic Channels by Blending Fully Sulfonated Graft Copolymers with PVDF Homopolymer. Submitted to *Journal of Polymer Science Part A: Polymer Chemistry*, February 2013.

Throughout the course of the project, fragments of the results constituting the three manu-

scripts have been presented at conferences, as talks or in posters and in the yearly update on ongoing PhD projects at the DTU Chemical Engineering, *KT Graduate Schools Yearbook*. Furthermore, a popular scientific article has been published in a Danish journal. These contributions are presented in the following.

Other publications

A
M. M. Nielsen. Tailoring Proton Exchange Membranes for Fuel Cells.*KT Graduate Schools Yearbook 2011*, 137-140.

B
M. M. Nielsen. Hydrocarbon Architectures for Fuel Cell Membranes. *KT Graduate Schools Yearbook 2012*, in print.

C - *Appendix II*
M. M. Nielsen, K. Jankova and S. Hvilsted. Nytænkning i Brændselscellemembraner. *Dansk Kemi* 95 (1-2) 2013, 18-21 (in Danish).

Conference contributions

a
M. M. Nielsen, K. Jankova and S. Hvilsted. New Polymer Architectures for Proton Conducting Fuel Cell Membranes. *Annual Polymer Day.* DTU, Kgs. Lyngby, Denmark, November 2010 (talk).

b
M. M. Nielsen, I. Dimitrov, S. Takamuku, P. Jannasch, K. Jankova and S. Hvilsted. Sulfonic Acid Functionalized Polysulfone by "Click" Chemistry. *Advances in Materials for Proton Exchange Membrane Fuel Cell Systems.* Asilomar Conference Grounds, California, USA, February 2011 (poster).

c
M. M. Nielsen, I. Dimitrov, S. Takamuku, P. Jannasch, K. Jankova and S. Hvilsted. Modification of Polysulfone for Proton Exchange Membranes. *Fundamentals and Developments in Polymer Processing Science and Technology* Palazzo Feltrinelli, Gargnano, Italy, May 2011 (poster).

d
M. M. Nielsen, I. Dimitrov, S. Takamuku, P. Jannasch, K. Jankova and S. Hvilsted. A Principal Route for Modification of Polysulfone Intended for Proton Exchange Membranes by "Click" Chemistry. *Frontiers in Polymer Science.* Centre de Congrès, Lyon, France, May 2011 (poster).

e
M. M. Nielsen, K. Jankova and S. Hvilsted. Proton Conducting Polysulfone Membranes by

ATRP and Click. *Nordic Polymer Days.* KTH Royal Institute of Technology, Stockholm, Sweden, June 2011 (talk).

f
M. M. Nielsen, A. C. C. Yang, K. Jankova, S. Hvilsted and S. Holdcroft. Partially Fluorinated Graft Copolymer Blends for Proton Exchange Membranes. *Nordic Polymer Days.* IDA House, Copenhagen, Denmark, May 2012 (talk).

g
M. M. Nielsen, I. Dimitrov, S. Takamuku, P. Jannasch, K. Jankova and S. Hvilsted. Dendronised Polymer Architectures for Fuel Cell Membranes. *MacroGroup UK International Conference on Polymer Synthesis & UKPCF International Conference on Polymer Colloids.* The University of Warwick, Coventry, England, July 2012 (poster).

h
M. M. Nielsen, A. C. C. Yang, K. Jankova, S. Hvilsted and S. Holdcroft. Fully Sulfonated Graft Copolymer Blends - A Structure-Property Relationship Study. *CARISMA International Conference on Medium and High Temperature Proton Exchange Membrane Fuel Cells.* Axelborg, Copenhagen, Denmark, September 2012 (poster).

j
M. M. Nielsen, K. Jankova and S. Hvilsted. Sulfonated Hydrocarbon Graft Architectures for Fuel Cell Membranes. *Annual Polymer Day.* DTU, Kgs. Lyngby, November 2012 (talk).

2

Background

When navigating in a research area as heavily investigated as that of fuel cells, it is a big help to be familiar with its history, and crucial to understand the underlying mechanisms driving the evolution. This section is meant as an explained short guide to the road of the fuel cell, from an electrochemical concept to a promising power generator that has found widespread uses and is on the brink to full-scale commercial entry to one of the three areas historically renowned to facilitate growth of societies: transportation [7] - with emphasis on the proton exchange membrane.

2.1 Proton exchange membrane fuel cell (PEMFC)

The first roughly 120 years after the electrochemical principle behind the fuel cell was discovered in 1838 by C. F. Schönbein [8] and the year after demonstrated by W. R. Grove were thin. The term "fuel cell" was introduced in 1858 by C. Langer and L. Mond, other than that, not much happened until the United States launched their high priority space programs that ultimately brought N. Armstrong and his crew to the moon. During the period of time leading on to this turning point in world history, the US electronics company General Electric experienced major breakthroughs in using a polymer proton exchange membrane (PEM) (sulfonated polystyrene) in 1955 and depositing catalyst platinum onto the PEM in 1958. F. T. Bacon was credited for a 5 kW stationary fuel cell the following year, and during space journeys in the 1960s Pratt & Whitney licensed Bacon's US patents for use in the air shuttles to supply electricity and drinking water, the sole byproduct from the electrochemical reaction between hydrogen and oxygen. The next landmark for PEM fuel cells (PEMFC) was the development of the PEMFC automobile by R. Billings in 1991. This discovery was a motivating factor for car companies, and research institutions across the northern hemisphere in particular. As opposed to the internal combustion engine, FC's are not restricted by the Carnot cycle, which implies that a larger amount of the chemical energy can be converted to electricity [9]. With the signed memorandum of understanding among leading personal vehicle manufacturing companies from 2009, stating that from 2015 they would provide fuel cell electric vehicles (FCEV) for commercialization, infrastructure

is now being developed, and FC's are getting ready to meet the general public [10]. According to the Fuel Cell Today 2012 Industry Review [10], there has been an almost eight-fold increase in FC shipments from 2008 to 2012 with Asia, Europe and North America as the main recipients. By type, PEMFC represent some 90% in 2012 with direct methanol fuel cells (DMFC) and solid oxide fuel cells (SOFC) having most of the remaining share. This should be seen in relation to a roughly 50:50 distribution between PEMFC and DMFC in 2008. From a capacity point of view the share of PEMFC makes up less than half, i.e. about as much as DMFC. In addition to the large scale transportation application, PEMFC's are incorporated into portable products, of which the educational portfolio of Singapore-based Horizon Fuel Cell Technologies is among the more remarkable market elements [11].

To operate PEMFC's, hydrogen is required. Hydrogen production can be done by a range of techniques, from fuel processing (e.g. hydrocarbon reforming, pyrolysis etc.) to non-reforming processes, from biomass or water (e.g. electrolysis) [12]. The discussion on how to best store hydrogen - and energy in general - has been ongoing for several years, that the energy economy has quite a way to go to become cost-competitive to alternatives [13]. There are cases, though, where the potential is so large, that a solution simply has to be found. For instance, in societies exploiting renewable energy sources like wind or water energy, supply and demand for electricity do not always go hand in hand. In autumn it is typically more windy, in spring there is more melt water etc. Here, excess energy (if not sold to other communities) can power the electrolysis of water [12], thereby generating hydrogen (see Figure 2.1).
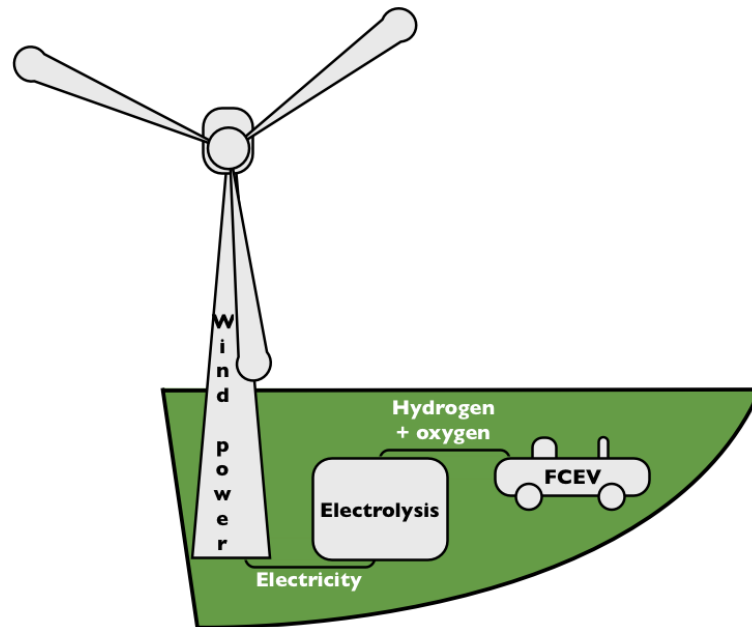

FIGURE 2.1: *Excess electricity from wind energy can be used to run electrolysis, then the generated hydrogen can be used in fuel cell powered vehicles.*

In countries where green energy have top priority this is particularly valid. Take for

instance Denmark, with the recent ambitious goal to be fossil-free in 2050 [14]. Here technologies utilizing hydrogen will be highly relevant. The environment will benefit, and societies can reduce their dependency on fossil fuel providers by strengthening the local energy production in a future that could see more alternative fuels for the transportation sector rather than a fossil fuel monopoly [15]. It is beyond the scope of the work presented here to conclude on the economic benefits in a hydrogen powered society. There are too many uncertainties as of yet, including hydrogen production, hydrogen storage, construction of a refueling intranet, which is so far only in its verge and mainly restricted to Western Europe, North America and Southeast Asia [16].

2.2 Proton exchange membrane fuel cell (PEMFC)

PEMFC are also referred to as polymer electrolyte membrane fuel cell, named after the proton conducting component separating the electrodes (see Figure 2.2).
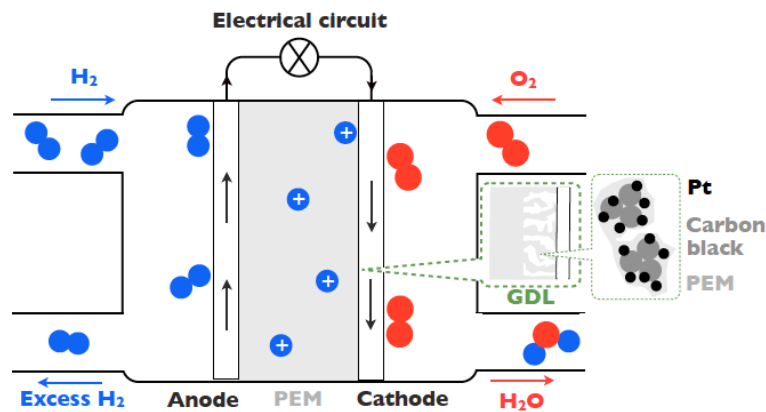

FIGURE 2.2: *Illustration of a single cell. The protons migrate over a polymer membrane while the electrons partake in an electrical circuit. Oxygen anions and protons form water, the only waste product - along with heat. GDL = gas diffusion layer.*

PEMFC runs on hydrogen, or purified reformed natural gas (carbon monoxide destroys the catalyst pla-tinum). The environment of the membrane is aqueous and acidic, whereas the electrodes are coated with a catalyst material, typically of platinum (extensive research for alternatives are ongoing due to the high prices and low abundance). PEMFC operated in an aqueous media, below the boiling point of water are referred to as low temperature PEMFC's (LT-PEMFC). However, the catalytic stability is increased and heat transfer improved by operating at higher temperatures. Thus systems have been developed to work with phosphoric acid instead of water as electrolyte, applying a different class of polymer membranes, that can be operated at temperatures up to 200 ^{o}C. These are called high temperature PEMFC's (HT-PEMFC). LT-PEMFC usually apply sulfonic acid (-SO$_3$H) as protogenic group due to its pK$_a$ value, whereas the protogenic group in HT-PEMFC is phosphonic acid (-PO(OH)$_2$), which has higher thermal stability. Details on proton con-

ductivity are provided in the next section. Figure 2.2 shows a graphical representation of a PEMFC single cell. The first zoom is showing the gas diffusion layer (GDL), and the second zoom shows the catalyst layer consisting of platinum, carbon black and PEM. The power output of a single cell is typically in the range of 0.5 to 1.0 V, so multiple cells are commonly arranged in a series of stacks, as illustrated in Figure 2.3. whereby the effect is increased according to the desired application.
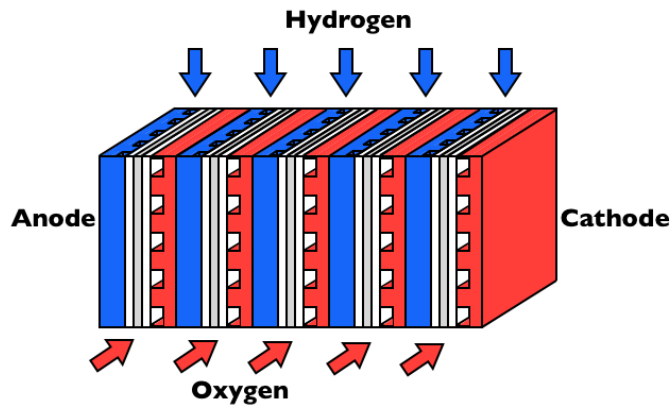

FIGURE 2.3: *Single cells are arranged in stacks to obtain a higher voltage.*

The DMFC works a lot like PEMFC, only methanol is the fuel, and not hydrogen, and the catalyst layer consists of platinum and ruthenium. The coordination chemistry of this complex enables the electrochemical reaction to proceed without the need of a fuel reformer [17]. DMFC's also deploy PEM's, and the most notable difference in requirements is the barrier properties towards the liquid methanol. On a side note, PEM's are cation ion exchange membranes, implying that PEM's for FC's are closely related to those of electro-dialysis, water purification, desalination, sensors etc. [18–20].

2.3   Proton exchange membrane (PEM)

In short, PEM's serve the purpose to allow for protons to migrate from the anode to the cathode side and simultaneously separate the reactant gases. This is obtained by tuning the macromolecular structure in a balance between acidic groups and the hydrophobic moiety that provides chemical, thermal and mechanical stability [20]. Comparison is of-tentimes done with reference to the most commonly referred to commercial benchmark, Nafion[R] [21, 22], which is a perfluorosulfonic acid (PFSA). Its chemical structure is shown in Figure 2.4. Research performed to make up for limitations of Nafion[R] and the likes usually addresses improvement of the proton conductivity or mechanical integrity upon water sorption, which is unavoidable for LT-PEMFC. Requirements to PEM's mostly address their stabi-lity; chemical, thermal and mechanical, and that they allow for percolated water channels through which protons can migrate. Differences in the microstructural features of ionomers are reported to be different from PFSA's (e.g. Nafion[R]) and hydrocarbon

systems (e.g. sulfonated polyetherketone) due to the higher flexibility of the former [23]. Consequently, wider channels are obtained with PFSA's, the separation between -SO$_3$H groups are smaller, and there is an overall good connectivity.

FIGURE 2.4: *Chemical structure of Nafion®.*

Figure 2.5 shows the orientation of ionomer in four different situations. When dissolved in a good solvent (upper left) the polymers are free to move around. When film cast and dry (upper right) the ionic groups will attract each other and potentially form clusters surrounded by hydrophobic segments. When brought in contain with water the water molecules enter the membrane through the hydrophilic ionic domains (lower left). As the level of hydration is increased percolation arises (lower right).

FIGURE 2.5: *Illustration of the orientation of the amphiphilic polymers when in solution (upper left), when the membrane is dry and ionic segregation appear (upper right), upon water uptake (lower left), and when hydration leads to percolation (lower right). Black = polymer; Red = sulfonic acid groups; Blue = water.*

The understanding of the ion transport mechanisms in Nafion® has received tremendous attention over the years [24–26]. Several hypotheses have been proposed for the non-linear relationship between ionic conductivity and swelling in Nafion®, from the percolation the-

ory of Hsu and Gierke [27] to more recent random network model by Eikerling et al. [28], Diat et al.'s fibrillar model [29] and parrallel cylindrical water nanochannels of Schmidt-Rohr et al. [30], and Kreuer's comparative studies of PFSA and hydrocarbon [31]. The kinetics of ion transport in Nafion$^{®}$ have been studied by AC impedance [32]. Model studies have been made on modified carbon nanotubes in the evaluation of the effects of the hydrophobic environment [33]. On a more general note, there is consensus that the interplay between permeability and conductivity is of vital importance for ion exchange membranes [34–37]. I.e. a specific hydration number is needed in order to get within the operating window of the PEM [38]. Likewise, high temperature proton exchange membrane (HT-PEM) research is performed on the ion conducting mechanisms on phosphoric acid [39]. Figure 2.6 is a schematic representation of a humidified sulfonic acid group attached to a hydrophobic backbone, experiencing the vehicle mechanism, which is one of the accepted explanations to how protons migrate across PEM's [23]. The Grotthuss mechanism - or proton hopping - is another. Here protons are believed to practically jump from acid group to acid group. Bicontinuous hydrophilic and hydrophobic domains of well ordered morphologies are enhanced when the hydrophilic channels are less than 6 nm in diameter [40]. The through-plane impedance technique has been used for the evaluation of anisotropy of PEM's [41].
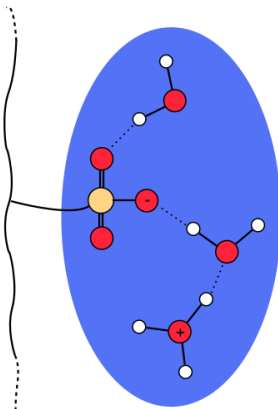

FIGURE 2.6: *Visualization of proton transfer* via *the vehicle mechanism. Black = polymer; Blue = water domain; Orange = S; Red = O; White = H.*

HT-PEMFC, typically operated at 180 ^{o}C, and using phosphoric acid-doped PEM's, are developed to circumvent the most frequent limitations of low temperature PEMFC's, e.g. CO catalyst poisoning, water and heat management and effects from changing humidification [1, 22, 42–46]. Polybenzimidazole (PBI) is the most common base of such structures [47–49]. Composite membranes is another promising field of HT-PEM's [50].

2.4   Membrane performance parameters

In the evaluation of the potential of a PEM candidate, some basic investigations are routinely performed in addition to proton conductivity measurements. The measurement is done by

NaOH back titration [51]. Water uptake quantified as the percentage wise weight gain upon water sorption of a dry membrane is a measure for the swelling behavior. Ion exchange capacity (IEC) [meq g^{-1}] is a measure for the ionic content in a dry membrane. The theoretical IEC value can be calculated from ^{1}H NMR or be determined experimentally. Deviations between the two are typically due to imperfect connectivity between ionic domains. Well-ordered networks are considered key to increase proton conductivity. Figure 2.7 graphically represents the cases where ionic channels in a hydrophobic matrix are interconnected (*i*)) and where the ionic channels form dead ends and some ionic domains are isolated *ii*). Dead ends are included in IEC but do not facilitate proton transport across the membrane. Isolated ionic domains neither contribute to conductivity, nor in the experimental determination of the IEC value.
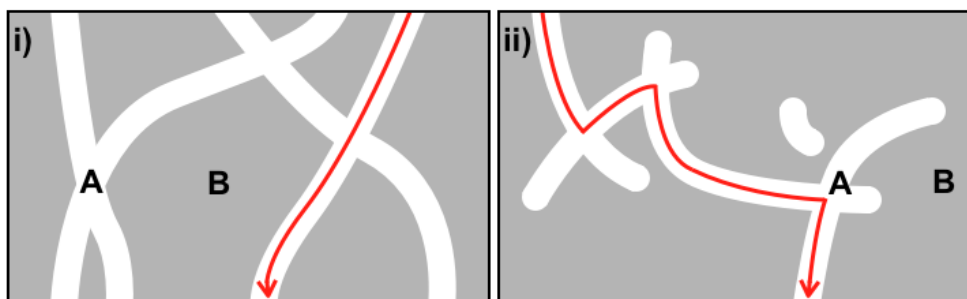
FIGURE 2.7: *Illustrations of i) perfectly interconnected ionic channels (A) in a hydrophobic matrix (B) and ii) a microstructure with dead ends and isolated ionic domains.*

The analytical acid concentration [-SO$_3$H] [M] strongly influences the conductivity, so knowledge on its acid and water content dependency is useful. At elevated IEC water uptake may be high, which dilutes the acid and subversively affects the conductivity [36]. The effective proton mobility, μ_{eff} is the proton conductivity "normalized" for the effects of acid concentration and provides information on acid dissociation, ionic channel tortuosity, and special proximity of neighbouring acid groups [36]. In the extreme case where no dissociation of the acid takes place, $\mu_{eff} = 0$. In pure water, $\mu_{eff} = 3.623 \cdot 10^{-3}$ cm^2 S^{-1} V^{-1} at RT [52].

PEM's belong to the category cation exchange membranes, and share many properties with other applications thereof, as sensors, water purification, desalination and electrodialysis [20]. Alternative routes to cation exchange membranes are for example radiation-induced grafting of styrene from preexisting membrane material [18, 19, 21, 53].

2.5 Current challenges facing PEMFC

For the assessment of current challenges to overcome for PEMFC technology to succeed in the long run, an overview of key factors price, lifecycle time and performance should come handy.
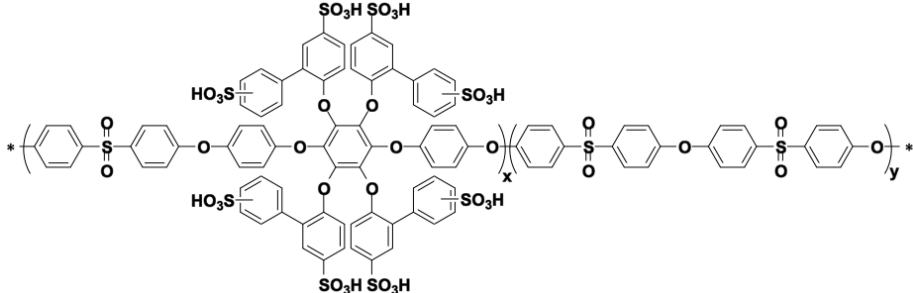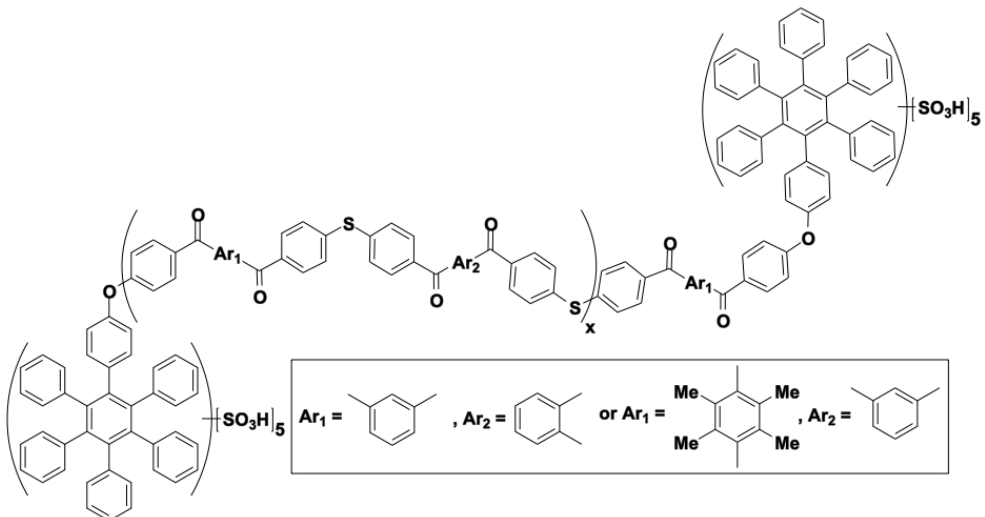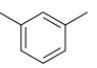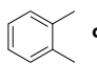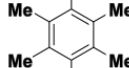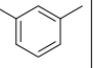
As already mentioned, there are multiple components in a PEMFC, and the costs of the individual parts depend on the scale of production. According to a US Department of Energy (DOE) estimate from 2011, in 2015 the catalyst ink and application will be the main cost driver at high production rates (500,000 units a year), making up 33% of the total cost 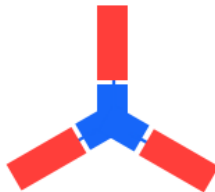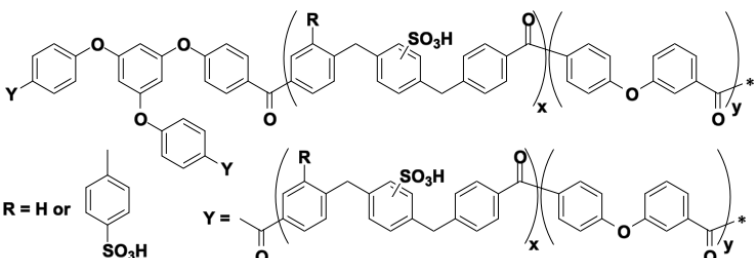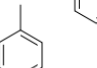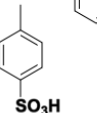[54]. Other expenses are: bipolar plates (22%), MEA frame/gaskets (15%), GDL (12%), PEM (12%), other (6%). However, at low production rate (1,000 units a year) PEM is the main cost driver, by 44%. The remaining components make up: GDL (18%), bipolar plates (15%), catalyst ink and application (11%), other (8%), MEA frame/gaskets (4%). The first scenario is the aim, and with fuel cell powered buses already in operation in e.g. British Columbia, London UK and Oslo, and a large-scale commercialization of personal vehicles scheduled for 2015 by automotive companies from all of the Northern hemisphere, e.g. Hyundai, Daimler and General Motors, it could be feasible. In either case, extensive research is ongoing on every single component, at universities, in companies and all sorts of research institutions. For instance, the required amount of Pt for the electrodes has been reduced remarkably in recent years [55], and research on recovery as well as non-precious metal catalysts have high priority [8,56], but this is also necessary. Based on the estimated abundance of Pt on Earth, if all cars that are currently equipped with an internal combustion engine were to be replaced by PEMFC, there would not be enough Pt to fulfill this vision. Updates on the challenges facing the industry are published continuously, with the US DOE as one of the main standard-bearers [57–59].
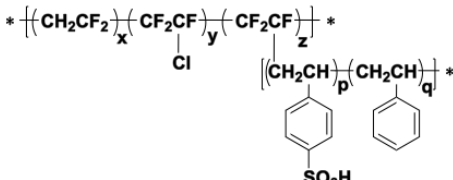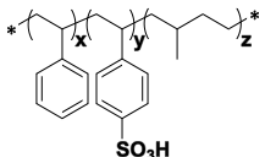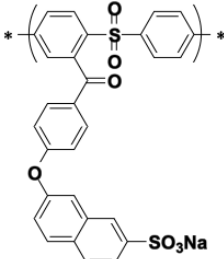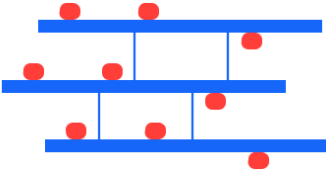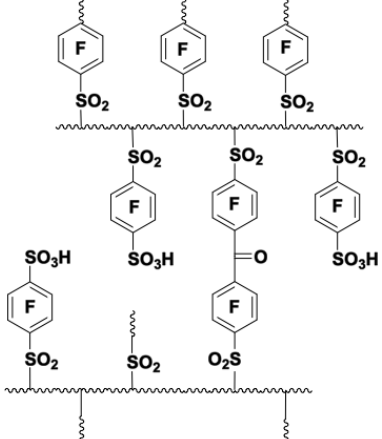
The lifetime of a PEM is typically caused by flooding, drying-out, pollution/corrosion/dissolution of the catalyst, membrane rupture and crossover of the gases [56,60–62]. In short, flooding obstructs the electrochemical processes on the cathode side (where water is formed), and on the anode side water molecules leave along with the protons in the vehicle mechanism leaving that side water deficient. Humidifiers are used to keep the right humidity in the cell. As the membrane dries out, the resistance increases. The catalyst degradation occurs grace to the harsh operating conditions and the low temperature (especially true for DMFC, where carbon monoxide is a severe threat towards Pt). At higher temperatures this issue is reduced, and heat management facilitated [42]. Membrane fracture or pin-hole formation [63] are consequences of changing humidities throughout the cell. The cross-over phenomenon is difficult to avoid, in part due to the small membrane thickness and the aforementioned degradation and constant changes in the FC environment. Accelerated tests are used in the investigations of these on single cells [64], and in addition stack testing [65] and modeling studies [66] are carried out. Thermal and degradation studies made on the isolated PEM is a more simple method that still yields useful data. The Fenton test is an example of a commonly applied method in the evaluation of chemical stability [67,68]. Fenton's reagent contains ferrous iron salts and hydrogen peroxide, thus the membrane gets exerted to aggressive radical attack in an oxidative environment. Chemical degradation of PFSA's are typically followed by ^{19}F NMR spectroscopy [69].

PFSA's dominate the commercial PEM landscape for reasons already mentioned. In a trade-off between price, real lifetime and performance other PEM candidates may enter the scene. However, they do have performance-related limitations, especially at elevated temperatures [70]. Hence, numerous alterations of e.g. Nafion$^{\textcircled{R}}$ have been made, where the inherent properties of the PFSA are attempted preserved at the same time as the weak-

nesses are made up for [71]. Research on alternatives to PFSA's, include the development of partially sulfonated ionomers, of which the BAM (Ballard Advanced Materials) was a strong candidate due to its styrenic base allowing for straight forward chemistry and low cost [72]. An overview of some structurally different model studies are included in Table 2.1. They all exploit well defined ionic and hydrophobic regions. Overall, it is important to keep in mind the necessity of compromising parameters like conductivity, and water uptake [73]. In order to determine which member of a certain category performs better, as in the case of PFSA's [74], it is useful to do model studies on different morphologies. Research trends have gone in directions of sulfonated hydrocarbon-based structures [21, 75–78], and aromatic systems developed to perform better at low RH [79]. Much attention has been directed towards block copolymer structures [80], e.g. styrenic tri-blocks [81], due to their self-assembling properties. MEA processing deploying hydrocarbon-based PEM's rather than PFSA's were investigated by McGrath and coworkers [82]. The compromise in using hydrocarbon-based PEM systems is the lower oxidative stability rela-tive to PFSA's, which is less of an issue when applied in low capacity power sources operated at low temperatures, as is often the case for portable FC's [83]. Plenty of work has also been done on partially fluorinated systems [84, 85]. An alternative route to PEM synthesis, which has received a fair amount of attention (from industry too) is radiation-induced grafting, which has the useful feature that the inhe-rent properties of an existing polymeric material is preserved even during chemical and/or physical surface alteration [86, 87]. The creation of highly ordered mesoporous Nafion$^{\circledR}$ membranes by micelle templating is another [88]. Due to the complexity in the polymeric systems and many variables, simulation studies are carried out in parallel with experimental work [23, 66, 89, 90].

TABLE 2.1: *Examples of architectural strategies pursued by research groups in recent years in investigating the structure-property relationships, excluding blends [91,92], composite systems [93] and alterations of PFSA systems.*

Class	Examples
Highly sulfonated backbone segments	Ueda et al. [94]

| *Highly sulfonated end-groups* | Hay et al. [95] |

| *Star copolymers* | Hay et al. [96] |

Class	Examples
Graft copolymers	Holdcroft et al. [3]
Block copolymers	Balsara et al. [97]
Comb-type structures	Jannasch et al. [98]
Cross-linked networks	Kerres et al. [92]

3

Chemical tools

In the creation of amphiphilic polymers with features of exhibiting interconnected phase-morphologies, a palette of chemical reactions, including polymerization reactions are necessary. The synthetic pathways should be efficient, reliable, and the polymer syntheses controllable. Thereby the presence of undesired functionalities should be reduced to a minimum, as these can contribute to degradation or the like of the membranes. A selection of synthetic disciplines applied in the project work is presented in the following.

3.1 Lithiation

One of the reasons for using polyarylenes as backbones in PEM systems is that they are chemically stable under even harsh conditions. Yet proton conducting functionality must be incorporated in a way, so a selective modification is needed. In the case of the polysulfones Udel$^{®}$, various sites can be directly sulfonated [21,99,100] or the *ortho* proton to the sulfone bridge can be attacked by *n*-BuLi and the resulting lithiated site can be quenched by an electrophile possessing a desired functionality, as shown by Jannasch et al. [2,98]. In the case of the work presented here, this is a chloromethyl group that can serve as ATRP-initiating site or as a precursor for azide functionality leading up to click chemistry.

3.2 Copper-catalyzed azide-alkyne cycloaddition (CuAAC) or click chemistry

Click chemistry is a term covering highly efficient coupling reactions that have attracted much interest over the past years as it allows for a high degree of control when introducing functionalities in even complex macromolecular structures [101–103]. For this reason it has found widespread use within e.g. bioapplications [104], drug delivery systems [105], conductive polymers [106] and in the creation of multlayer films [107]. CuAAC was originally reported by Huisgen [108] and later developed to become the selective click reaction we know today by Meldal et al. [109] and Sharpless et al. [110]. In the reaction between an azide and
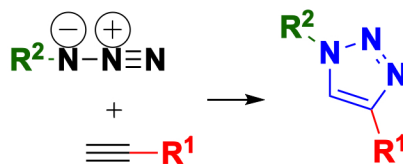
SCHEME 3.1: *The general click reaction.*

terminal alkyne the link between two connected molecules is always a 1,2,3-triazole. Scheme 3.1 displays the general CuAAC click reaction. It may be surprising that there are only few publications on click chemistry applied in PEM research. Highly sulfonated comb-type crosslinked structures by Norris et al. [111] and graft structures by Dimitrov et al. [112] showed that there is a considerable potential in the chemistry for PEM's. The Brønsted base 1,2,3-triazole (pK_B = 0 - 1) [113] could potentially serve as an enhancer of phase separation grace to acid-base interactions with the -SO$_3$H groups. The interesting feature here is that a high degree of control can be obtained as compared to other non-quantitative reactions, incl. chain lengths and degree of sulfonation (DS). Within the frames of this work, of click reactions, only CuAAC was used.

3.3　Atom transfer radical polymerization (ATRP)

ATRP has its roots in the Kharasch reaction, an atom transfer radical additon [114], and ATRP was initially reported by Matyjaszewski [115] et al. and Sawamoto et al. [116]. The fundamental concept of the controlled radical polymerization technique is depicted in Scheme 3.2. Copper(I) forms a complex with a halide from a (macro)initiator and thereby leaves the initiator with a radical site. The equilibrium lies towards to dormant state (left side in Scheme 3.2), i.e. the key to the high control of the technique lies in the persistent radical effect-induced equilibrium between activation and deactivation of the halide metal complex [117]. Upon the encounter with a vinylic monomeric unit the radical will react on the least stable vinylic carbon in generating the most stable new radical (Scheme 3.2, middle right image). Again the equilibrium between the active and dormant states is towards the far left, meaning that the compound is insusceptible to propagation the vast majority of the time. The addition of vinylic monomeric units thus repeats itself over time, whereby a polymer chain is formed.

ATRP has gained immense interest due to the high degree of control that can be obtained, and the wide range of monomers, ligands, initiators and solvents that can be applied [118–121]. A strong asset is the high degree of control with the polymerization of a wide range of vinylic monomers. This means that polymer chain lengths can be targeted and synthesized, at narrow polydispersities (PDI). ATRP has found widespread use, structurally (e.g. multiblocks, grafts etc.) and application-wise (e.g. ion exchange membranes, biocompatible materials, drug delivery systems etc. [122,123]). The reaction can be performed in a solvent or in bulk, where the monomer serves as solvent. Depending on the application there are some limitations to conventional ATRP: it requires an air (oxygen) free
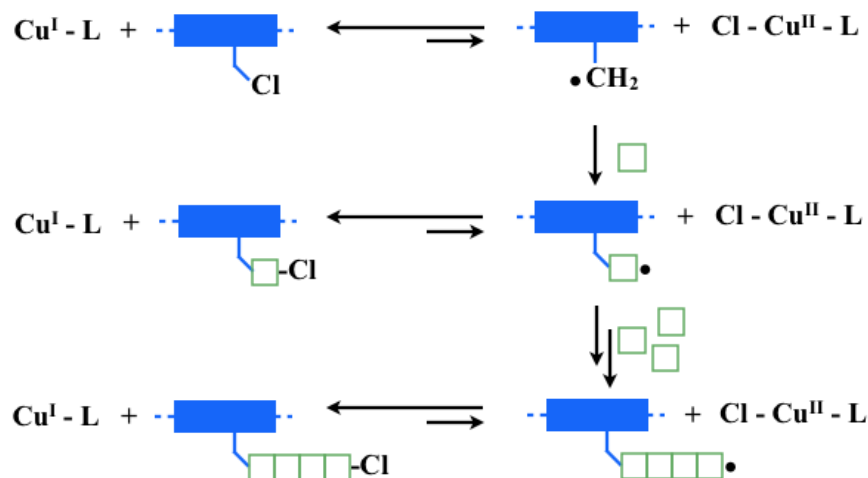
SCHEME 3.2: *Graphical reproduction of monomer (squares) grafting from a macroinitiator (rectangles) by ATRP in the general case; L = ligand.*

environment and it is often difficult to get rid of all copper, the latter is mainly challenging when developing products for bioapplications as copper is a reducing agent and cytotoxic. In order to counteract these limitations, notably Matyjaszewski and coworkers have evolved ATRP in various directions: *i)* AGET (activators generated by electron transfer) ATRP employing a reducing agent and copper(II); *ii)* ARGET (activators regenerated by electron transfer) ATRP developed to work at ppm copper levels [124]; *iii)* electrochemically controlled ATRP (eATRP), which avoids the reducing agent deployed in ARGET; *iv)* ATRP in aqueous media [121]. The reason should be found in the diversity of conditions under which it can take place. A key to the identification of the basic reaction components is provided below [120, 121, 125].

Initiator: Typically contains a halide (e.g. chloride or bromide) on primary, secondary or tertiary carbon. Can be small molecules or macromolecules, in which case it is called a macroinitiator.
Catalyst: Based on transition metals, typically copper halides, but also based on ruthenium and iron.
Ligand: Depending on solubility and other reaction components, ligands of different valency usually influence differently on the kinetics.
Monomer: Typically substituted monomers where stabilization of the propagating radicals can be obtained, including examples of ring-opening.

The combination of ATRP and click chemistry is a natural evolution of the two efficient chemical tools, hence a palette of clickable initiators, monomers and macromolecules now exist [126, 127]. An interesting feature is the potential in one-pot syntheses. ATRP is widely used in the synthesis of PEM model compounds [122]. Within the frames of this work, mostly conventional ATRP in bulk was applied, utilizing a protected, functional initiator or a macroinitiator. AGET ATRP was applied in a few reactions.

3.4   Blending

The term "blending" covers the resulting liquid or dry material from the mixing of two or more chemically or/and physically different polymers. This approach is oftentimes used to make up for less desirable properties of a polymer that otherwise has valuable characteristics. For example, to reduce cost, improve processability - or as is the case in the work presented here: to decrease swelling by the introduction of a hydrophobic polymer. The morphology upon blending depends on factors like the kinetics of the mixing process, processing temperature, choice of solvent and additives [128]. Hence the optimization process in blend formation is non-trivial, and within the frames of the work presented here, blend systems have been optimized to the extent where arguably homogeneous membranes could be obtained. Blends can be fully segregated, phase separated or both. Transmission electron microscopy is a useful tool in such morphological investigations [5].

Different approaches to blended PEMs include: *i)* blends with covalent and/or ionic crosslinking; *ii)* blends of hydrocarbon and partially fluorinated sulfonated copolymers; *iii)* blends of non-sulfonated homopolymer and partially sulfonated partially fluorinated graft copolymer; *iv)* sulfonated poly(arylene ether) (PAE) blended with functionalized imidazoles; *v)* blends with sulfonated PAE with benzimidazole-functionalized PAE [5,91,92,100,129–132].

4

Settling on strategies

In tailoring new chemical structures and evaluating their structure-property relationships three overall strategies have been singled out of which two are based on a commercial, hydrophobic backbone, PSU, Udel®. The pristine PSU structure is shown in Figure 4.1. The arylene ether segment (green) is apolar and electron-rich, while the arylene sulfone segment (orange) is polar and electron-poor. This enabled the application of various kinds of chemistry, and on top of that, products made from such a backbone have shown good film forming properties, as reported by Jannasch et al. [2, 98, 133–136].
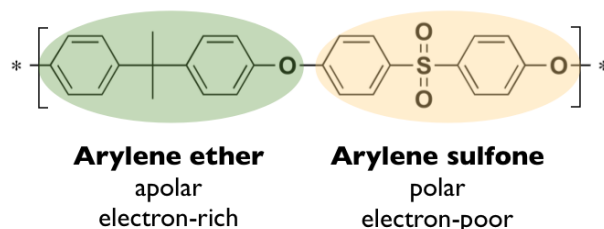
FIGURE 4.1: *Molecular properties of the backbone component, PSU.*

The PSU is chemically modified by lithiation and subsequent insertion of an ATRP-initiating group that can be converted to a click chemistry reagent rather easily. Flexible side chains of varying length and branching are synthesized, thereby generating various local ionic concentrations. The side chains are then attached to the backbone and their PEM properties are investigated (*Manuscript 1*). The novel dendronised structure draws elements from dendrimers [137]. When applying the modified PSU for grafting purposes, styrenic side chains are grown from it. The system is subsequently sulfonated, with the intention to restrict sulfonation to the grafts (*Manuscript 2*). Partially fluorinated graft co-polymer systems with sulfonated graft side chains have previously gained interest in PEM design [3]. Figure 4.2 provides a graphic representation of the approaches to establish a new macromolecular family.

Introducing dendronised side chains by CuAAC is motivated by the potentially phase-segregation enhancing effect of the resulting Brønsted base 1,2,3-triazole [113]. Previous reports on non-covalent acid-base interactions to mediate physical cross-linking of sulfonated polytriazole with resulting well-connected ion channels, as a means to suppress membrane swelling and improved proton conductivity [138] support this perception. A contributing effect on conductivity upon addition of triazoles has also been reported [139]. Resembling strategies from literature include blend systems of PSU and PBI [85], and preparation of anhydrous PEM's based on Nafion®/azole composites [140]. Chemically, the strategies applied in Manuscript 1 and 2 are tied together by previous work from our group, where linear, partially fluorinated, phosphonated grafts (rather than short side chains) are clicked onto the same backbone structure [112]. In the synthesis of the side chains, inspiration is collected from an earlier applied strategy utilizing the Williamson ether synthesis from a hydroxystyrene [141]. In a resembling approach, Norris et al. [111] introduced short linear sulfonated side chains by use of click chemistry, and subsequently cross-linked these.
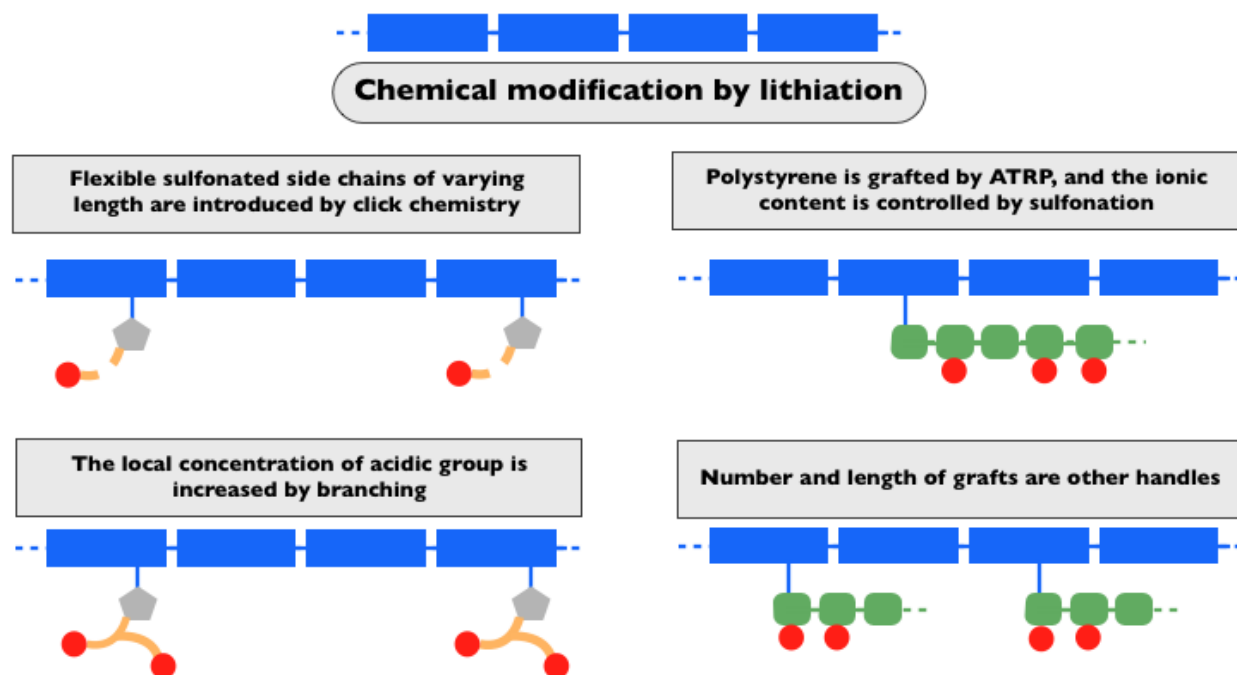
FIGURE 4.2: *Cartoon-style overview of the family tree from ancestor, PSU. Blue = PSU; Grey = 1,2,3-triazole; Orange = aliphatic chains; Red = sulfonic acid; Green = PS.*

The third main strategy is the exploitation of the blending benefits of a highly sulfonated graft copolymer with resulting potential for high ionic purity in the proton conducting water channels, but also IEC. The strategy is illustrated in Figure 4.3. P(VDF-*co*-CTFE)-SPS is sulfonated to completion and thereafter blended with high molecular weight PVDF homopolymer, to improve the mechanical integrity of the hydrated state by increasing entanglement and crystallinity of the system (*Manuscript 3*).
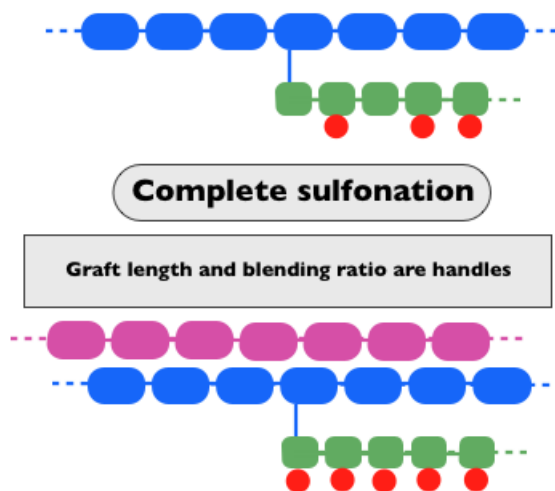
FIGURE 4.3: *Cartoon-style overview of the applied strategy to new knowledge on blends of fully sulfonated graft copolymers. Blue = P(VDF-co-CTFE); Pink = PVDF; Green = PS; Red = sulfonic acid.*

The potential in blend systems has driven massive research on the field of PEM's. Work include hydrocarbon and partially fluorinated sulfonated copolymer blends [129], sulfonated poly(etheretherketone) (SPEEK) and polysulfone bearing benzimidazole side groups [131], sulfonated poly(etherketoneketone) (SPEKK) and a poly(ether imide) [142], polyaryl blend membranes with covalent and/or ionic cross-linking density [91, 92]. Also, blending with small molecules that contribute to the pK_a have been reported [130]. Important when designing blend systems is blend miscibility, as it influences PEM properties [143]. This motivated the investigations on phase behaviour of e.g. sulfonated block copolymers [144].

On a general note, membranes of the amphiphilics can be prepared by various approaches, depending on the chemical nature and microstructure of the polymer, and the choice will affect the morphology so crucial to the performance of the PEM [73, 145, 146]. Commercial PFSA's like Nafion® are typically extruded or dispersion cast and optimized with additives etc. Other treatments that will alter the film's physical and/or thermal properties include the addition of reinforcing agents or plasticizers, annealing, stretching, film thickness and when using a solvent, the choice thereof along with the evaporation rate. When working on model compounds in lab scale, there is not resources for optimizing all of these parameters, so typically researchers decide on using solution casting, potentially with annealing [146]. Electrospinning is a more advanced technique for the fabrication of nanofibrous membranes [147].

Dendronised architectures

The sulfonated hydrocarbon-based structures in the PSU family are shown in Scheme 5.1. Those prepared by click chemistry follow the reaction arrow *Manuscript 1* from **PSU-Cl**.
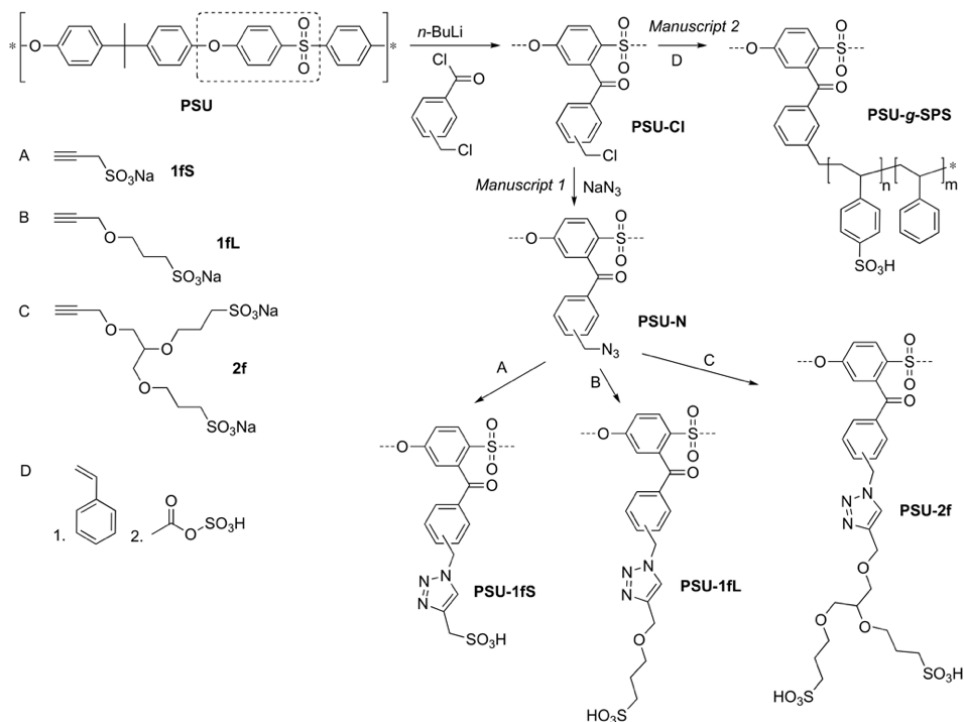
SCHEME 5.1: *Synthetic route to PSU with flexible sulfonated side chains attached via a 1,2,3-triazole.*

5.1   Preparation

The first step in creating a structural family based on the PSU backbone was the introduction of (chloromethyl)benzoyl groups. Lithiated PSU was reacted with *meta* and *para* versions of (chloromethyl)benzoyl chloride, and the negatively charged carbon in *ortho* position to SO_2 reacted with the electrophilic carbonyl group, rendering an aryl chloromethylene group tethered to PSU *via* a ketone linkage. During the reaction a colour change was observed, from colourless PSU *via* green and later light brown of the negatively charged polymer, then upon the electrophilic substitution the colour went over orange to yellow. No further differences between the two electrophiles appeared further down the road, besides the *meta* version being liquid at RT and the *para* version solid. In the following, structures from both analogue modified backbones are presented, whereas the former was preferred for the graft structures described in the next chapter. The functionalization into **PSU-Cl** was confirmed and quantified with ^{1}H NMR. The obtained degrees of substitution are: 18%, 25%, 54% and 67%. The colour changed from brown to yellow/white as the chlorine was readily converted quantitatively into an azide by overnight stirring at RT with sodium azide. Confirmation of **PSU-N** is acquired from the characteristic azide stretch at 2097 cm^{-1} observed by FTIR combined with the ^{1}H NMR spectra revealing a shift of the methylene peak upfield, from 4.61-4.56 ppm to 4.45-4.25. FTIR spectra of the four deployed **PSU-N** are shown in Figure 5.1. The intensity of the azide peak (highlighted green) relative to the C-H sp^3 stretch from the backbone (highlighted orange) increases by concentration.
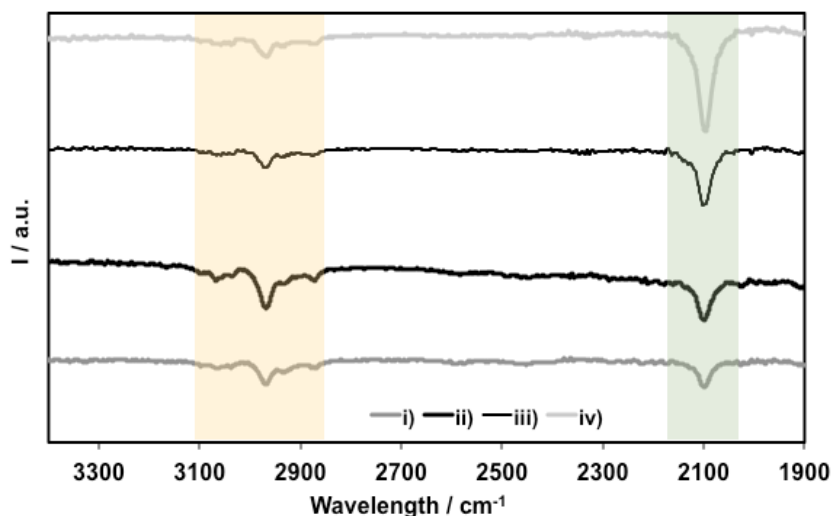
FIGURE 5.1: *Stacked view of **PSU-N** FTIR spectra at DG's of i) 18%; ii) 25%, iii) 54% and iv) 67%. Green: N_3 region; Orange: C-H sp^3 stretch.*

The next step was synthesis of the aliphatic, alkyne-terminated side chains. A short, linear variant, **1fS** (intended for pathway A in Scheme 5.1), was prepared according to a method reported by Ryu et al. [148], where propargyl bromide is reacted with sodium sulfite at 65 ^{o}C overnight (Scheme 5.2). A longer, linear version, **1fL** (for the B route in Scheme 5.1) was synthesized by Williamson ether synthesis, by activating propargyl alcohol with sodium
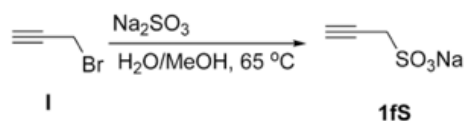
SCHEME 5.2: *Reaction conditions for the synthesis of **1fS**.*
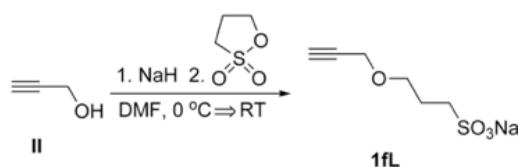
SCHEME 5.3: *Synthetic conditions for **1fL**.*
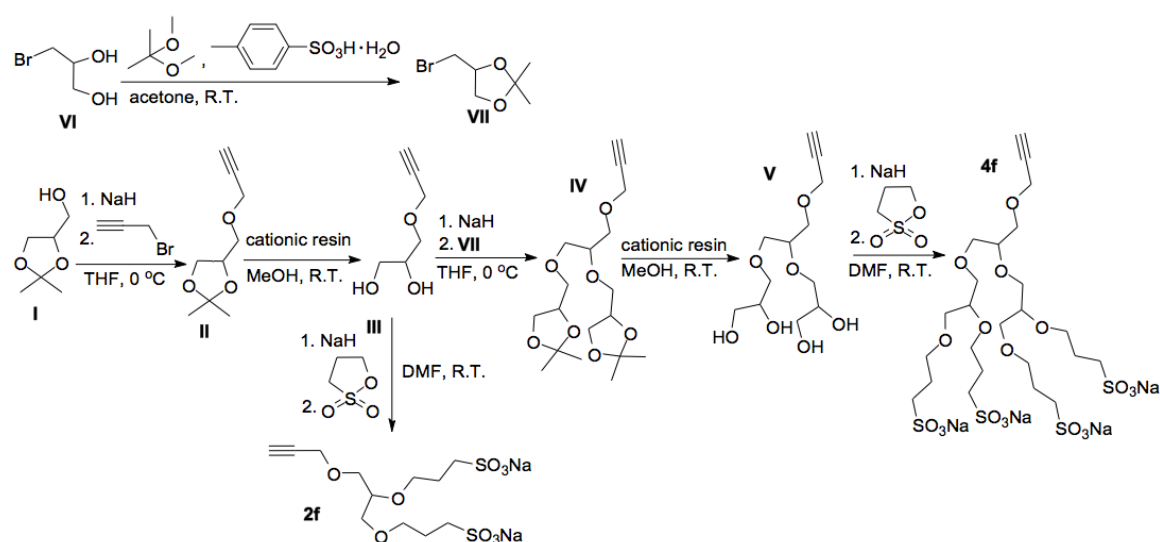
SCHEME 5.4: *Synthetic route to bisulfonated first generation and tetrasulfonated second generation dendritic side chains, **2f** and **4f**.*

hydride (NaH) followed by nucleophilic ring-opening of 1,3-propanesultone, applying similar conditions as Dimitrov et al. used with a poly(2,3,5,6-tetrafluoro-4-hydroxystyrene) [141] (Scheme 5.3). In addition to the monosulfonated, linear compounds, a branched, bisulfonated structure, **2f** (for the C arrow in Scheme 5.1) was developed. It is the simplest version - or first generation - of a dendronised side chain. The three-step procedure developed (Scheme 5.4) takes offset in solketal, which is activated by NaH, whereafter alkyne-functionality is introduced upon addition of propargyl bromide. Second, the ether linkages are cleaved by overnight stirring in a cationic resin, and then, in the final step, a double Williamson ether synthesis is carried out on the diol.

A second generation dendritic structure was developed by the chemical pathway shown in Scheme 5.4. ^{1}H NMR and FTIR analyses supported the conversion. This system was
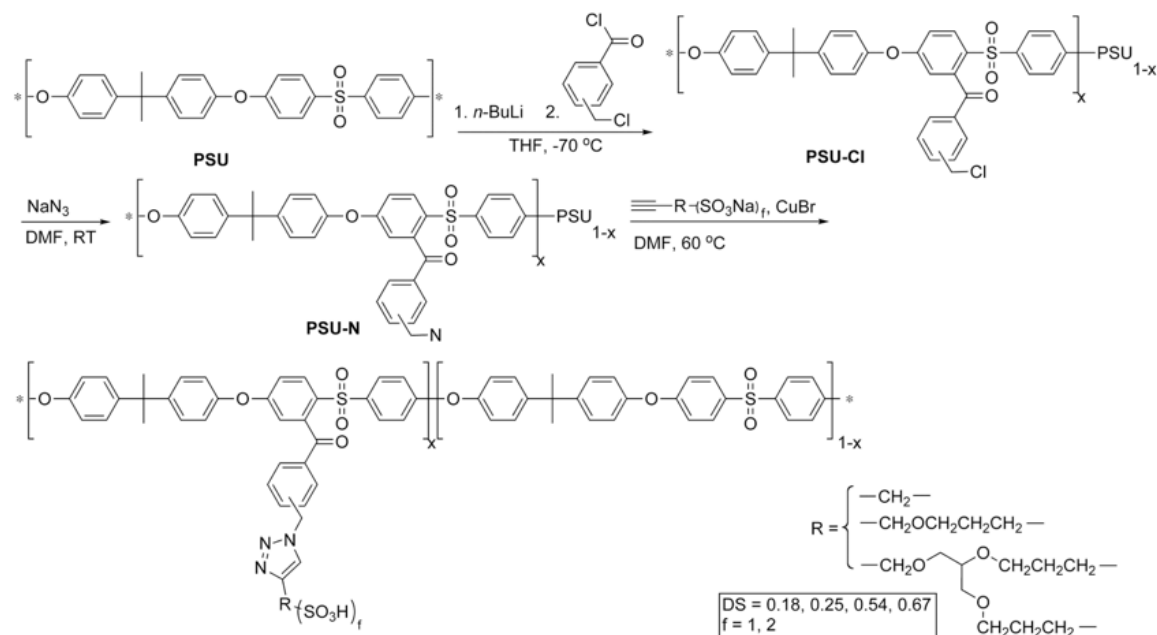
SCHEME 5.5: *Synthetic pathway from PSU, via **PSU-Cl**, **PSU-N** and to sulfonated comb-type or dendronised architectures.*

not investigated further. Due to the many non-SO$_3$H atoms, the IEC will be low unless the degree of substitution on the backbone is higher than any of the obtained **PSU-Cl**'s.

   Three different substitution degrees of amphiphilic polymers were prepared, by clicking the alkyne compounds with **PSU-N** chosen among the four prepared **PSU-Cl**, with 18%, 25%, 54% and 67% modified repeat units. **PSU-2f** employed 18% instead and not 25%, which is used for the linear chains. The click reactions were carried out in DMF with CuBr as initiator at 60 ºC overnight, as shown in Scheme 5.5. All products from the click reaction were dialyzed against deionized water to enhance purity. In an evaluation of the effect of sulfonation before versus after the click reaction, **PSU-2f** was prepared in both ways - with no remarkable advantages by one method over the other. For removal of excess alkyne an azide-functionalized Merrifield's peptide was used. The resin was prepared as previously reported [149, 150]. However, the effect was never evaluated, since dialysis was performed successively. ^{1}H NMR spectra confirming the transformation of **PSU-N**$_{0.67}$ into **PSU-2f**$_{0.67}$ are shown in Figure 5.2.
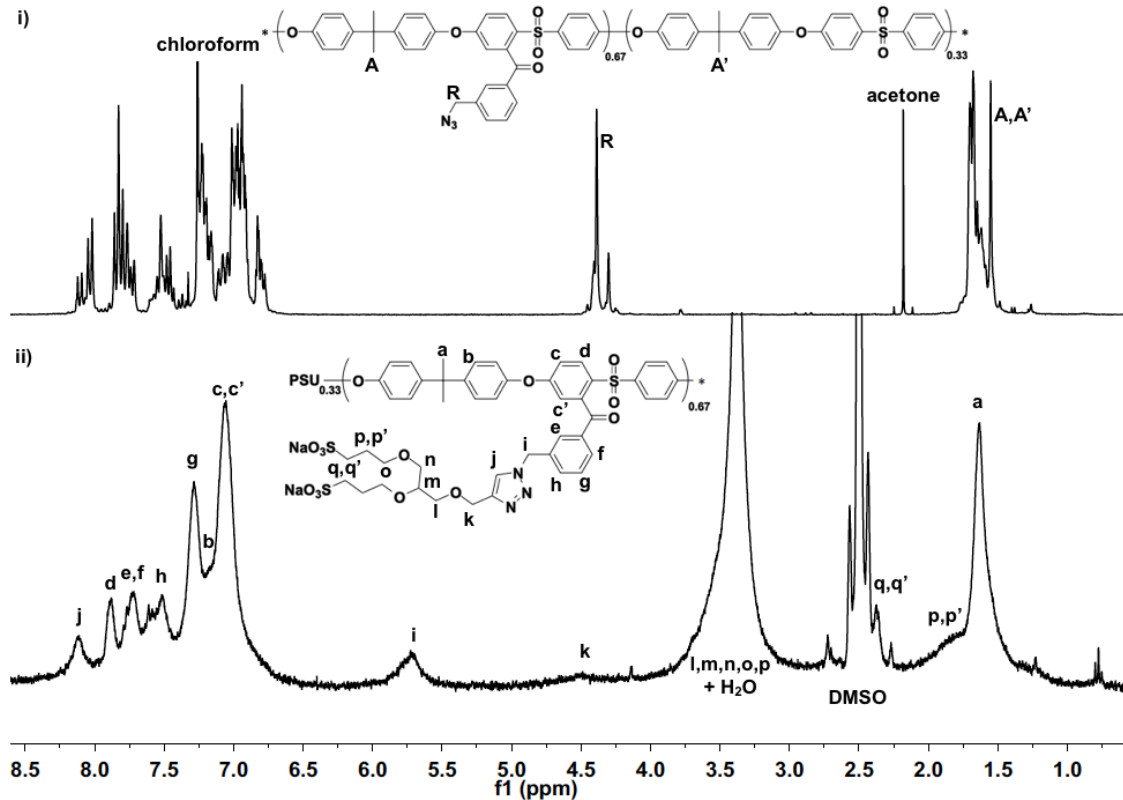
FIGURE 5.2: ^1H NMR spectra of i) **PSU-N**$_{0.67}$ (CDCl$_3$) and ii) **PSU-2f**$_{0.67}$ (in DMSO-d$_6$).

5.2 Membrane properties

Membranes were cast from DMSO on 4 x 1 cm glass substrates leveled on a hot plate at approximately 80 ^{o}C and subsequently dried in vacuum oven at 80 ^{o}C. The films were detached from the glass substrate by immersion in deionized (DI) water. The membranes, all in their sodium salt form, where protonated through stirring for 1 hour in 1M H$_2$SO$_4$, followed by stirring for 1 hour in DI water - both at 80 ^{o}C. Excess acid was washed out over several washes with DI water, and the membranes were stored in DI water until conductivity measurements were performed. The obtained wet film thicknesses ranged from 11 to 118 μm (the wet thickness of internal reference, Nafion$^{\circledR}$ 212 (N212), was 7 μm). Film casting in an inert nitrogen atmosphere was investigated in parallel, but with no resulting difference in membrane appearance.

In a PEMFC operated at elevated temperature the thermal properties of the PEM is pivotal. Hence the thermal stability of the dendronised structure is quantified by thermogravimetric analysis (TGA) as the temperature at which the sample has lost 10% of its initial weight, referred to as the degradation temperature at 10% ($T_{d\ 10\%}$). Due to the use of high boiling solvents in the preparation process 100% is defined as the weight at 150 ^{o}C. Glass transition temperatures (T_g)/exothermal responses (T_{exo}) are estimated by

differential scanning calorimetry (DSC). The values are stated in Table 5.1. The thermal degradation of **PSU-2f** occurs in two steps, the first one up to around 370 ^oC, which is attributed to the decomposition of the dendrons. Thereafter the membranes experience a weight loss that can be attributed to the backbone. The more dendrons there are, the larger is the ratio between these two losses. An important observation is that introduction of an aliphatic spacer between the -SO_3H groups and the aromatic backbone does not reduce the thermal ionomer stability to an extent where it is more prone to degradation than what the loss of -SO_3H of analogue fully aromatic membranes, which are known to degrade at approximately 250 ^oC [98,151]. DSC data suggest two almost identical exothermal responses for the different DS's around 86 ^oC and 190 ^oC. In addition, **PSU-2f**$_{0.18}$ exhibits one at 162 ^oC, a peak that could be hiding in the DSC curves of the higher IEC versions (see Table 5.1). The peak around 190 ^oC is believed to be related to the backbone as T_g of PSU is measured to be 189 ^oC. At first, this behavior is different from the trend of increasing T_g upon sulfonation that is usually reported [98,146]. However, examples of the opposite are known too, e.g. *i)* the sulfonation of polystyrene or polycarbonate [152], *ii)* if residual solvent plasticizes the membrane [146], or *iii)* when introducing aliphatic side chains [153] to an aromatic system. An endothermal response that is observed between the exothermal responses, which is indicative of annealing and potentially cross-linking effects - between the -SO_3H groups, as also described by Smitha et al. [152] and observed with N212, which is deployed as internal reference. The T_{exo} around 86 ^oC corresponds to a transition temperature of the dendritic side chains. This suggests that even though the ionomer does not degrade at an earlier point than its fully aromatic analogues, it loses its mechanical integrity earlier, an attribute of the aliphatic side chains. For LT-PEMFC applications this may not be a hindrance, but it will not be suited for medium to high temperature applications.

TABLE 5.1: *Membrane properties of PSU,* ***PSU-g-1fS****,* ***PSU-g-1fL****,* ***PSU-g-2f*** *and N212.*

Sample	T_{exo}/°C			$T_{d\ 10\%}$/°C	IEC$_{NMR}$/meq g^{-1}	σ/mS cm^{-1}	WU/$wt\%$
PSU		189		527	-	-	-
PSU-1fS$_{0.25}$		-		-	0.49	<1	7
PSU-1fS$_{0.54}$		-		-	0.91	<1	2
PSU-1fS$_{0.67}$		-		-	1.06	1	14
PSU-1fL$_{0.25}$		-		-	0.47	<1	5
PSU-1fL$_{0.54}$		-		-	0.86	2	11
PSU-1fL$_{0.67}$		-		-	1.00	2	28
PSU-2f$_{0.18}$	86	162	188	340	0.33	12	19
PSU-2f$_{0.54}$	86	191		307	0.74	24	25
PSU-2f$_{0.67}$	85	190		292	0.84	62	141
N212		120		352	0.91	92	19

Note: IEC$_{NMR}$ is calculated from the assumption that both the click reaction and DS are complete, based on ^{1}H NMR. For N212, IEC is from the product specifications, and $T_{exo} = T_g$ is a literature value for Nafion$^®$ NRE 212 [112]. Thermal data were not recorded for comb-type structures.

Water sorption is a key parameter in PEM evaluation, as it is associated with proton conductivity as well as mechanical stability. If a membrane does not take up enough water, there will be no interconnecting channels between ionic groups for the protons to use to cross the membrane. If water swelling becomes excessive, mechanical integrity will be lost and the PEM fail in the PEMFC. The water sorption and proton conductivity under fully

humidified conditions were investigated for both dendronised and linear PSU structures (see Figure 5.3). **PSU-1fS** and **PSU-1fL** exhibit water uptakes in the region of N212, 5 - 28 wt% vs. 19 wt% in the IEC span of 0.47 - 1.06 meq g^{-1} (determined from ^{1}H NMR) vs. 0.91 meq g^{-1} (product specification). **PSU-2f** from 0.33 meq g^{-1} to 0.74 meq g^{-1} takes up from 19 wt% to 25%, and at 0.84 meq g^{-1} it experiences a 141 wt% water uptake, i.e. several times higher than the linear side chain analogues. It turns out that the proton conductivites under immersed conditions of the comb-type relative to dendronised architectures are proportional to the water sorption. Thus, only negligible conductivities are obtained of the former: 0 - 2 mS cm^{-1}, whereas **PSU-2f** reaches 12, 24 and 62 mS cm^{-1} as the ionic content is increased. The jumps from the medium to high IEC ionomer in both water sorption and conductivity are pronounced in ways that indicate that percolation of the water system and improved conductivity is happening here. The low conductivity values of the comb-type structures reminisce resembling structures investigated by Norris et al. [111]. The most plausible explanation is believed to be the low IEC values, a similar behavior is observed for PAE sulfonated directly to the backbone in *ortho* position with resulting poor phase separation [27]. The higher water uptake and conductivities of the dendronised system are ascribed to the increased flexibility of the spacer between the sulfonic acid groups in combination with the increased local -SO$_3$H concentration. The comb-type structures serve as reference compounds for the dendronised structure, but the comb-type structures will likely see increased water uptake and conductivity along with it upon increased IEC, as is observed with other systems [3,4,154]. Decreasing T_g upon sulfonation has previously been reported for PS [152].
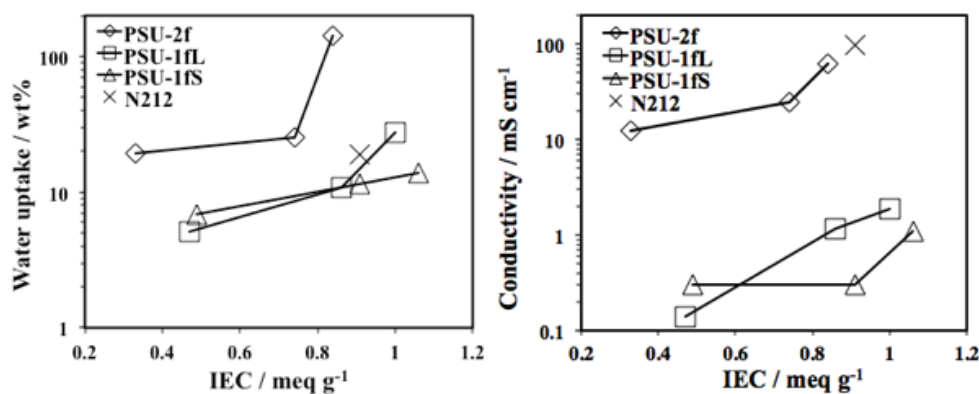
FIGURE 5.3: *Water uptake (left) and proton conductivity (right) versus IEC. Reproduced from Manuscript 1.*

6

Grafts

In this study **PSU-Cl** is applied as macroinitiator (MI) for creating a sulfonated graft copolymer system. Two pathways are approached: *i)* ATRP-grafting of sodium styrene sulfonate (SSS) directly from **PSU-Cl** (Scheme 6.1), *ii)* ATRP-grafting of styrene from **PSU-Cl** followed by post-sulfonation. In a third approach, alkyne functionalized PS is prepared with the intention to attach these onto **PSU-N** applying CuAAC. Within the frames of what was attempted, polymerization of SSS gave a too low degree of polymerization (DP), and the click reaction did not proceed as expected. From a proof of concept point of view, the ATRP-grafting appears to be the best suited for the present system. However, sulfonation was not restricted to the grafts, but took also place on the backbone. Therefore a new way of sulfonating the PS grafts selectively would be an improvement.

6.1 Sulfonated monomer

The ATRP-grafting of SSS was carried out in DMSO and DMF respectively, with no difference in the outcome. Conditions used for homopolymerization of SSS to become poly(sodium styrene sulfonate (PSSS) were used (details are provided in the suppoting information of *Manuscript 2*): from initiator ethyl-2-bromoisobutyrate (EBiB) with CuCl$_2$/L-ascorbic acid/bpy run at 60 ^{o}C. During the initially attempts from MI **PSU-Cl** no polymerization took place even after 48 hours, so the temperature was stepwise raised and the other reaction conditions altered until a run for 5 days at 100 ^{o}C gave something useful. The applied conditions are shown in Scheme 6.1.

In brief, the reaction conditions are left with room for improvement, maybe at further increased temperatures or by converting the monomer to an organic salt to improve solubility. However, from a **PSU-Cl** with 67% modification (other substitution degrees were used along the way, hence the unspecified location of the chloromethyl group in Scheme 6.1), an average of 1 - 2 repeat units per site was obtained, which would theoretically place the amphiphile in the sweet spot IEC - wise. Film casting at first resulted in brittle films that cracked upon drying, but after a few attempts with the same material, incorporating a
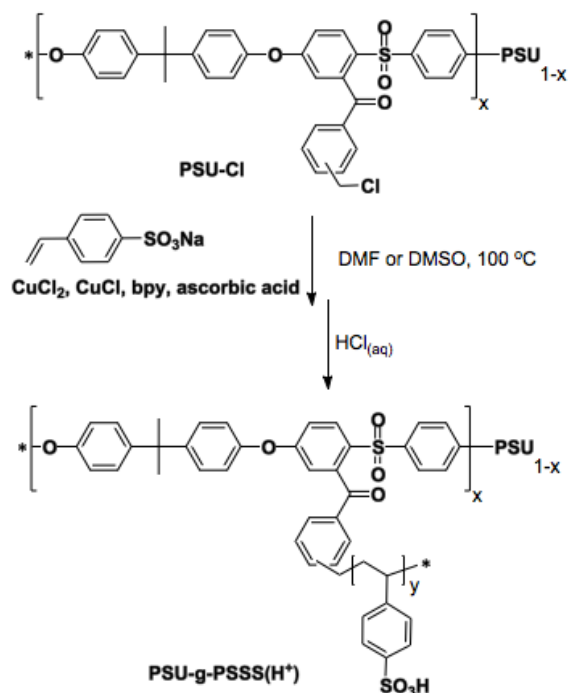
SCHEME 6.1: *SSS is grafted from **PSU-Cl** in protic solvent, and protonated upon film casting.*

filtration, somewhat stable films appeared. Film casting was attempted from DMSO, DMF and DMAc on a PTFE sheet at RT or a glass substrate at RT or at elevated temperatures. Decent films were formed when casting from DMSO on a glass substrate at around 80 ^oC. The membranes were converted to their acidic form upon immersion in 1M HCl. Back titration with NaOH of the film showed an IEC value of 2.5 meq g^{-1}. The water uptake was 29 wt% and conductivity 5 mS cm^{-1} under immersed conditions. The relatively high IEC value and low water uptake and low conductivity could be signs of a poor percolation of the membrane. Due to the many variables to optimize (e.g. reaction conditions, monomer form, casting conditions etc.) and the less promising membrane properties, the method was abandoned for an approach aiming at post-sulfonation.

6.2 Post-sulfonation

In the post-sulfonation approach, PS side chains were grown from **PSU-Cl** in a bulk reaction at 100 ^oC with CuBr/PMDETA catalyst/ligand system. The reaction was also performed with bpy as ligand, a reaction that proceeded considerably slower, an observation well in accordance with the activation rate constants of the two [121]. Three graft copolymers were synthesized: **g3-47** (DG = 3%, DP$_{PS}$ = 47), **g18-8** (DG = 18%, DP$_{PS}$ = 8) and **g18-10** (DG = 18%, DP$_{PS}$ = 10).

After characterization, the PSU-*g*-PS were dissolved in 1,2-dichloroethane (DCE) at 50

^{o}C while acetyl sulphate, was prepared in a separate flask cooled to 0 ^{o}C by mixing acetic anhydride and H_2SO_4 in DCE under N_2-purging. The sulfonation agent was immediately, yet slowly, transferred to the graft copolymer that changed from colourless to brown when left for an overnight reaction. Different DS were targeted by different reaction times, ranging from 2 hours to 2 days. two or three different DS were prepared from each graft copolymer, and the resulting products were named with a prefix S and suffix letter after the sulfonation reaction time, S = short, M = medium, L = long, e.g. **S*g*3-47-S**. To quench the reaction, IPA was added, then the solvents were evaporated by air stripping, then the products were stirred with DI water and subsequently dialyzed against DI water for several days, and then freeze dried. In addition to sulfonating the graft copolymers, in the evaluation of the selectivity of the reaction, **PSU-Cl** with DG of 18% underwent the same treatment (= **S-PSU-Cl-18**). All samples were examined with ^{1}H NMR, FTIR, TGA and DSC. Stacked ^{1}H NMR spectra of **S-PSU-Cl-18**, **PSU-Cl-18**, ***g*18-10** and **S*g*18-10-L** are shown in Figure 6.1, and the appearance of new peaks upon acetyl sulphate treatment were clear for both the MI [*i)* and *ii)*] and the graft copolymers [*iii)* and *iv)*]. The non-sulfonated compounds are dissolved in chloroform [*ii)* and *iii)*], whereas the sulfonated compounds [*i)* and *iv)*] are dissolved in DMSO. This may explain what appears to be a slight downfield shift, but in addition, new peaks appear. The phenomenon is most pronounced of the MI, since the peaks of the sulfonated PS are broad and not easily separated. A full attribution of the protons would require further investigations, but most likely, the part of the backbone being modified is on the *ortho* position to the SO_2 group of PSU. Based on the intensities of the peaks observed in Figure 6.1*i)* it can be concluded that sulfonation of the introduced benzoyl alone would not account for changed spectrum. TGA results could indicate that probably one third of the introduced -SO_3H groups are introduced to the backbone, and the remaining two thirds are attributed to the sulfonated PS grafts (SPS). However, the stated DS in *Manuscript 2* are based on the assumption that only grafts are sulfonated. A reason is that the two by far highest integrating peaks around 7.7-7.2 ppm and 6.8-6.0 ppm in the spectrum of **S*g*18-10-L** are in regions with no new peaks appearing in that of **S-PSU-Cl-18**.

TGA and DSC data of the graft copolymers are included in Table 6.1. It appears the $T_{d\ 10\%}$ depends on graft length rather than DS, as those of **S*g*3-47** lie from 350 to 368 ^{o}C while **S*g*18-8** exhibit $T_{d\ 10\%}$'s of 259 ^{o}C and the **S*g*18-10** have $T_{d\ 10\%}$'s of 309-358 ^{o}C. This would imply that the shorter the grafts, the lower the thermal stability. The hypothesis is that the -SO_3H groups form anhydrides in a cross-linking reaction upon heating, whereby the resulting cross-linked structure increases in thermal stability. This supports the observation that the longer chains of **S*g*18-10** cross-link to a higher extent than **S*g*18-8**. As for the T_g, two values are observed in some case, i.e. one at 85-109 ^{o}C and one between 150 ^{o}C and 210 ^{o}C. The lowest is in the range of pure PS [155], while the higher is closer to that of T_g of pure PSU: 189 ^{o}C. The differences in T_g that are attributed to PS may be due to differences in DS [152]. An observation made when performing DSC up to 250 ^{o}C compared to 220 ^{o}C is that the T_g recorded during the second heating cycle shows an increase. In case of **S*g*18-8-S** the increase is from 150 ^{o}C to 209 ^{o}C. The reason is believed to be the aforementioned anhydride formation, possibly combined with thermal annealing.
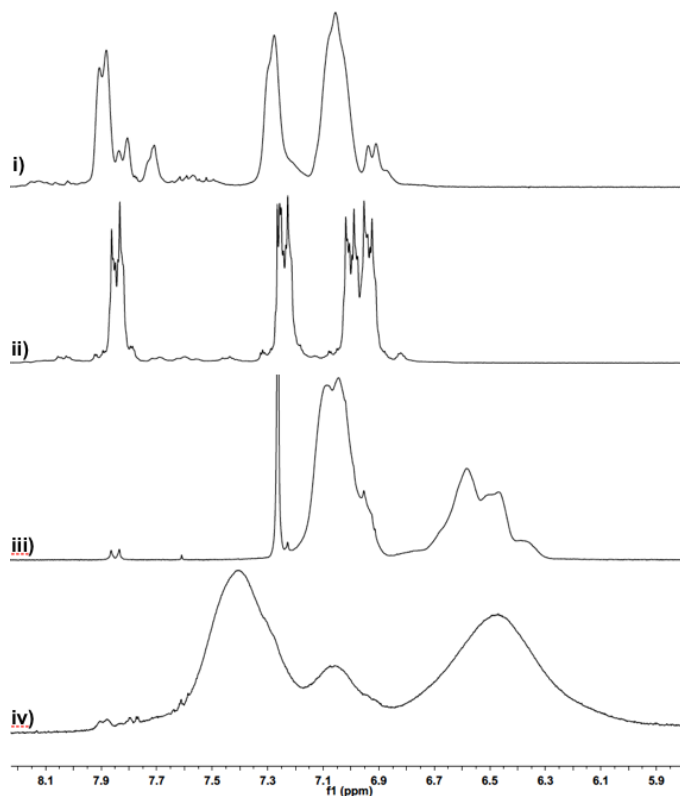
FIGURE 6.1: ^1H *NMR spectra of i)* **S-PSU-Cl-18**, *ii)* **PSU-Cl-18**, *iii)* **g18-10** *and iv)* **Sg18-10-L**.

TABLE 6.1: *Membrane properties of non-sulfonated and sulfonated samples.*

Sample	$T_{d\ 10\%}$ / $^{\circ}$C	T_g / $^{\circ}$C	
PSU	527	189	
PSU-Cl-3	524	183	
PSU-Cl-18	496	181	
g18-8	413	110	
g18-10	408	109	
Sg3-47-S	350	177	
Sg3-47-M	368	85	191
Sg3-47-L	350	99	201
Sg18-8-S	259	150	
Sg18-8-L	259	109	206
Sg18-10-S	358	188	
Sg18-10-M	309	152	
Sg18-10-L	309	210	
S-PSU-Cl-18	397	171	
PSSS	496	134	

Note: **g3-47** is not included due to material scarcity.

6.3 Applying click chemistry

Inspired by the efficient click reaction applied in obtaining the dendronised architectures and the work of Dimitrov et al. [112], a chemical route to PSU-*g*-PS harnessing the 1,2,3-triazole coupling is explored. Here, polymer chains with a terminal alkyne groups is selected for the click reaction with **PSU-N** synthesized as described in the previous chapter. The obtained degrees of substitution were 3%, 6% and 7%. In the first step, shown in Scheme 6.2, styrene (St) is grafted from trimethylsilyl protected propargyl bromide (TMSPrBr).
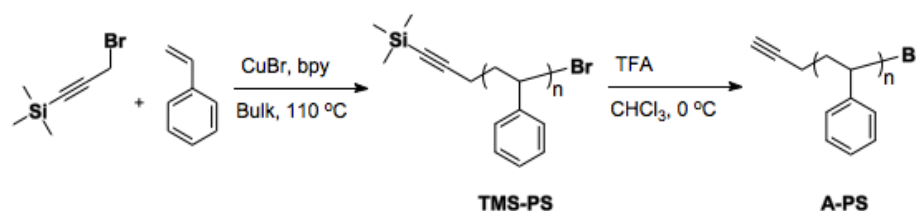
SCHEME 6.2: *Synthetic route to **A-PS** for click chemistry, prepared from the TMSPrBr initiator.*

St, CuBr and bpy in the ratio [200]:[1]:[2] were mixed in a Schlenk tube and degassed thrice by the freeze-pump-thaw process. 1 eq TMSPrBr was added and yet a degassing was performed before bulk polymerization by ATRP at 110 ºC to give **TMS-PS**. Propagation was followed by SEC (DMF), as shown in Figure 6.2, and verified by ^{1}H NMR and FTIR.
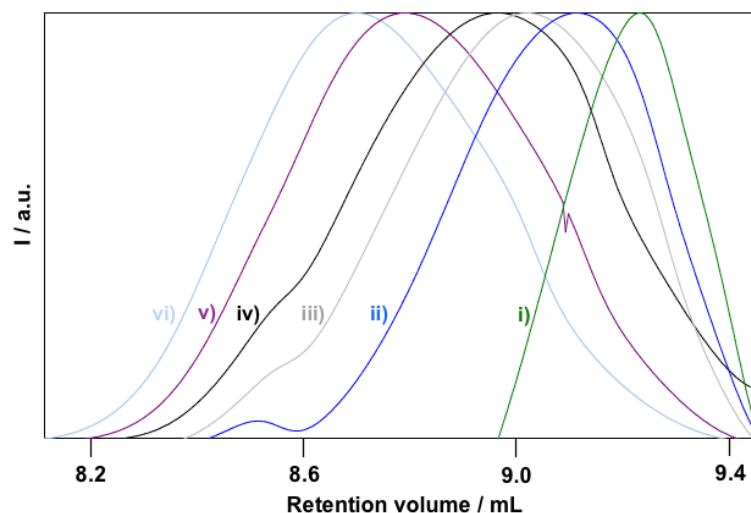
FIGURE 6.2: *Normalized SEC (DMF) trace of TMS-PS after i) 15 min., ii) 30 min., iii) 45 min., iv) 60 min., v) 90 min. and vi) 120 min.*

The polymerization was also investigated, employing PMDETA as ligand. Homopolymers of number average molecular weight 62 kDa and PDI of 1.35 (applying a PMMA standard calibration curve) were obtained with PMDETA. With bpy, five homopolymers were prepared, ranging from 2.5 kDa to 8 kDa. The alkyne was then deprotected by cleav-

ing the TMS off by a modified version of the procedure of Dimitrov et al. [112]: 0.15 mmol **TMS-PS** were dissolved in 10 mL CHCl$_3$ and under nitrogen and cooled to 0 ^{o}C when 37.3 mmol trifuoroacetic acid (TFA) was added and the reaction run overnight. Conversion was confirmed by ^{1}H NMR and FTIR. ^{1}H NMR spectra of the alkyne functionalized PS, **A-PS**, before and after deprotection are shown in Figure 6.3.
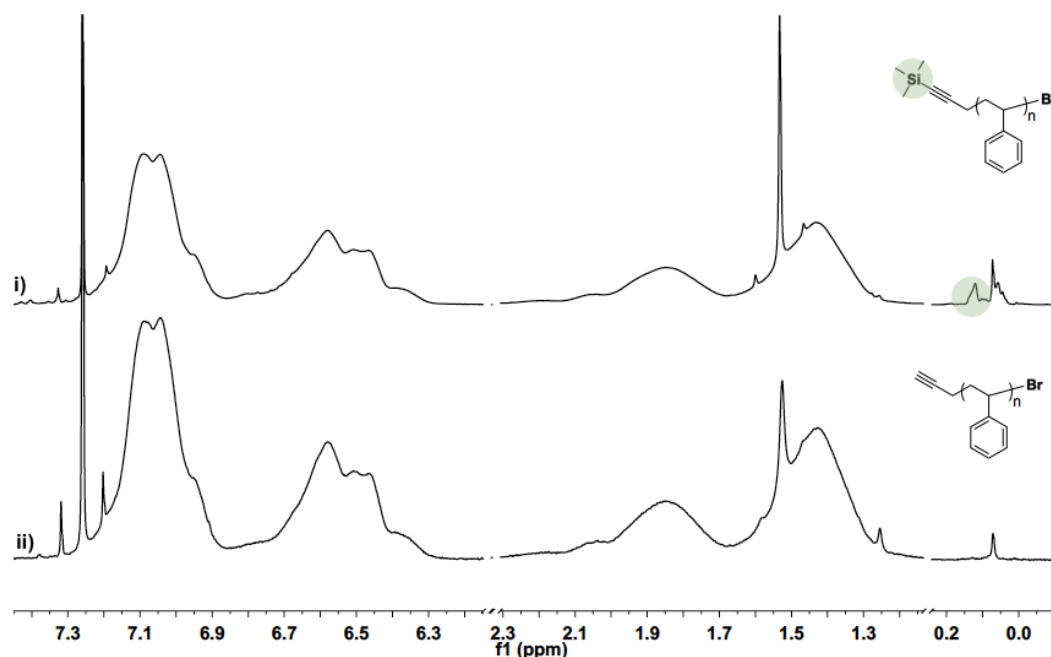
FIGURE 6.3: ^{1}*H NMR spectra of i)* ***TMSPr-PS*** *and ii)* ***A-PS***.

In the click reaction that followed, three different reaction conditions were applied, all to no avail, as shown in Scheme 6.3. In the first approach, *i)* 1 eq **A-PS** and 6 eqs CuBr were stirred in DMF at 60 ^{o}C overnight. Then, *ii)* **A-PS** was stirred overnight with 6 eqs CuBr and 6 eqs PMDETA in THF at 35 ^{o}C. In the last method deployed, *iii)* **A-PS** was stirred overnight in THF at 35 ^{o}C with 6 eqs CuI and 24 eqs triethylamine (TEA). In all cases precipitation from MeOH were performed.
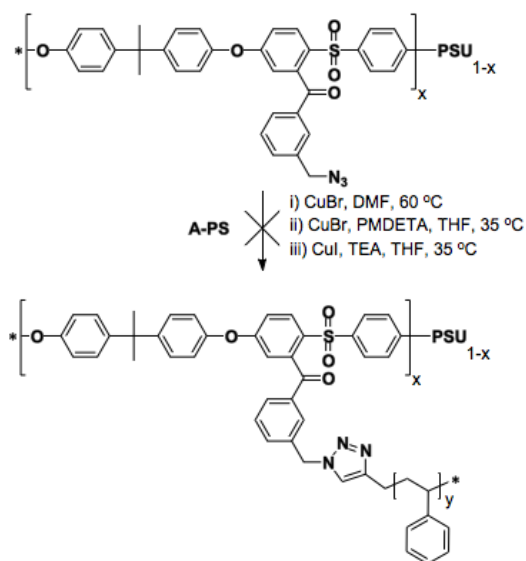
SCHEME 6.3: *Three different sets of reaction conditions were applied on two differently substituted* **PSU-N**.

7

Blends

The idea of generating a graft copolymer system with high ionic purity lies in continuation of previous work by Holdcroft and coworkers [3–5,122,154,156] where diblock morphologies are compared to graft copolymer morphologies at various DG, chain lengths and DS. Low DG graft copolymers have promising water sorption features, but non-sulfonated grafts in partially sulfonated poly(vinylidene fluoride-*co*-chlorotrifluoroethylene)-*g*-polystyrene (P(VDF-*co*-CTFE)-*g*-SPS) restrict the ionic domains. This would be circumvented by increasing the ionic purity by sulfonation to completion. As a result the IEC will become higher and instead of DS the IEC-handle can be the ionomer content in a blend system. Blend systems have previously been investigated with partially sulfonated ionomer and short PVDF homopolymer chains [5], and comparative studies of the effect of the blend component showed that water uptake was best controlled through the utilization of crystalline polymer of high molecular weight, where increasing entanglement is a key factor [6]. Hence, P(VDF-*co*-CTFE)-*g*-SPS with fully sulfonated grafts of various lengths are blended with high molecular weight PVDF homopolymer in this study.

7.1 Preparation

Partially sulfonated P(VDF-*co*-CTFE)-*g*-SPS from the comparative study of the influence of DS [154] was sulfonated to completion as shown in Scheme 7.1 by the same sulfonation applied on PSU-*g*-PS in previous chapter. The complete sulfonation of graft copolymers with an average of 39, 62 and 79 St repeat units per chain (referred to as $\mathbf{Graft}_{2.6-S}$, $\mathbf{Graft}_{2.6-M}$ and $\mathbf{Graft}_{2.6-L}$ after the molar percentage of 2.6% chlorotrifluoroethylene (CTFE) in the backbone, and the graft length: Short, Medium and Long) was confirmed with ^{1}H NMR.

Blends were prepared by dissolving ionomer and PVDF in dimethylacetamide (DMAc), whereupon the solution was concentrated to a viscosity high enough for 50 - 75 μm thick membranes to form. Casting was done on a leveled poly(tetrafluoroethylene) (PTFE) sheet, and the membranes were subsequently dried overnight at 80 ^{o}C. Blends containing 40 vol% ionomer and 60 vol% PVDF were prepared from each fully sulfonated graft copolymer.

SCHEME 7.1: *Synthetic pathway from partially to fully sulfonated P(VDF-co-CTFE)-g-SPS.*

These samples are referred to as **SB40-60**, **MB40-60** and **LB40-60**, named after graft length (S, M, L), that they are blends (B) and their ionomer-to-PVDF ratio (40-60). Likewise a series with 25 vol% ionomer was made, with the resulting samples being termed **SB25-75**, **MB25-75** and **LB25-75**. Membranes of the pure graft copolymers were prepared by a similar method too.

7.2 Membrane properties

The aim with the study is to evaluate the effect of the increased ionic purity of the channels in the PEM when blending fully sulfonated graft copolymers relative to when controlling IEC by the degree of sufonation. The two scenarios are illustrated in Figure 7.1.

FIGURE 7.1: *Cartoon image of the effect by regulating IEC by tuning DS (left) or by blending with PVDF homopolymer (right).*

Therefore, blends of fully sulfonated graft copolymers are evaluated against previous data recorded for the same system at partial sulfonation. Equally important is the evalu-

ation of the same blends against a fully sulfonated pure graft copolymer of equal IEC (and hence with lower DG and graft length). Transmission electron microscopy was employed in the evaluation of the microstructural effect of blending. In Figure 7.2 are shown TEM images of the pure graft copolymers (left column), the 40-60 blend series (middle column) and the 25-75 blend series (right column).
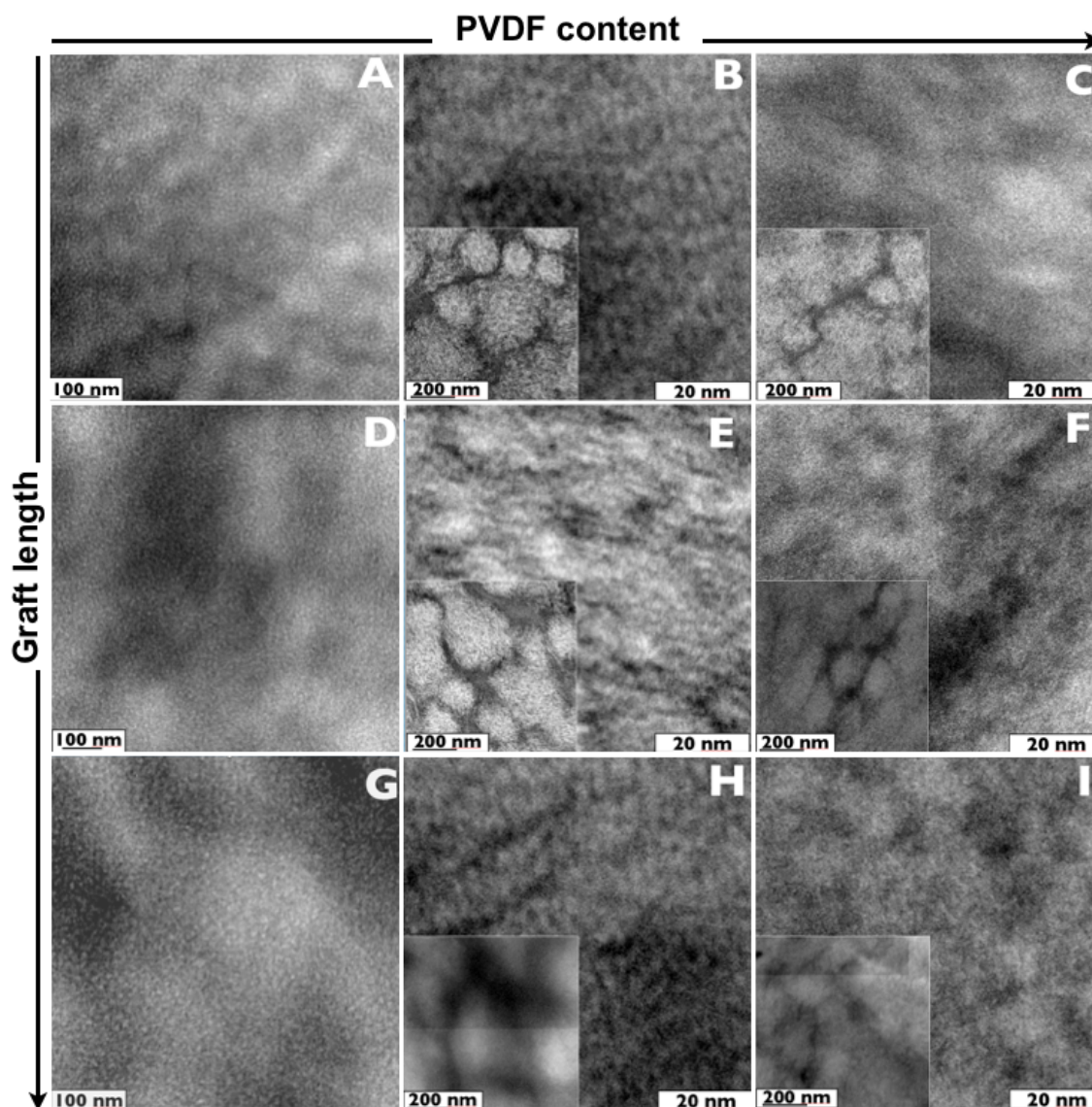
FIGURE 7.2: *TEM images of A)* **Graft**$_{2.6-S}$, *B)* **SB40-60**, *C)* **SB25-75**, *D)* **Graft**$_{2.6-M}$, *E)* **MB40-60**, *F)* **SB25-75** *G)* **Graft**$_{2.6-L}$, *H)* **LB40-60**, *I)* **SB25-75**.

Each row is made from the same pure graft copolymer, hence the upper row is based on **Graft**$_{2.6-S}$, the middle row is based on **Graft**$_{2.6-M}$ and the lower row is based on **Graft**$_{2.6-L}$. Dark areas represent stained ionic domains, and bright areas represent fluorous regions. The pure graft copolymers (images A, D and G) exhibit interconnected ionic

groups in a hydrophobic matrix. At low magnification of the 40-60 blend series (images B, E and H at scale bar 200 nm) a macro-phase-separation into mainly ionic and fluorous domains is clearly visible. The bright fluorous domains appear well distinguishable from the dark ionic domains. In the 25-75 blend series there is more PVDF, which is visible upon comparison at similar level of magnification (images C, F and I). At higher magnification (scale bar 20 nm) of the predominantly fluorous region of the 40-60 blend series, there appears to be a repetitive interconnected pattern of ionic domains. This is valid for all three membranes, and more pronounced than of the 25-75 blend series. A similar phenomenon is observed with bright areas appearing in the ion-rich areas. Especially the patterns of **SB40-60** (image B) and **LB40-60** (image H) resemble the ordered structures found with self-assembling structures [157]. Figure 7.3 illustrates how water fills the ionic domains of the membrane with the fluorous moieties providing mechanical stability.
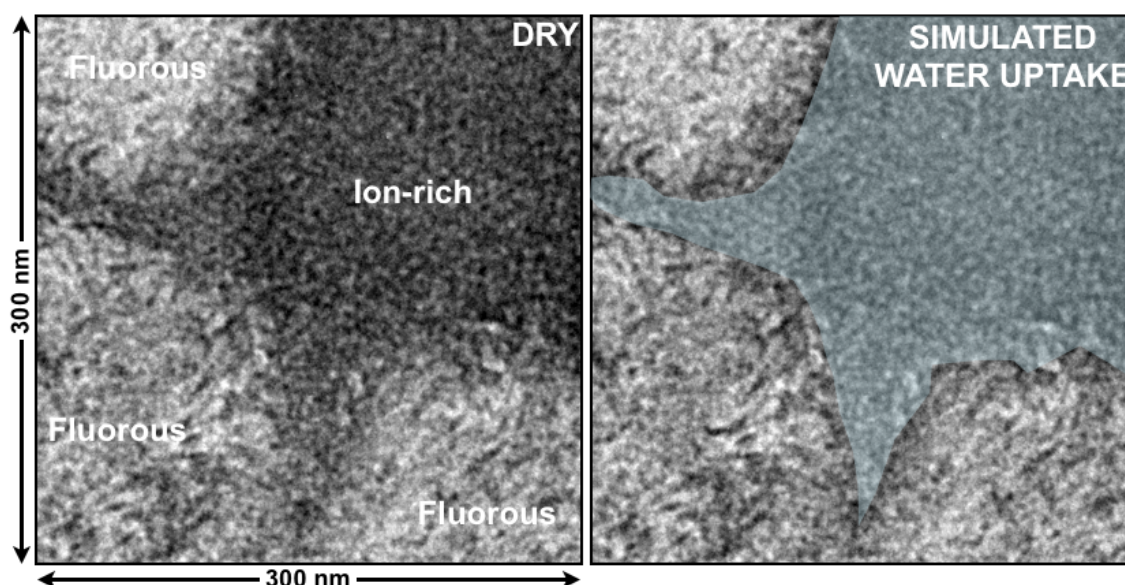
FIGURE 7.3: *TEM image of **SB40-60** in the borderland between the macro phases. Dark represents ionic domains and bright represents fluorous domains. To the right is a simulation of where water will mainly be located upon swelling.*

IEC was determined of all samples, and upon comparison with the theoretical values, the measured valued are overall 10 - 35% lower (see Table 7.1). This indicates that not all acidic groups are well connected. The theoretical IEC's of blend series 40-60 and blend series 25-75 are 1.72 meq g^{-1} and 0.85 meq g^{-1}, respectively, and the measured values are in the range of 1.15 - 1.31 meq g^{-1} and 0.60 - 0.75 meq g^{-1}, respectively. The measured IEC of **Graft**$_{1.1}$ is slightly lower than the 40-60 blend series: 1.10 meq g^{-1}.

Dynamic vapor sorption (DVS) was used in estimating the water uptake per -SO$_3$H group, i.e. the hydration number, λ, of the 40-60 blend series, **Graft**$_{1.1}$ and Nafion$^{®}$ 117 (N117) (See Figure 7.4). The 25:75 series exhibited poor conductivities at reduced relative humidity (RH) and were therefore not included here. Both blends and the pure **Graft**$_{1.1}$

TABLE 7.1: *Theoretical and measured IEC valued of the blends and* **Graft**$_{1.1}$.

Polymer	IEC$_{theoretical}$ / meq g^{-1}	IEC$_{measured}$ / meq g^{-1}
SB40-60	1.72	1.22 ± 0.18
SB25-75	0.85	0.60 ± 0.02
MB40-60	1.72	1.31 ± 0.10
MB25-75	0.85	0.75 ± 0.09
LB40-60	1.72	1.15 ± 0.09
LB25-75	0.85	0.64 ± 0.02
Graft$_{1.1}$	1.72	1.10 ± 0.07

exhibited λ inferior to N117 throughout the investigated RH range. At 45% RH λ = 1 - 3 for the 40:60 blends and **Graft**$_{1.1}$, while λ = 5 for N117. At 95% RH, the λ was 9 - 14 for the 40:60 blends and **Graft**$_{1.1}$ and 19 for N117. The blend series seem to follow the trend that longer grafts result in higher λ values. The pure graft obtains similar values
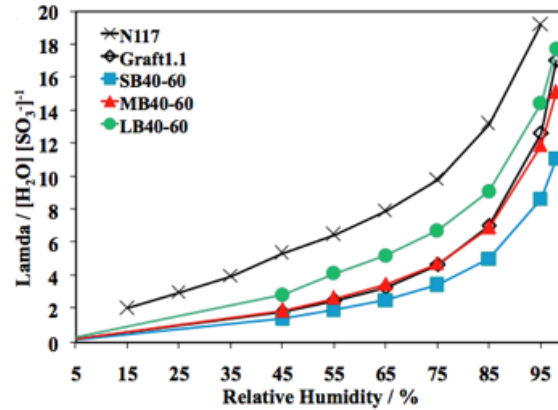
FIGURE 7.4: *Hydration number as function of RH.*

The influence of temperature and RH on the conductivity was evaluated by measuring the conductivity at three different temperatures and RH values: 25 ^{o}C, 50 ^{o}C and 80 ^{o}C, and 55% RH, 75% RH and 95% RH. **Graft**$_{1.1}$ and the 40-60 blend series show similar dependencies on both temperature and RH. At RH = 95% the slopes of the 40-60 series and **Graft**$_{1.1}$ are about half as big as that of N117: 0.42 - 0.57 vs. 1.04. The same trend is observed at 80 ^{o}C at different RH: The 40-60 series and **Graft**$_{1.1}$ slopes span 0.78 - 1.06, while that of N117 is 2.50. The temperature and RH dependence of blends and pure graft copolymers are thus considerably lower than that of N117. Despite this promising trend, the absolute conductivities of blends and graft copolymers are much lower than N117: $\sigma(80^{o}$C$)$ = 41 mS cm^{-1} of **Graft**$_{1.1}$ 45 mS cm^{-1} of **MB40-60** vs. 122 mS cm^{-1} of N117. Conductivity is plotted against temperature at RH = 95% and against RH at 80 ^{o}C in Figure 7.5.
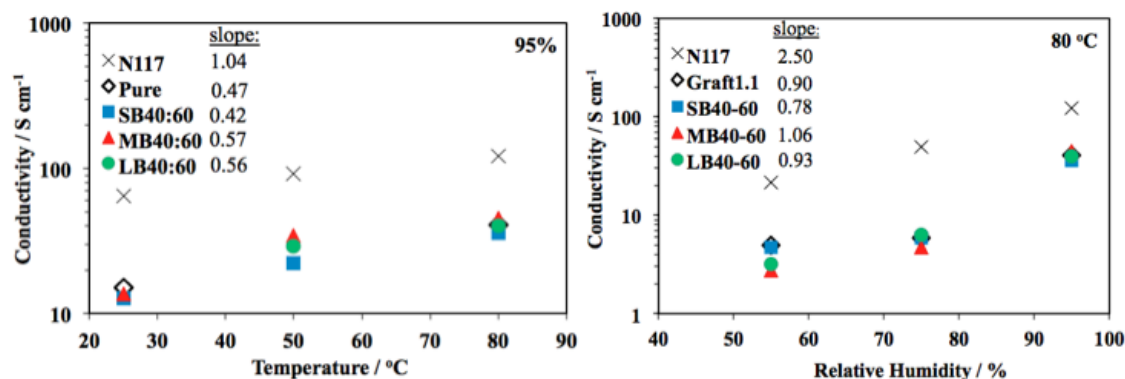
FIGURE 7.5: *Conductivity plotted against temperature at RH = 95% (left) and against RH at 80 °C (right) of 40-60 blend series, **Graft**$_{1.1}$ and N117.*

7.2.1 Partial sulfonation vs blending upon complete sulfonation

At similar IEC (approximately 1 meq g^{-1}) the blends take up three to four times as much water as the partially sulfonated grafts (66 - 98 wt% vs. 18 - 29 wt%). The blends are believed to allow for an improved water percolation due to the absence of structurally restricting non-sulfonated PS. The water uptake is still double or thrice that of N117, however. The proton conductivities of the blends are at least four times higher those of partially sulfonated grafts (62 - 63 mS cm^{-1} vs. 1 - 15 mS cm^{-1}), which correlates well with the increased water uptake. The analytical acid concentration, [-SO$_3$H], of blends and partially sulfonated grafts are fluctuating between the same order of magnitude and a factor of two difference (0.68 - 0.72M vs. 0.82M and 1.26M, respectively). This discrepancy can be explained to a certain extent by the spread in IEC of the partially sulfonated grafts, which leads to uneven water uptakes (18 - 29 wt%). [-SO$_3$H] of N117 is 0.97M, which is closer to the blends than what can be explained by the factor two to three difference in water uptake that causes acid dilution. The blends exhibit μ_{eff} values several times larger than the partially sulfonated grafts (0.89 $\cdot$ 10^3 - 0.95 $\cdot$ 10^3 cm^2 sV^{-1} vs. 0.01 $\cdot$ 10^3 - 0.14 $\cdot$ 10^3 cm^2 sV^{-1}), i.e. more than they differ in conductivity. This suggests a morphological gain by blending. The proton mobilities in the blends are greater than in N117, where it is 0.75 $\cdot$ 10^3 cm^2 sV^{-1}.

7.2.2 Full sulfonation vs blending

All numbers discussed in the following can also be found in Table 7.2. At equal IEC, the 40-60 blend series exhibit water uptakes two to three times smaller than **Graft**$_{1.1}$ (66 - 98 wt% vs. 192 wt%). At half IEC, the 25-75 blend series show water uptakes that are reduced proportionally to 25 - 40 wt%, i.e. the same range as N117 (33 wt%) - however, IEC's are also lower (0.60 - 0.75 meq g^{-1} vs. 0.89 meq g^{-1}). The 40-60 blend series show conductivities of 62 - 63 mS cm^{-1}, i.e. 35% higher than the pure graft copolymer **Graft**$_{1.1}$, displaying 46 mS cm^{-1}. The IEC's of the 25-75 series are about half that of **Graft**$_{1.1}$, but the conductivities are similar: 48 - 51 mS cm^{-1}. The same ratio applied relative to the 40-60 series, yet the conductivity is only approx. 30% higher of the blends with the highest

ionomer content. No blends reach the conductivity of N117, which is 70 mS cm^{-1}, but the 40-60 series get close.

TABLE 7.2: *Membrane properties of the blends and* **Graft**$_{1.1}$.

Polymer	WU / wt%	σ / mS cm^{-1}	[-SO$_3$H] / M	μ_{eff} / cm^2 sV^{-1}
SB40-60	66 $\pm$ 2	63 $\pm$ 3	0.71	0.92
SB25-75	32 $\pm$ 10	48 $\pm$ 6	0.97	0.51
MB40-60	98 $\pm$ 3	62 $\pm$ 1	0.68	0.95
MB25-75	40 $\pm$ 3	49 $\pm$ 5	0.90	0.57
LB40-60	91 $\pm$ 9	62 $\pm$ 4	0.72	0.89
LB25-75	25 $\pm$ 3	51 $\pm$ 6	0.90	0.59
Graft$_{1.1}$	192 $\pm$ 28	46 $\pm$ 3	0.77	0.63

As for [-SO$_3$H] the 40-60 blend series show concentrations approximately 40% higher than **Graft**$_{1.1}$, i.e. 0.68 - 0.72M vs. 0.49M. This gap will be partially explained by the considerably higher water uptake of the pure graft copolymer. The 25-75 series reach at least 25% higher concentrations: 0.90 - 0.97M. This is similar to N117, which reaches [-SO$_3$H] of 0.97M. As for μ_{eff}, blends and pure grafts display the same behavior: 0.89 $\cdot$ 10^3 cm^2 sV^{-1} - 0.95 $\cdot$ 10^3 cm^2 sV^{-1} versus 0.97 $\cdot$ 10^3 cm^2 sV^{-1}, and the effect of increasing the PVDF-content in the 25-75 series results in about half the μ_{eff}, i.e. 0.51 $\cdot$ 10^3 cm^2 sV^{-1} - 0.59 $\cdot$ 10^3 cm^2 sV^{-1}. IEC of N117 is between those of the blend series, and so is its μ_{eff} (0.75 $\cdot$ 10^3 cm^2 sV^{-1}) between the two.

8

Orphans

As the main objective with the work underlying this research project is the discovery and development of new macromolecular architectures, there was a lot of freedom from the very start. As a consequence, multiple synthetic paths were subjected to a screening process that ultimately resulted in the three manuscripts. However, some concepts, though promising, could not be pursued further than to the preliminary investigations level due to time constraints. In this section, some of these are presented, and are thus leading on to the future perspectives, which are given in the next section. For the sake of completion, it should briefly be mentioned that a preliminary attempt made with phoshonated monomer for the ATRP-grafting from the PSU MI proceeded successfully with diethyl vinylphosphonate, but was never investigated further. The intention was to create a phosphonated non-fluorous graft copolymer system with potential for high IEC values at fairly short graft length.

8.1   Blend - SnO$_2$ composite membrane

During the work with P(VDF-*co*-CTFE)-*g*-SPS/PVDF blend membranes it turned out that the series with low ionomer content (25 vol%) showed promising water sorption properties. Hence a series with 60 wt% ionomer content thereof was briefly examined. The water uptakes of these membranes were negligible, indicative of a too low ionomer content. Studies of inorganic particles embedded in PEM have shown that these can have an enhancing effect on water uptake and proton conductivity [158], so this strategy was picked up, but applied on the blend systems containing 40 vol% and 25 vol% ionomer. Preparation of composite membranes was performed as applied by Nørgaard et al. on Nafion$^{\circledR}$ membranes [159], except the H$_2$O$_2$ washing step is avoided as oxidation may follow. Due to a scarcity of graft copolymer material the characterization steps had to be planned carefully, saving the destructive thermal property determinations (TGA and DSC) for last. Water sorption and conductivity measurements were obtained, and looked promising at first, but the limited sample material and improvised nature of the setups caused the error bars to be too large to truly rely on the data. Next move was to evaluate the influence on the mechanical properties of the blend membranes from before the introduction of SnO$_2$ particles to after. This

was done in a microindentation setup like the one shown in Figure 8.1, where the film was subjected to a range of different forces to which the stress was measured, and following the elasticities were calculated. The idea was conceived too late for unambiguous data to be presented. Setup is currently scheduled for further development.
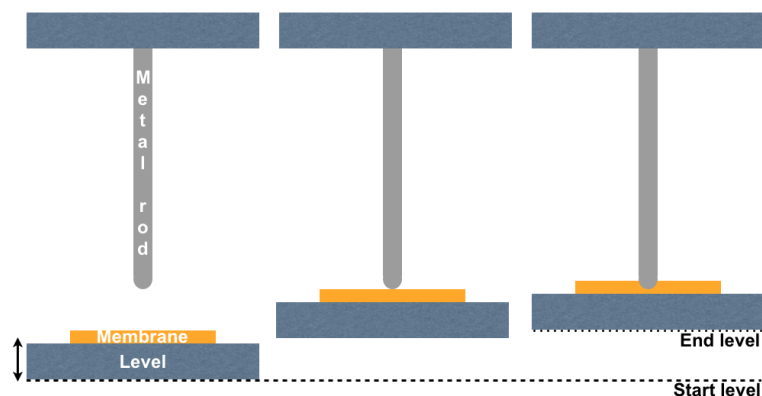
FIGURE 8.1: *Illustration of the microindentation principle.*

8.2 Surface-initiated ATRP (SI-ATRP) from PVDF

Surface-initiated ATRP (SI-ATRP) has proven to be a useful tool in modifying polymer surfaces [160]. A vital aspect in PEM design is the phase separation of ionic and hydrophobic domains. The idea was thus to use preformed hydrophobic matrix and then graft sulfonated chains onto the surface. Despite reports on low initiating efficiency of PVDF [161], a porous PVDF membrane was chosen as the substrate, and sodium styrene sulfonate (SSS) was chosen as IEC-contributing monomer. SSS is known to be polymerizable in MeOH/water mixture, in which PVDF is insoluble [162]. Different reaction conditions were carried out, including the same reaction run in ultrapure water and a 1:1 mixture of ultrapure water and methanol (MeOH), of which the latter proved successful. The reaction was carried out as follows. In a 10 mL Schlenk is placed 1.353 g SSS, 9.3 mg copper(I)chloride, 32.9 mg bpy and 8.1 mL H_2O/MeOH. The mixture is purged with N_2 for 30 minutes, a PVDF film (Millipore, 0.2 μm, hydrophobic) of 18.8 mg is added, a freeze-pump-thaw degassing cycle is performed and the reaction commenced at 90 ^{o}C. At this point the colour was brown. After 48 hours and 30 minutes the reaction is quenched in dry ice/IPA, the film is washed with 1:1 ultrapure H_2O/MeOH and washed overnight. After two days of washing in fresh H_2O/MeOH the membrane is dried in vacuum oven at 50 ^{o}C overnight.

Characterization was performed with FTIR, ^{1}H NMR and TGA. Figure 8.2 shows the TGA curves of the pristine PVDF membrane and the surface graft film respectively. There appears to be a 9 wt% gain which can be attributed to PSSS grafts. The system proved feasible but was abandoned for time reasons. Later, the strategy was pursued by our group, where high in-plane conductivities were recorded [163]. Energy-dispersive X-ray spectroscopy (EDX) showed sulfur abundances throughout the cross section, however, electron

microscopy would be useful in the determination of the -SO$_3$H distribution inside the pores relative to the outer surface of the membrane.
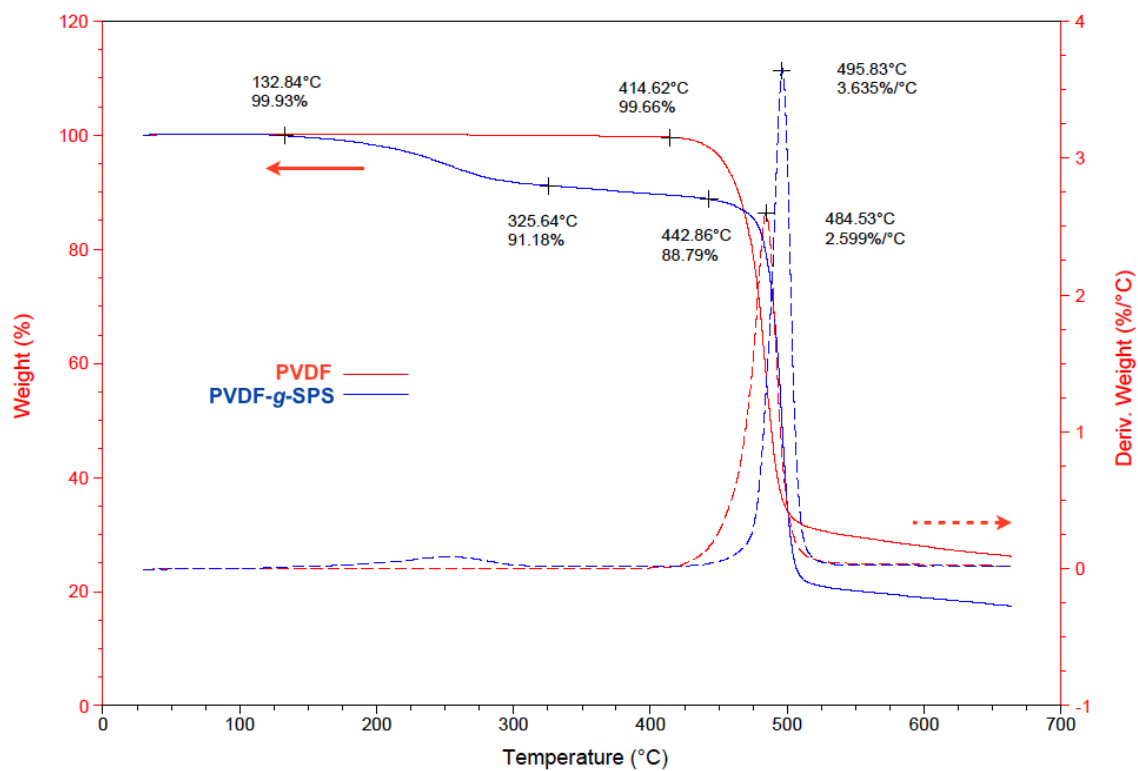
FIGURE 8.2: *TGA curves of pristine porous PVDF membrane and PVDF-g-PSSS.*

9

Summary & Outlook

The environment in a fuel cell is harsh, with fluctuating temperature, elevated pressure and changing humidification levels. Water management, proton conductivity, thermal stability and mechanical integrity determine the membrane's potential, so understanding and being able to tune the macromolecular structure accordingly is paramount. In the molecular design process the interplay between proton conducting groups and stability providing segments are pivotal for percolated water systems to form. Hence, the quest for deeper knowledge on structure-property relationships is a main driver in the evolution of proton conducting membranes for the future.

By applying three distinctly different strategies without changing all parameters in the process, the present dissertation addresses the need for re-thinking the macromolecular architectonic PEM-landscape. All along the way, the intention has been to focus on efficient and versatile synthetic routes, keeping a door open for the range of alternative applications that ion exchange membranes have.

In the first approach, a commercial PSU is modified to become a potential ATRP-macroinitiator that is easily turned into a click reagent. Dendronised and short linear aliphatic side chains are synthesized and clicked onto the PSU backbone at various degrees of substitution. The dendronised structure has a higher local concentration of sulfonic acid groups, and shows higher water uptake and conductivity than equivalent-IEC linear side chains. A gap is observed from when almost no water sorption occurs to when a well percolated water system forms. The finding suggests that the needed amount of protogenic groups can be reduced by increasing the local ionic concentration. Preliminary steps towards a second generation dendronised system have been taken, thus a synthetical route is developed.

In the second approach, the ATRP-macroinitiator is used to graft PS side chains at various DG. The system is subsequently partially sulfonated. The applied sulfonation procedure is not selective for the grafts, as the backbone is substituted with sulfonic acid too. Consequently, most graft copolymers loose mechanical integrity upon immersion into water. With handles in DG, graft length - or the use of different (pre-functionalized) monomers as

preliminary studies showed - the system possesses valuable possibilities in the creation of hydrocarbon graft copolymer architectures.

In the third approach, the PS grafts on a partially fluorinated copolymer are sulfonated to completion, leaving the backbone non-sulfonated. Thereby a higher purity of the ionic channels is obtained. Using different graft lengths, a span of IEC is obtained, all of which swell tremendously when submerged in water. To counteract this, the ionomers are blended with high molecular weight PVDF, which increases the entanglement and crystallinity, and because of its chemical nature is embedded in primarily the hydrophobic backbone. Different PVDF contents are investigated, and it turns out the phase separation takes place on two levels, a micro scale level phase separation into ion-rich domains with smaller PVDF content and primarily fluorous domains with smaller ionic abundances. Notable observations include the little, if any, effect of the graft length in the blend systems, the increase in analytical acid concentration of blends with high PVDF content, and the reduced dependence on relative humidity relative to Nafion$^{\circledR}$.

Parameters that can be changed and characterizations that can be performed are numerous, and of course far from all have been investigated here. A new macromolecular family, based on the commercial PSU has seen the light of day, and the architectures that can be constructed by ATRP and click chemistry are many. Higher generation dendronised side chains, higher molecular weight backbone or investigating a different segment than bisphenol A, fine tuning the degree of substitution/grafting, the choice of monomers, post- or pre-functionalization - there are too many to mention them all. Probably most useful would have been a more thorough investigation of the PSU-based architectures, by SAXS (briefly approached but not mentioned in this dissertation), electron microscopy, and fuel cell related characterizations like conductivity at low humidity and dynamic vapor sorption. As a means to highly sulfonated, short side chains to provide reasonably high IEC values, ATRP grafting of vinylsulfonic acid could also be interesting. Due to its highly hydrophilic nature, it would probably have to be converted to an organic salt prior to the grafting. Strategies only briefly mentioned in the previous chapter that were only touched upon briefly suggest other directions the research presented here could have been taken. They all appear promising, and would be interesting to investigate further in future projects.

Bibliography

[1] M. Schuster, T. Rager, A. Noda, K. D. Kreuer, and J. Maier. About the Choice of the Protogenic Group in PEM Separator Materials for Intermediate Temperature, Low Humidity Operation: A Critical Comparison of Sulfonic Acid, Phosphonic Acid and Imidazole Functionalized Model Compounds. *Fuel Cells*, 5(3):355–365, 2005.

[2] L. E. Karlsson and P. Jannasch. Polysulfone Ionomers for Proton-Conducting Fuel Cell Membranes: Sulfoalkylated Polysulfones. *J. Membr. Sci.*, 230(1-2):61–70, 2004.

[3] E. M. W. Tsang, Z. Zhang, Z. Shi, T. Soboleva, and S. Holdcroft. Considerations of Macromolecular Structure in the Design of Proton Conducting Polymer Membranes: Graft Versus Diblock Polyelectrolytes. *J. Am. Chem. Soc.*, 129(49):15106–15107, 2007.

[4] E. M. W. Tsang, Z. Zhang, A. C. C. Yang, Z. Shi, T. J. Peckham, R. Narimani, B. J. Frisken, and S. Holdcroft. Nanostructure, Morphology, and Properties of Fluorous Copolymers Bearing Ionic Grafts. *Macromolecules*, 42(24):9467–9480, 2009.

[5] T. Weissbach, E. M. W. Tsang, A. Yang, R. Narimani, B. Frisken, and S. Holdcroft. Structural Effects of the Nano-Scale Morphology and Conductivity of Ionomer Blends. *J. Mater. Chem.*, 22:24348–24355, 2012.

[6] R. Narimani. Morphological Studies of Ionic Random Graft Copolymers Based on Scattering Techniques. *Ph.D. Dissertation, Simon Fraser University*, 2012.

[7] D. J. Capeci. Course HST 122: History of U.S. Since 1877, Department of History Missouri State University (iTunesU), 2009.

[8] Various authors. The Fuel Cell Today Industry Review 2011. Technical report, 2011.

[9] M. Winter and R. J. Brodd. What Are Batteries, Fuel Cells, and Supercapacitors? *Chem. Rev.*, 104(10):4245–4269, 2004.

[10] D. Carter, M. Ryan, and J. Wing. The Fuel Cell Industry Review 2012. Technical Report 4, Fuel Cell Today, 2012.

[11] http://www.horizonfuelcell.com/. February 27, 2013.

[12] J. D. Holladay, J. Hu, D. L. King, and Y. Wang. An Overview of Hydrogen Production Technologies. *Catal. Today*, 139(4):244–260, 2009.

[13] M. Balat. Potential Importance of Hydrogen as a Future Solution to Environmental and Transportation Problems. *Int. J. Hydrogen Energy*, 33(15):4013–4029, 2008.

[14] H. H. Larsen and L. S. Petersen, editors. *DTU International Energy Report 2012 - Energy Efficiency Improvements*. DTU National Laboratory for Sustainable Energy, 2012.

[15] E. Spiegel, N. McArthur, and R. Norton. *Energy Shift - Game-Changing Options for Fueling the Future*. strategy+business, McGraw Hill, 2009.

[16] http://www.netinform.net/H2/H2Stations/. February 27, 2013.

[17] S. Takamuku. Durable Polysulfones with Densely Sulfonated Segments for Highly Proton Conducting Membranes. *Ph.D. Dissertation, Lund University*, 2012.

[18] T. Xu. Ion Exchange Membranes: State of Their Development and Perspective. *J. Membr. Sci.*, 263(1-2):1–29, 2005.

[19] R. S. L. Yee, R. A. Rozendal, K. Zhang, and B. P. Ladewig. Cost Effective Cation Exchange Membranes: A Review. *Chem. Eng. Res. Des.*, 90(7):950–959, 2012.

[20] K.-D. Kreuer. On the Development of Proton Conducting Materials for Technological Applications. *Solid State Ionics*, 97:1–15, 1997.

[21] C. H. Park, C. H. Lee, M. D. Guiver, and Y. M. Lee. Sulfonated Hydrocarbon Membranes for Medium-Temperature and Low-Humidity Proton Exchange Membrane Fuel Cells (PEMFCs). *Prog. Polym. Sci.*, 36(11):1443–1498, 2011.

[22] S. Bose, T. Kuila, T. X. H. Nguyen, N. H. Kim, K.-T. Lau, and J. H. Lee. Polymer Membranes for Hgh Temperature Proton Exchange Membrane Fuel Cell: Recent Advances and Challenges. *Prog. Polym. Sci.*, 36(6):813–843, 2011.

[23] K.-D. Kreuer, S. J. Paddison, E. Spohr, and M. Schuster. Transport in Proton Conductors for Fuel-Cell Applications: Simulations, Elementary Reactions, and Phenomenology. *Chem. Rev.*, 104(10):4637–4678, 2004.

[24] M. Laporta, M. Pegoraro, and L. Zanderighi. Perfluorosulfonated Membrane (Nafion): FT-IR Study of the State of Water with Increasing Humidity. *Phys. Chem. Chem. Phys.*, 1:4619–4628, 1999.

[25] P. J. James, J. A. Elliott, T. J. McMaster, J. M. Newton, A. M. S. Elliott, S. Hanna, and M. J. Miles. Hydration of Nafion Studied by AFM and X-Ray Scattering. *J. Mater. Sci.*, 5:5111–5119, 2000.

[26] K. A. Mauritz and R. B. Moore. State of Understanding of Nafion. *Chem. Rev.*, 104(10):4535–4585, 2004.

[27] W. Y. Hsu and T. D. Gierke. Ion Transport and Clustering in Nafion Perfluorinated Membranes. *J. Membr. Sci.*, 13:307–326, 1983.

[28] M. Eikerling, A. A. Kornyshev, and U. Stimming. Electrophysical Properties of Polymer Electrolyte Membranes: A Random Network Model. *J. Phys. Chem. B*, 101(97):10807–10820, 1997.

[29] L. Rubatat, G. Gebel, and O. Diat. Fibrillar Structure of Nafion: Matching Fourier and Real Space Studies of Corresponding Films and Solutions. *Macromolecules*, 37(20):7772–7783, 2004.

[30] K. Schmidt-Rohr and Q. Chen. Parallel Cylindrical Water Nanochannels in Nafion Fuel-Cell Membranes. *Nat. Mater.*, 7(1):75–83, 2008.

[31] K.-D. Kreuer. On the Development of Proton Conducting Polymer Membranes for Hydrogen and Methanol Fuel Cells. *J. Membr. Sci.*, 185(1):29–39, 2001.

[32] C. Gavach, G. Pemboutoglou, M. Nedyalkov, and G. Pourcelly. AC Impedance Investigation of the Kinetics of Ion Transport in Nafion Perfluorosulfonic Membranes. *J. Membr. Sci.*, 45:37–53, 1989.

[33] B. F. Habenicht, S. J. Paddison, and M. E. Tuckerman. The Effects of the Hydrophobic Environment on Proton Mobility in Perfluorosulfonic Acid Systems: An Ab Initio Molecular Dynamics Study. *J. Mater. Chem.*, 20:6342–6351, 2010.

[34] S. J. Paddison. Proton Conduction Mechanisms At Low Degrees of Hydration in Sulfonic Acid-Based Polymer Electrolyte Membranes. *Annu. Rev. Mater. Res.*, 33(1):289–319, 2003.

[35] M. A Hickner. Water-Mediated Transport in Ion-Containing Polymers. *J. Polym. Sci. Part B: Polym. Phys.*, 50(1):9–20, 2012.

[36] T. J. Peckham, J. Schmeisser, M. Rodgers, and S. Holdcroft. Main-Chain, Statistically Sulfonated Proton Exchange Membranes: The Relationships of Acid Concentration and Proton Mobility to Water Content and Their Effect Upon Proton Conductivity. *J. Mater. Chem.*, 17(30):3255–3268, 2007.

[37] B. Smitha, S. Sridhar, and A. A. Khan. Solid Polymer Electrolyte Membranes for Fuel Cell Applications - A Review. *J. Membr. Sci.*, 259(1-2):10–26, 2005.

[38] X. Kong and K. Schmidt-Rohr. Water-Polymer Interfacial Area in Nafion: Comparison with Structural Models. *Polymer*, 52(9):1971–1974, 2011.

[39] L. Vilciauskas, M. E. Tuckerman, G. Bester, S. J. Paddison, and K.-D. Kreuer. The Mechanism of Proton Conduction in Phosphoric Acid. *Nat. Chem.*, 4, 2012.

[40] N. P. Balsara and K. M. Beers. Proton Conduction in Materials Comprising Conducting Domains with Widths Less than 6 nm. *Eur. Polym. J.*, 47(4):647–650, 2011.

[41] T. Soboleva, Z. Xie, Z. Shi, E. M. W. Tsang, T. Navessin, and S. Holdcroft. Investigation of the Through-Plane Impedance Technique for Evaluation of Anisotropy of Proton Conducting Polymer Membranes. *J. Electroanal. Chem.*, 622(2):145–152, 2008.

[42] P. Thounthong, V. Chunkag, P. Sethakul, S. Sikkabut, S. Pierfederici, and B. Davat. Energy Management of Fuel Cell/Solar Cell/Supercapacitor Hybrid Power Source. *J. Pow. Sour.*, 196(1):313–324, 2011.

[43] L. Gubler and G. G. Scherer. Trends for Fuel Cell Membrane Development. *Desalination*, 250(3):1034–1037, 2010.

[44] Q. Li, R. He, J. O. Jensen, and N. J. Bjerrum. Approaches and Recent Development of Polymer Electrolyte Membranes for Fuel Cells Operating Above 100 Degrees C. *Chem. Mater.*, 15(26):4896–4915, 2003.

[45] M. F. H. Schuster and W. H. Meyer. Anhydrous Proton-Conducting Polymers. *Annu. Rev. Mater. Res.*, 33(1):233–261, 2003.

[46] C. Yang, P. Costamagna, S. Srinivasan, J. Benziger, and A. B. Bocarsly. Approaches and Technical Challenges to High Temperature Operation of Proton Exchange Membrane Fuel Cells. *J. Pow. Sour.*, 103:1–9, 2001.

[47] Q. Li, J. O. Jensen, R. F. Savinell, and N. J. Bjerrum. High Temperature Proton Exchange Membranes Based on Polybenzimidazoles for Fuel Cells. *Prog. Polym. Sci.*, 34(5):449–477, 2009.

[48] J. Mader, L. Xiao, T. J. Schmidt, and B. C. Benicewicz. Polybenzimidazole/Acid Complexes as High-Temperature Membranes. *Adv. Polym. Sci.*, 216:63–124, 2008.

[49] O. D. Thomas, T. J. Peckham, U. Thanganathan, Y. Yang, and S. Holdcroft. Sulfonated Polybenzimidazoles: Proton Conduction and Acid-Base Crosslinking. *J. Polym. Sci. Part A: Polym. Chem.*, 48(16):3640–3650, 2010.

[50] O. Savadogo. Emerging Membranes for Electrochemical Systems Part II. High Temperature Composite Membranes for Polymer Electrolyte Fuel Cell (PEFC) Applications. *J. Pow. Sour.*, 127(1-2):135–161, 2004.

[51] M. Sankir, Y. S. Kim, B. S. Pivovar, and J. E. McGrath. Proton Exchange Membrane for DMFC and H_2/Air Fuel Cells: Synthesis and Characterization of Partially Fluorinated Disulfonated Poly(arylene ether benzonitrile) Copolymers. *J. Membr. Sci.*, 299(1-2):8–18, 2007.

[52] P. Atkins and J. de Paula. *Atkins' Physical Chemistry*. Oxford University Press, New York, 7th edition, 2002.

[53] J. A. Horsfall and K. V. Lovell. Synthesis and Characterisation of Sulfonic Acid-Containing Ion Exchange Membranes Based on Hydrocarbon and Fluorocarbon Polymers. *Eur. Polym. J.*, 38(8):1671–1682, 2002.

[54] N. Garland and J. Kopasz. DOE View of Advanced Materials for Fuel Cells. Advances in Materials for Proton Exchange Membrane Fuel Cell Systems, Asilomar, CA, 2011.

[55] H. A. Gasteiger, S. S. Kocha, B. Sompalli, and F. T. Wagner. Activity Benchmarks and Requirements for Pt, Pt-Alloy, and Non-Pt Oxygen Reduction Catalysts for PEMFCs. *Appl. Catal., B*, 56(1-2):9–35, 2005.

[56] Z. Chen, D. Higgins, A. Yu, L. Zhang, and J. Zhang. A review on Non-Precious Metal Electrocatalysts for PEM Fuel Cells. *Energy Environ. Sci.*, 4(9):3167–3192, 2011.

[57] K. E. Martin, J. P. Kopasz, and K. W. McMurphy. Status of Fuel Cells and the Challenges Facing Fuel Cell Technology Today. In A. M. Herring, T. A. Zawodzinski Jr., and S. J. Hamrock, editors, *Fuel Cell Chemistry and Operation*, volume 1040, chapter 1. ACS Symp. Ser., Washington, DC, 2012.

[58] J. S. Spendelow and D. C. Papageorgopoulos. Progress in PEMFC MEA Component R&D at the DOE Fuel Cell Technologies Program. *Fuel Cells*, 11(6):775–786, 2011.

[59] Y. Wang, K. S. Chen, J. Mishler, S. C. Cho, and X. C. Adroher. A Review of Polymer Electrolyte Membrane Fuel Cells: Technology, Applications, and Needs on Fundamental Research. *Appl. Energy*, 88(4):981–1007, 2011.

[60] T. T. H. Cheng, E. Rogers, A. P. Young, S. Ye, V. Colbow, and S. Wessel. Effects of Crossover Hydrogen on Platinum Dissolution and Agglomeration. *J. Pow. Sour.*, 196(19):7985–7988, 2011.

[61] R. Borup, J. Meyers, B. Pivovar, Y. S. Kim, R. Mukundan, N. Garland, D. Myers, M. Wilson, F. Garzon, D. Wood, P. Zelenay, K. More, K. Stroh, T. Zawodzinski, J. Boncella, J. E. McGrath, M. Inaba, K. Miyatake, M. Hori, K. Ota, Z. Ogumi, S. Miyata, A. Nishikata, Z. Siroma, Y. Uchimoto, K. Yasuda, K.-I. Kimijima, and N. Iwashita. Scientific Aspects of Polymer Electrolyte Fuel Cell Durability and Degradation. *Chem. Rev.*, 107(10):3904–3951, 2007.

[62] N. Zamel and X. Li. Effect of Contaminants on Polymer Electrolyte Membrane Fuel Cells. *Prog. Energ. Combust.*, 37(3):292–329, 2011.

[63] J. Yu, T. Matsuura, Y. Yoshikawa, M. Nazrul Islam, and M. Hori. Lifetime Behavior of a PEM Fuel Cell with Low Humidification of Feed Stream. *Phys. Chem. Chem. Phys.*, 7(2):373–378, 2005.

[64] M. P. Rodgers, L. J. Bonville, H. R. Kunz, D. K. Slattery, and J. M. Fenton. Fuel Cell Perfluorinated Sulfonic Acid Membrane Degradation Correlating Accelerated Stress Testing and Lifetime. *Chem. Rev.*, 112(11):6075–6103, 2012.

[65] M. Miller and A. Bazylak. A Review of Polymer Electrolyte Membrane Fuel Cell Stack Testing. *J. Pow. Sour.*, 196(2):601–613, 2011.

[66] A. A. Shah, K. H. Luo, T. R. Ralph, and F. C. Walsh. Recent Trends and Developments in Polymer Electrolyte Membrane Fuel Cell Modelling. *Electrochim. Acta*, 56(11):3731–3757, 2011.

[67] J. Healy, C. Hayden, T. Xie, K. Olson, R. Waldo, M. Brundage, H. Gasteiger, and J. Abbott. Aspects of the Chemical Degradation of PFSA Ionomers Used in PEM Fuel Cells. *Fuel Cells*, 5(2):302–308, 2005.

[68] D. W. Rhoades, M. K. Hassan, S. J. Osborn, R. B. Moore, and K. A. Mauritz. Broadband Dielectric Spectroscopic Characterization of Nafion Chemical Degradation. *J. Pow. Sour.*, 172(1):72–77, 2007.

[69] L. Ghassemzadeh, K.-D. Kreuer, J. Maier, and K. Müller. Evaluating Chemical Degradation of Proton Conducting Perfluorosulfonic Acid Ionomers in a Fenton Test by Solid-State ^{19}F NMR Spectroscopy. *J. Pow. Sour.*, 196(5):2490–2497, 2011.

[70] S. J. Osborn, M. K. Hassan, G. M. Divoux, D. W. Rhoades, K. A. Mauritz, and R. B. Moore. Glass Transition Temperature of Perfluorosulfonic Acid Ionomers. *Macromolecules*, 40(10):3886–3890, 2007.

[71] S. J. Peighambardoust, S. Rowshanzamir, and M. Amjadi. Review of the Proton Exchange Membranes for Fuel Cell Applications. *Int. J. Hydrogen Energy*, 35(17):9349–9384, 2010.

[72] H. Chang, H. Kim, Y. S. Choi, and W. Lee. Critical Issues in the Commercialization of DMFC and Role of Membranes. In Zaidi S.M. Javaid and Takeshi Matsuura, editors, *Polymer Membranes for Fuel Cells*, chapter 13, pages 307–339. Springer US, Boston, MA, 2009.

[73] Y. Yang, A. Siu, T. J. Peckham, and S. Holdcroft. Structural and Morphological Features of Acid-Bearing Polymers for PEM Fuel Cells. *Adv. Polym. Sci.*, 215:55–126, 2008.

[74] K.-D. Kreuer, M. Schuster, B. Obliers, O. Diat, U. Traub, A. Fuchs, U. Klock, S. J. Paddison, and J. Maier. Short-Side-Chain Proton Conducting Perfluorosulfonic Acid Ionomers: Why They Perform Better in PEM Fuel Cells. *J. Pow. Sour.*, 178:499–509, 2008.

[75] Y. Chikashige, Y. Chikyu, K. Miyatake, and M. Watanabe. Poly(arylene ether) Ionomers Containing Sulfofluorenyl Groups for Fuel Cell Applications. *Macromolecules*, 38(16):7121–7126, 2005.

[76] T. Higashihara, K. Matsumoto, and M. Ueda. Sulfonated Aromatic Hydrocarbon Polymers as Proton Exchange Membranes for Fuel Cells. *Polymer*, 50(23):5341–5357, 2009.

[77] D. S. Kim, G. P. Robertson, Y. S. Kim, and M. D. Guiver. Copoly(arylene ether)s Containing Pendant Sulfonic Acid Groups as Proton Exchange Membranes. *Macromolecules*, 42:957–963, 2009.

[78] T. Okayasu, K. Hirose, and H. Nishide. Sulfonic Acid Polymer-Densely Grafted Poly(ethersulfone)s for a Highly Proton-Conducting Membrane. *Polym. Adv. Technol.*, 22(8):1229–1234, 2011.

[79] M. L. Einsla, Y. S. Kim, M. Hawley, H.-S. Lee, J. E. McGrath, B. Liu, M. D. Guiver, and B. S. Pivovar. Toward Improved Conductivity of Sulfonated Aromatic Proton Exchange Membranes at Low Relative Humidity. *Chem. Mater.*, 20(17):5636–5642, 2008.

[80] Y. A. Elabd and M. A. Hickner. Block Copolymers for Fuel Cells. *Macromolecules*, 44(1):1–11, 2011.

[81] Y. A. Elabd, E. Napadensky, C. W. Walker, and K. I. Winey. Transport Properties of Sulfonated Poly(styrene-b-isobutylene-b-styrene) Triblock Copolymers at High Ion-Exchange Capacities. *Macromolecules*, 39(1):399–407, 2006.

[82] A. Roy, M. A. Hickner, O. Lane, and J. E. McGrath. Investigation of Membrane Electrode Assembly (MEA) Processing Parameters on Performance for Wholly Aromatic Hydrocarbon-Based Proton Exchange Membranes. *J. Pow. Sour.*, 191(2):550–554, 2009.

[83] M. A. Hickner, H. Ghassemi, Y. S. Kim, B. R. Einsla, and J. E McGrath. Alternative Polymer Systems for Proton Exchange Membranes (PEMs). *Chem. Rev.*, 104(10):4587–4612, 2004.

[84] Y. Li, A. Roy, A. S. Badami, M. Hill, J. Yang, S. Dunn, and J. E. McGrath. Synthesis and Characterization of Partially Fluorinated Hydrophobic-Hydrophilic Multiblock Copolymers Containing Sulfonate Groups for Proton Exchange Membrane. *J. Pow. Sour.*, 172(1):30–38, 2007.

[85] A. Katzfuss, K. Krajinovic, A. Chromik, and J. Kerres. Partially Fluorinated Sulfonated Poly(arylene sulfone)s Blended with Polybenzimidazole. *J. Polym. Sci. Part A: Polym. Chem.*, 49:1919–1927, 2011.

[86] J. Chen, M. Asano, Y. Maekawa, and M. Yoshida. Chemically Stable Hybrid Polymer Electrolyte Membranes Prepared by Radiation Grafting, Sulfonation, and Silane-Crosslinking Techniques. *J. Polym. Sci. Part A: Polym. Chem.*, 46:5559–5567, 2008.

[87] M. M. Nasef and E.-S. A. Hegazy. Preparation and Applications of Ion Exchange Membranes by Radiation-Induced Graft Copolymerization of Polar Monomers Onto Non-Polar Films. *Prog. Polym. Sci.*, 29(6):499–561, 2004.

[88] J. Lu, S. Lu, and S. P. Jiang. Highly Ordered Mesoporous Nafion Membranes for Fuel Cells. *Chem. Commun.*, 47(11):3216–3218, 2011.

[89] P. V. Komarov, I. N. Veselov, P. P. Chu, and P. G. Khalatur. Mesoscale Simulation of Polymer Electrolyte Membranes based on Sulfonated Poly(ether ether ketone) and Nafion. *Soft Matter*, 6(16):3939–3956, 2010.

[90] K. Malek, M. Eikerling, Q. Wang, Z. Liu, S. Otsuka, K. Akizuki, and M. Abe. Nanophase Segregation and Water Dynamics in Hydrated Nafion: Molecular Modeling and Experimental Validation. *J. Chem. Phys.*, 129(20):204702, 2008.

[91] J. Kerres, W. Zhang, A. Ullrich, C.-M. Tang, M. Hein, V. Gogel, T. Frey, and L. Jörissen. Synthesis and Characterization of Polyaryl Blend Membranes Having Different Composition, Different Covalent and/or Ionical Cross-linking Density, and their Application to DMFC. *Desalination*, 147:173–178, 2002.

[92] J. A. Kerres. Blended and Cross-Linked Ionomer Membranes for Application in Membrane Fuel Cells. *Fuel Cells*, 5(2):230–247, 2005.

[93]   B. P. Tripathi, M. Kumar, and V. K. Shahi. Highly Stable Proton Conducting Nanocomposite Polymer Electrolyte Membrane (PEM) Prepared by Pore Modifications: An Extremely Low Methanol Permeable PEM. *J. Membr. Sci.*, 327(1-2):145–154, 2009.

[94]   K. Matsumoto, T. Higashihara, and M. Ueda. Locally Sulfonated Poly (ether sulfone)s with Highly Sulfonated Units as Proton Exchange Membrane. *J. Polym. Sci. Part A: Polym. Chem.*, 47:3444–3453, 2009.

[95]   S. Matsumura, A. R. Hlil, C. Lepiller, J. Gaudet, D. Guay, and A. S. Hay. Ionomers for Proton Exchange Membrane Fuel Cells with Sulfonic Acid Groups on the End Groups: Novel Linear Aromatic Poly(sulfide-ketone)s. *Macromolecules*, 41:277–280, 2008.

[96]   S. Matsumura, A. R Hlil, N. Du, C. Lepiller, J. Gaudet, D. Guay, Z. Shi, S. Holdcroft, and A. S. Hay. Ionomers for Proton Exchange Membrane Fuel Cells with Sulfonic Acid Groups on the End-Groups: Novel Branched Poly (ether-ketone)s with 3,6-Ditrityl-9H-Carbazole End-Groups. *J. Polym. Sci. Part A: Polym. Chem.*, 46:3860–3868, 2008.

[97]   M. J. Park, K. H. Downing, A. Jackson, E. D. Gomez, A. M. Minor, D. Cookson, A. Z. Weber, and N. P. Balsara. Increased Water Retention in Polymer Electrolyte Membranes at Elevated Temperatures Assisted by Capillary Condensation. *Nano Lett.*, 7(11):3547–3552, 2007.

[98]   B. Lafitte, M. Puchner, and P. Jannasch. Proton Conducting Polysulfone Ionomers Carrying Sulfoaryloxybenzoyl Side Chains. *Macromol. Rapid Commun.*, 26(18):1464–1468, 2005.

[99]   L. M. de Carvalho, A. R. Tan, and A. de Souza Gomes. Nanostructured Membranes Based on Sulfonated Poly(aryl ether sulfone) and Silica for Fuel-Cell Applications. *J. Appl. Polym. Sci.*, 110(3):1690–1698, 2008.

[100] W. Li, A. Manthiram, and M. D. Guiver. Acid-Base Blend Membranes Consisting of Sulfonated Poly(ether ether ketone) and 5-amino-benzotriazole Tethered Polysulfone for DMFC. *J. Membr. Sci.*, 362(1-2):289–297, 2010.

[101] C. J. Hawker and K. L. Wooley. The Convergence of Synthetic Organic and Polymer Chemistries. *Science*, 309(5738):1200–5, 2005.

[102] W. H. Binder and R. Sachsenhofer. Click Chemistry in Polymer and Materials Science. *Macromol. Rapid Commun.*, 28(1):15–54, 2007.

[103] S. Hvilsted. Facile Design of Biomaterials by Click Chemistry. *Polym. Int.*, 61(4):485–494, 2012.

[104] M. Karadag, G. Yilmaz, H. Toiserkani, D. O. Demirkol, S. Sakarya, L. Torun, S. Timur, and Y. Yagci. Polysulfone/Pyrene Membranes: A New Microwell Assay Platform for Bioapplications. *Macromol. Biosci.*, 11(9):1235–1243, 2011.

[105] I. Javakhishvili. Nanoscale Polymeric Amphiphiles by Combination of Controlled Polymerizations and "Click" Reactions: Implications for Drug Delivery. *Ph.D. Dissertation, Technical University of Denmark*, 2010.

[106] A. E. Daugaard. Functional Materials by Click Chemistry. *Ph.D. Dissertation, Technical University of Denmark*, 2009.

[107] G. Rydzek, J. S. Thomann, N. Ben Ameur, L. Jierry, P. Mésini, A. Ponche, C. Contal, A. E. El Haitami, J. C. Voegel, B. Senger, P. Schaaf, B. Frisch, and F. Boulmedais. Polymer Multilayer Films Obtained by Electrochemically Catalyzed Click Chemistry. *Langmuir*, 26(4):2816–24, 2010.

[108] R. Huisgen. 1.3-Dipolare Cycloadditionen. *Angew. Chem.*, 75(13):604–637, 1963.

[109] C. W. Tornøe, C. Christensen, and M. Meldal. Peptidotriazoles on Solid Phase: [1,2,3]-triazoles by Regiospecific Copper(I)-Catalyzed 1,3-dipolar Cycloadditions of Terminal Alkynes to Azides. *J. Org. Chem.*, 67(9):3057–3064, 2002.

[110] H. C. Kolb, M. G. Finn, and K. B. Sharpless. Click Chemistry: Diverse Chemical Function from a Few Good Reactions. *Angew. Chem., Int. Ed.*, 40(11):2004–2021, 2001.

[111] B. C. Norris, W. Li, E. Lee, A. Manthiram, and C. W. Bielawski. Click-Functionalization of Poly(sulfone)s and a Study of Their Utilities as Proton Conductive Membranes in Direct Methanol Fuel Cells. *Polymer*, 51(23):5352–5358, 2010.

[112] I. Dimitrov, S. Takamuku, K. Jankova, P. Jannasch, and S. Hvilsted. Polysulfone Functionalized with Phosphonated Poly(pentafluorostyrene) Grafts for Potential Fuel Cell Applications. *Macromol. Rapid Commun.*, 33(16):1368–1374, 2012.

[113] J.-L. M. Abboud, C. Foces-Foces, R. Notario, R. E. Trifonov, A. P. Volovodenko, V. A. Ostrovskii, I. Alkorta, and J. Elguero. Basicity of N-H- and N-Methyl-1,2,3-triazoles in the Gas Phase, in Solution, and in the Solid State - An Experimental and Theoretical Study. *Eur. J. Org. Chem.*, 2001:3013–3024, 2001.

[114] M. S. Kharasch, E. V. Jensen, and W. H. Urry. Addition of Carbon Tetrachloride and Chloroform to Olefins. *Science*, 102:128, 1945.

[115] J.-S. Wang and K. Matyjaszewski. Controlled/"Living" Radical Polymerization. Halogen Atom Transfer Radical Polymerization Promoted by a Cu(I)/Cu(II) Redox Process. *Macromolecules*, 28(23):7901–7910, 1995.

[116] M. Kato, M. Kamigaito, M. Sawamoto, and T. Higashimuras. Polymerization of Methyl Methacrylate with the Carbon Tetrachloride/Dichlorotris-(triphenylphosphine)ruthenium(II)/Methylaluminum Bis(2,6-di-tert-butylphenoxide) Initiating System: Possibility of Living Radical Polymerization. *Macromolecules*, 28:1721–1723, 1995.

[117] W. A. Braunecker and K. Matyjaszewski. Controlled/Living Radical Polymerization: Features, Developments, and Perspectives. *Prog. Polym. Sci.*, 32(1):93–146, 2007.

[118] J. Xia and K. Matyjaszewski. Controlled/Living Radical Polymerization. Atom Transfer Radical Polymerization Using Multidentate Amine Ligands. *Maromolecules*, 30:7697–7700, 1997.

[119] K. Matyjaszewski, Y. Nakagawa, and S. G. Gaynor. Synthesis of Well-Defined Azido and Amino End-Functionalized Polystyrene by Atom Transfer Radical Polymerization. *Macromol. Rapid Commun.*, 18:1057–1064, 1997.

[120] K. Matyjaszewski and J. Xia. Atom Transfer Radical Polymerization. *Chem. Rev.*, 101(9):2921–2990, 2001.

[121] K. Matyjaszewski. Atom Transfer Radical Polymerization: From Mechanisms to Applications. *Isr. J. Chem.*, 52(3-4):206–220, 2012.

[122] Z. Shi and S. Holdcroft. Synthesis of Block Copolymers Possessing Fluoropolymer and Non-Fluoropolymer Segments by Radical Polymerization. *Macromolecules*, 37(6):2084–2089, 2004.

[123] W. Jakubowski. Adapting Atom Transfer Radical Polymerization to Industrial Scale Production: The Ultimate ATRP Technology. In K. Matyjaszewski, B. S. Sumerlin, and N. V. Tsarevsky, editors, *Progress in Controlled Radical Polymerization: Mechanisms and Techniques*, chapter 13. ACS Symp. Ser., Washington, DC.

[124] T. Pintauer and K. Matyjaszewski. Atom Transfer Radical Addition and Polymerization Reactions Catalyzed by ppm Amounts of Copper Complexes. *Chem. Soc. Rev.*, 37(6):1087–1097, 2008.

[125] X.-P. Chen and A. B. Padias. Atom Transfer Radical Polymerization of Methyl Bicyclobutane-1-carboxylate. *Macromolecules*, 34(11):3514–3516, 2001.

[126] S. O. Kyeremateng, E. Amado, A. Blume, and J. Kressler. Synthesis of ABC and CABAC Triphilic Block Copolymers by ATRP Combined with Click Chemistry. *Macromol. Rapid Commun.*, 29(12-13):1140–1146, 2008.

[127] U. Mansfeld, C. Pietsch, R. Hoogenboom, C. R. Becer, and U. S. Schubert. Clickable Initiators, Monomers and Polymers in Controlled Radical Polymerizations - a Prospective Combination in Polymer Science. *Polym. Chem.*, 1(10):1560–1598, 2010.

[128] J. R. Fried. *Polymer Science & Technology*. Prentice Hall, Upper Saddle River, NJ, 2nd edition, 2003.

[129] N. Y. Arnett, W. L. Harrison, A. S. Badami, A. Roy, O. Lane, F. Cromer, L. Dong, and J. E. McGrath. Hydrocarbon and Partially Fluorinated Sulfonated Copolymer Blends as Functional Membranes for Proton Exchange Membrane Fuel Cells. *J. Pow. Sour.*, 172(1):20–29, 2007.

[130] W. Li, B. C. Norris, P. Snodgrass, K. Prasad, A. S. Stockett, V. Pryamitsyn, V. Ganesan, C. W. Bielawski, and A. Manthiram. Evaluating the Role of Additive pKa on the Proton Conductivities of Blended Sulfonated Poly(ether ether ketone) Membranes. *J. Phys. Chem. B*, 113(30):10063–10067, 2009.

[131] Y. Fu, A. Manthiram, and M. D. Guiver. Blend Membranes Based on Sulfonated Poly(ether ether ketone) and Polysulfone Bearing Benzimidazole Side Groups for Proton Exchange Membrane Fuel Cells. *Electrochem. Commun.*, 8:1386–1390, 2006.

[132] N. Gourdoupi, J. K. Kallitsis, and S. Neophytides. New Proton Conducting Polymer Blends and Their Fuel Cell Performance. *J. Pow. Sour.*, 195(1):170–174, 2010.

[133] S. Takamuku and P. Jannasch. Fully Aromatic Block Copolymers for Fuel Cell Membranes with Densely Sulfonated Nanophase Domains. *Macromol. Rapid Commun.*, 32(5):474–480, 2011.

[134] S. Takamuku and P. Jannasch. Properties and Degradation of Hydrocarbon Fuel Cell Membranes: A Comparative Study of Sulfonated Poly(arylene ether sulfone)s with Different Positions of the Acid Groups. *Polym. Chem.*, 3:1202–1214, 2012.

[135] S. Takamuku and P. Jannasch. Multiblock Copolymers Containing Highly Sulfonated Poly(arylene sulfone) Blocks for Proton Conducting Electrolyte Membranes. *Macromolecules*, 45(16):6538–6546, 2012.

[136] S. Takamuku and P. Jannasch. Multiblock Copolymers with Highly Sulfonated Blocks Containing Di- and Tetrasulfonated Arylene Sulfone Segments for Proton Exchange Membrane Fuel Cell Applications. *Adv. Energ. Mater.*, 2(1):129–140, 2012.

[137] S. Svenson and D. A. Tomalia. Dendrimers in Biomedical Applications - Reflections on the Field. *Adv. Drug Delivery Rev.*, 57(15):2106–2129, 2005.

[138] Y. J. Huang, Y. S. Ye, Y. C. Yen, L. D. Tsai, B. J. Hwang, and F. C. Chang. Synthesis and Characterization of New Sulfonated Polytriazole Proton Exchange Membrane by Click Reaction for Direct Methanol Fuel Cells (DMFCs). *Int. J. Hydrogen Energy*, 36(23):15333–15343, 2011.

[139] Z. Zhou, S. Li, Y. Zhang, M. Liu, and W. Li. Promotion of Proton Conduction in Polymer Electrolyte Membranes by 1*H*-1,2,3-triazole. *J. Am. Chem. Soc.*, 127(31):10824–10825, 2005.

[140] U. Sen, S. Unugurcelik, A. Ata, and A. Bozkurt. Anhydrous Proton Conducting Membranes for PEM Fuel Cells Based on Nafion/Azole Composites. *Int. J. Hydrogen Energy*, 33(11):2808–2815, 2008.

[141] I. Dimitrov, K. Jankova, and S. Hvilsted. Controlled Synthesis of Fluorinated Copolymers with Pendant Sulfonates. *J. Polym. Sci. Part A: Polym. Chem.*, 46:7827–7834, 2008.

[142] J. V. Gasa, R. A. Weiss, and M. T. Shaw. Structured Polymer Electrolyte Blends Based on Sulfonated Polyetherketoneketone (SPEKK) and a Poly(ether imide) (PEI). *J. Membr. Sci.*, 320(1-2):215–223, 2008.

[143] J. V. Gasa, R. A. Weiss, and M. T. Shaw. Influence of Blend Miscibility on the Proton Conductivity and Methanol Permeability of Polymer Electrolyte Blends. *J. Polym. Sci. Part B: Polym. Phys.*, 44:2253–2266, 2006.

[144] M. J. Park and N. P. Balsara. Direct Imaging of Hydrated Polymer Electrolyte Membranes for Fuel Cell Application. *ECS Trans.*, 16(2):1357–1363, 2008.

[145] M. Lee, J. K. Park, H.-S. Lee, O. Lane, R. B. Moore, J. E. McGrath, and D. G. Baird. Effects of Block Length and Solution-Casting Conditions on the Final Morphology and Properties of Disulfonated Poly(arylene ether sulfone) Multiblock Copolymer Films for Proton Exchange Membranes. *Polymer*, 50(25):6129–6138, 2009.

[146] C. H. Lee, K.-S. Lee, O. Lane, J. E. McGrath, Y. Chen, S. Wi, S. Y. Lee, and Y. M. Lee. Solvent-Assisted Thermal Annealing of Disulfonated Poly(arylene ether sulfone) Random Copolymers for Low Humidity Polymer Electrolyte Membrane Fuel Cells. *RSC Adv.*, 2(3):1025, 2012.

[147] S. Cavaliere, S. Subianto, I. Savych, D. J. Jones, and J. Rozière. Electrospinning: Designed Architectures for Energy Conversion and Storage Devices. *Energy Environ. Sci.*, 4(12):4761–4785, 2011.

[148] E.-H. Ryu and Y. Zhao. Efficient Synthesis of Water-Soluble Calixarenes Using Click Chemistry. *Org. Lett.*, 7(6):1035–1037, 2005.

[149] S. Löber, P. Rodriguez-Loaiza, and P. Gmeiner. Click Linker: Efficient and High-Yielding Synthesis of a New Family of SPOS Resins by 1,3-Dipolar Cycloaddition. *Org. Lett.*, 5 (10)(3):9717–9719, 2003.

[150] J. A. Opsteen and J. C. M. van Hest. Modular Synthesis of Block Copolymers via Cycloaddition of Terminal Azide and Alkyne Functionalized Polymers. *Chem. Commun.*, 1:57–59, 2005.

[151] J. Rozière and D. J. Jones. Non-Fluorinated Polymer Materials for Proton Exchange Membrane Fuel Cells. *Annu. Rev. Mater. Res.*, 33(1):503–555, 2003.

[152] B. Smitha, S. Sridhar, and A. A. Khan. Synthesis and Characterization of Proton Conducting Polymer Membranes for Fuel Cells. *J. Membr. Sci.*, 225(1-2):63–76, 2003.

[153] S. Borkar, K. Jankova, H. W. Siesler, and S. Hvilsted. New Highly Fluorinated Styrene-Based Materials with Low Surface Energy Prepared by ATRP. *Macromolecules*, 37(3):788–794, 2004.

[154] A. C. C. Yang, R. Narimani, Z. Zhang, B. J. Frisken, and S. Holdcroft. Controlling Crystallinity in Graft Ionomers, and Its Effect on Morphology, Water Sorption, and Proton Conductivity. *Submitted*, 2013.

[155] D. Plackett, K. Jankova, H. Egsgaard, and S. Hvilsted. Modification of Jute Fibers with Polystyrene via Atom Transfer Radical Polymerization. *Biomacromolecules*, 6(5):2474–2484, 2005.

[156] E. M. W. Tsang, Z. Shi, and S. Holdcroft. Ionic Purity and Connectivity of Proton-Conducting Channels in Fluorous-Ionic Diblock Copolymers. *Macromolecules*, 44(22):8845–8857, 2011.

[157] F. S. Bates and G. H. Fredrickson. Block Copolymers - Designer Soft Materials. *Phys. Today*, 52(2):32, 1999.

[158] P. Dimitrova, K. A. Friedrich, B. Vogt, and U. Stimming. Transport Properties of Ionomer Composite Membranes for Direct Methanol Fuel Cells. *J. Electroanal. Chem.*, 532(1-2):75–83, 2002.

[159] C. F. Nørgaard, U. G. Nielsen, and E. M. Skou. Preparation of Nafion 117-SnO$_2$ Composite Membranes Using an Ion-Exchange Method. *Solid State Ionics*, 213:76–82, 2012.

[160] C. J. Fristrup, K. Jankova, and S. Hvilsted. Surface-Initiated Atom Transfer Radical Polymerization - a Technique to Develop Biofunctional Coatings. *Soft Matter*, 5(23):4623–4634, 2009.

[161] T. Cai, K.-G. Neoh, and E.-T. Kang. Functionalizable Poly(vinylidene fluoride) Membranes via Controlled/Living Radical Polymerization and Click Chemistry. In K. Matyjaszewski, B. S. Sumerlin, and N. V. Tsarevsky, editors, *Progress in Controlled Radical Polymerization: Materials and Applications*, volume 1101, chapter 14. ACS Symp. Ser., Washington, DC, 2012.

[162] P. D. Iddon, K. L. Robinson, and S. P. Armes. Polymerization of Sodium 4-Styrenesulfonate via Atom Transfer Radical Polymerization in Protic Media. *Polymer*, 45:759–768, 2004.

[163] K. Jankova et al. in preparation.

Appendices

I

Analytical Techniques

NMR spectra were recorded in CDCl$_3$, DMSO-d_6 or D$_2$O using a Bruker 300 MHz, and in acetone-d_6 applying a Varian MercuryPlus 400 MHz.

Molecular weights and polydispersities were estimated by SEC, employing two instruments: 1) Samples dissolved in THF were run on a Viscotek 200 instrument using two PLgel mixed-D columns (Polymer Laboratories) assembled in series and a refractive index (RI) detector at a 1 mL min^{-1} flow speed. Calculations were performed from a PS standard calibration. 2) Samples dissolved in DMF (with 5 mM LiCl) were investigated on a Tosoh Corporation Bioscience Division HLC-8320GPC equipped with three PFG micro columns (100 Å, 1000 Å, and 4000 Å) from Polymer Standards Service, with an RI detector, at 50 ^{o}C at 0.3 mL min^{-1}). Calculations were performed utilising WinGPC Unity 7.4.0 software and PMMA standards.

Attenuated total reflectance FTIR spectra were recorded on a Perkin-Elmer Spectrum One instrument in the 4000-650 cm^{-1} operating range over 16 scans.

Samples for TEM were first stained with lead acetate, then epoxy embedded, microtomed and collected on a copper grid. A Leica UC6 ultramicrotome was deployed at RT, whereas cryo-microtomed was performed on a Leica Ultracut UCT with a Cryo 35° Waterblade. Electron micrographs were obtained with a Hitachi H7600 TEM at 100 keV and a Tecnai T20 G^2 at 200 keV. Calculations were done with ImageJ software.

TGA was operated at a heating speed of 20 ^{o}C min^{-1} from RT to 650 ^{o}C under nitrogen on a TA Instruments TGA Q500.

DSC was operated at a heating speed of 10 ^{o}C min^{-1} from RT to 220 ^{o}C or 250 ^{o}C under nitrogen on a TA Instruments DSC Q1000. Data collection was performed over three to five heating-cooling cycles. Thermal responses were calculated from the last heating cycle.

In-plane proton conductivities were recorded by two instrumental setups: 1) A homemade bench with two electrodes, a GW Instek laboratory DC power supply, model GPS-3030DD and two Fluke True RMS Multimeter 189's. 2) AC impedance spectroscopy, applying a Solartron 1260 frequency response analyzer employing a two-electrode configuration at a 100 mV sinusoidal AC voltage over a frequency range of 10 MHz - 100 Hz. The latter setup was also used for conductivity measurements at varying temperature and RH in combination with an ESPEC SH-241 temperature/humidity chamber. Conductivity measurements were obtained *in situ*.

Dynamic vapour sorption was carried out on a DVS-1000 from Surface Measurement Systems, UK. The target RH was reached by using a mixed gas flow of fully saturated water vapour and dry nitrogen. RH was maintained and controlled by a dew-point sensor. Typically, the membranes were kept at 25 ^{o}C in an RH range of 0 - 98% with steps of 10% from 0 to 90%, then to 95% and finally 98%. The mass of the membrane was recorded *in situ* every 10 seconds.

II

Nytænkning i Brændselscellemembraner

M. M. Nielsen, K. Jankova, S. Hvilsted

pop SCI

I 2020 skal 50% af danskernes elforbrug komme fra vindenergi.

Nytænkning i brændselscellemembraner

Brændselscellen blev alment kendt som vandgenererende kraftværk i 1960'ernes rumprogrammer. I dag er den en vigtig brik i energipuslespillet, og udviklingen fortsætter – bl.a. gennem arkitektonisk nytænkning af dens hjerte: en polymermembran.

Af Mads Møller Nielsen, Katja Jankova, Søren Hvilsted, Dansk Polymercenter, DTU Kemiteknik

Når Danmarks regering har indgået en energiaftale, hvor rundt regnet 35% af nationens energibehov skal dækkes gennem vedvarende energi og 50% af elektricitetsforbruget skal komme fra vindenergi i 2020 (mod 23% i 2012), så har det afgørende betydning, at den strøm, der genereres på tidspunkter af døgnet eller året, hvor vi ikke har behov for den, ikke går til spilde [1]. En løsning på dette problem er, at overskydende energi bruges til at drive elektrolyse af vand som derved spaltes i sine grundkomponenter brint (H_2) og ilt (O_2):

$$2\,H_2O \;\rightarrow\; 2\,H_2 + O_2$$
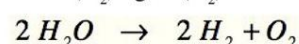
Disse to gasser udgør tilsammen reagenserne - brændstoffet som man vil sige i denne sammenhæng - til den type brændselsceller (PEMFC = *proton exchange membrane fuel cell*) man anvender i elbiler (FCEV = *fuel cell electric vehicle*). Elbiler er i disse år genstand for megen fokus grundet minimal lokal forurening og reducerede støjgener. Dertil kommer, at brint,
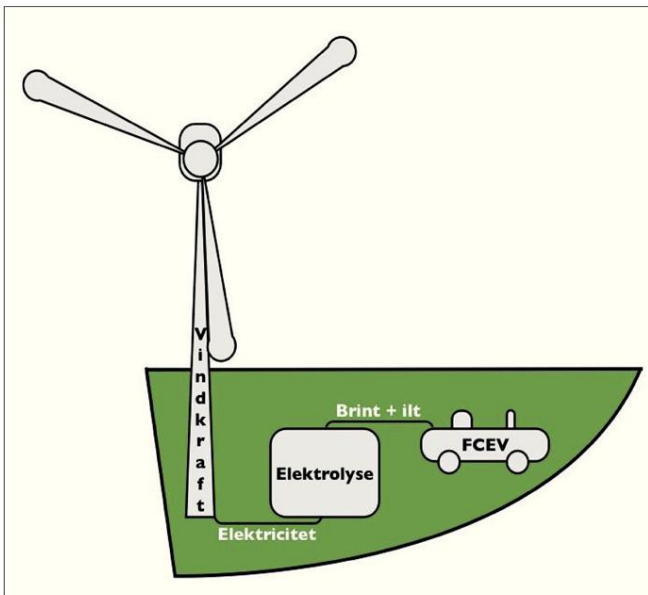
Figur 1. Overskydende el fra vindenergi bruges til at elektrolysere vand til ilt og brint som tankes på brændselscelledrevne elbiler.

der ligesom metanol ligeledes kan bruges som brændstof, også fremstilles fra en anden energiressource i tidsånden: biomasse. Således skal potentialet i brændselscellen også ses ift. situationen i dag, hvor fossile brændsler er førstevalget i transportsektoren. Et stærkt fysiker-argument for brændselscellen er, at den – modsat forbrændingsmotoren – ikke er begrænset af Carnotcyklussen, en model, der beskriver den maks. tilførte energi, som kan omdannes til arbejde i en varmekraftmaskine (i det ideelle tilfælde). Således kan man med en brændselscelle opnå langt mindre energitab i omdannelsen fra kemisk energi til elektricitet [2].

Processen fra høst af vindkraft til FCEV-brændstof er skitseret i figur 1.

I PEMFC produceres strøm gennem det, der i princippet er den modsatrettede reaktion af den, der finder sted i elektrolysen, dvs. der dannes elektrisk strøm frem for at den forbruges:

$$2\,H_2 + O_2 \;\rightarrow\; 2\,H_2O$$
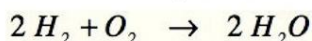
Den elektrokemiske proces er vist skematisk i figur 2.
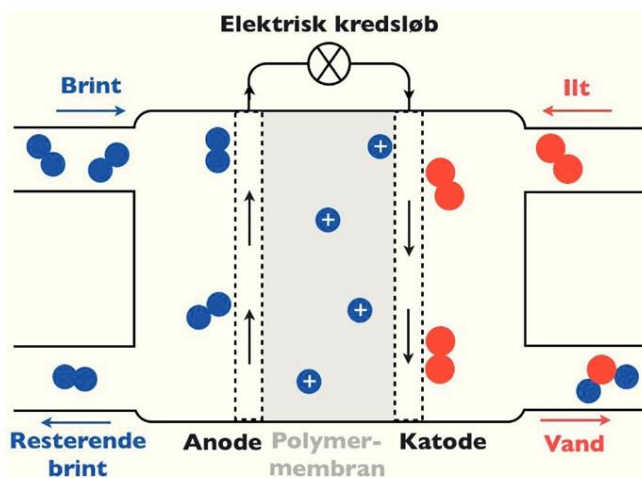
Figur 2. I en PEMFC spaltes brint i protoner og elektroner ved anoden, og mens protonerne bevæger sig gennem den protonledende polymermembran, løber elektronerne til katoden, hvor det eneste spildprodukt, vand, dannes.

Brint tilføres anoden (den negative elektrode), hvor den spaltes i protoner og elektroner. Protonerne bevæger sig gennem vandkanaler (figur 3) fra den ene side af en avanceret polymermembran til den anden [3] (ordet "polymer" er græsk for "mange dele" og dækker dét, at mange molekyler er bundet til hinanden i lange kæder; et eksempel herpå er plast). De forskellige mekanismer er beskrevet i boks 1. Elektronerne løber i et elektrisk kredsløb til katoden (den positive elektrode), hvor de sammen med protonerne og ilt danner det eneste spildprodukt: vand. Interessant nok var det en kombination af produkterne elektricitet og (drikke)vand, der fik NASA til at investere massivt i udviklingen af brændselsceller til Apollo-ekspeditionerne i anden halvdel af sidste århundrede.
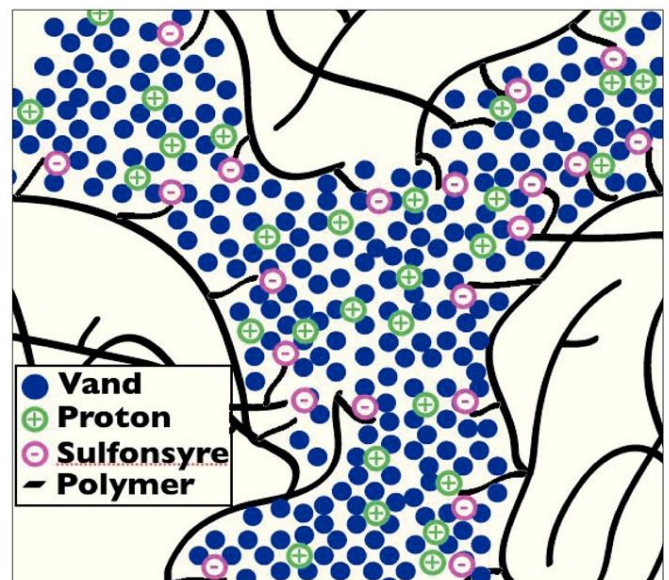
Figur 3. Protonerne bevæger sig over polymermembranen gennem vandkanaler, så det er vigtigt at opnå den rigtige balance mellem vandskyende og -elskende grupper.

Polymermembran og elektrodemateriale presses typisk sammen til én komponent (MEA = *membrane electrode assembly*). Sammen med endepladerne, der, via de til formålet designede kanaler, bringer ilt og brint i kontakt med MEA'en, udgør de en enkeltcelle. En enkeltcelle producerer 0,5-1,0 V, så for at opnå den større kapacitet, der skal til for at flytte eksempelvis en bil, bliver adskillige enkeltceller arrangeret i stakke i serie (figur 4, side 20).

Selvom PEMFC nu er nået til et punkt, hvor de er kommercielt tilgængelige, så står man stadig overfor nogle udfordringer, før de kan blive konkurrencedygtige ift. forbrændingsmotorer. F.eks. er der flere fordele ved at drive brændselscellen ved højere temperaturer, og desuden spiller levetid og pris vigtige roller. Forskning i membranen er her et vigtigt punkt, da den er med til at afgøre, under hvilke omstændigheder brændselscellen kan virke. ▶
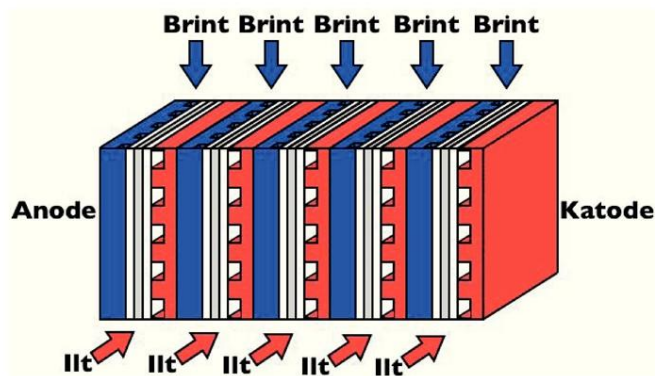
Figur 4. Brændselsceller stakkes i serie for at opnå tilstrækkeligt store kapaciteter.

$[x = 6\text{-}10,\ y = 1]$

Figur 5. Kemisk struktur af en *benchmark* PEM: Nafion®.

Membrandesign

For at en polymermembran kan bruges som PEM, skal den leve op til visse krav (boks 2). Bl.a. skal den kunne klare de betingelser, som brændselscellen drives under, uden at dekomponere. Den skal have en kemisk og fysisk formulering, som muliggør protonledning, og så skal den virke som barriere for reagensgasser samt elektroner. Et eksempel på en *state-of-the-art* PEM er den perfluorerede og sulfonsyre-funktionaliserede ($-SO_3H$) Nafion® (figur 5). Den længste sammenhængende kæde (*backbonet*) er her særdeles vandskyende (hydrofobt) og klarer temperaturer på over 100°C, hvor vand som bekendt antager gasform og bliver til damp. PEMFC som virker i et vandigt miljø bliver af denne årsag typisk drevet ved 80°C. Der findes imidlertid en version af PEMFC, som kan virke ved højere temperaturer. I den er sulfonsyre erstattet med fosfonsyre ($-PO(OH)_2$) som protonledende gruppe, og fosforsyre (H_3PO_4) erstatter vand i ionkanalerne.

Boks 2. Krav til PEM

Protonledningsevne. Syregrupper inkorporeres, f.eks. sulfonsyre. Dannelsen af vandholdige ionkanaler er afgørende for protonledningsevnen.
Kemisk, mekanisk og termisk stabilitet. *Backbonet* vælges, så det er vandskyende, kemisk stabilt og har en tilpas høj glasovergangstemperatur (herover mister polymeren sin karakteristiske struktur). Det er vigtigt, at membranen ikke ændrer sine dimensioner væsentligt i takt med forskelle i fugtningsgrad og temperatur.
Gasuigennemtrængelighed. Sikrer den kontrollerede cellereaktion.
Elektrisk isolering. De fleste polymerer er faktisk elektrisk isolerende.

Balancen mellem vandskyende og vandelskende (hydrofile) dele af polymeren er afgørende for, hvorvidt den ved membrandannelse viser sig at have sammenhængende ionkanaler, og hvorvidt den bevarer sin struktur, når den kommer i kontakt med vand. Det er med afsæt heri, at forskere over det meste af verden arbejder med målsætningen om, at finde frem til en kemisk struktur, som kan give forbedrede egenskaber ift. nutidens mest avancerede membraner. Dvs. holdbarhed, ydeevne og pris, hvor Nafion® og lignende strukturer kommer til kort [4]. Udviklingen af nye syntesemetoder gennem de senere år har bidraget med flere til rådighed stående arkitektoniske redskaber, så det er mere eller mindre kun fantasien (og kemien), der afgør, hvilke kemiske strukturer vi kan skabe.
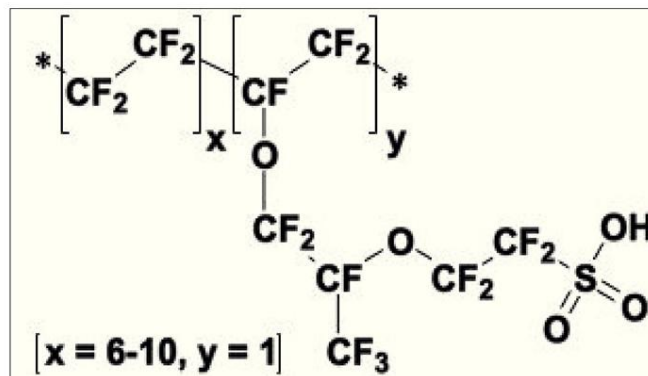
Boks 3. Nytænkning

MAProCon (*New Macromolecular Architectures and Functions for Proton Conducting Fuel Cell Membranes*) er et samarbejdsprojekt mellem Danmarks Tekniske Universitet, Syddansk Universitet, Lunds Universitet og Teknologisk Institut (overdraget midtvejs fra IRD A/S). Målsætningen er at bidrage til brændselscellemembranforskningen gennem fremstilling af nytænkende polymerstrukturer. Projektet er fireårigt og løber indtil marts 2013. Senere på foråret vil højdepunkter fra forskningssamarbejdet blive præsenteret på et symposium i IDA Huset.

Gennem MAProCon benytter vi forskellige tilgange til polymerarkitektur i nytænkningen af membranen i PEMFC. En af de strategier, vi har fulgt, er at benytte en kommercielt tilgængelig polysulfon som *backbone*, idet den tidligere har vist sig at have god kemisk og termisk stabilitet ud over at være velegnet til membrandannelse (den sorte struktur i figur 6) [5]. Vha. ”click”-kemi og atom transfer radikal polymerisering (ATRP)

Boks 4. Kemisk værktøjskasse

”Click”-kemi: Meget effektiv reaktion mellem funktionelle molekyler og polymerer. Gennem design af de enkelte byggeblokke udvides horisonten for membranarkitekturen betrageligt. Vi har her benyttet den kobberkatalyserede azid-alkyn-cykloaddition, der resulterer i en substitueret 1,2,3-triazol [7] (R angiver en vilkårlig restdel af molekylet):
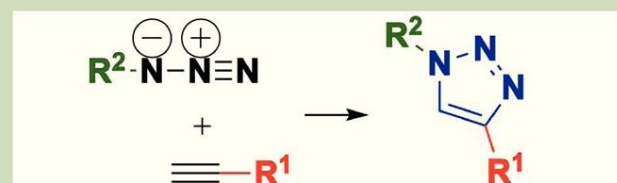
Atom transfer radikal polymerisering (ATRP): Polymeriseringsreaktion der muliggør en høj grad af kontrol over nøgleegenskaber som funktionalitet, arkitektur og kædelængde [8].
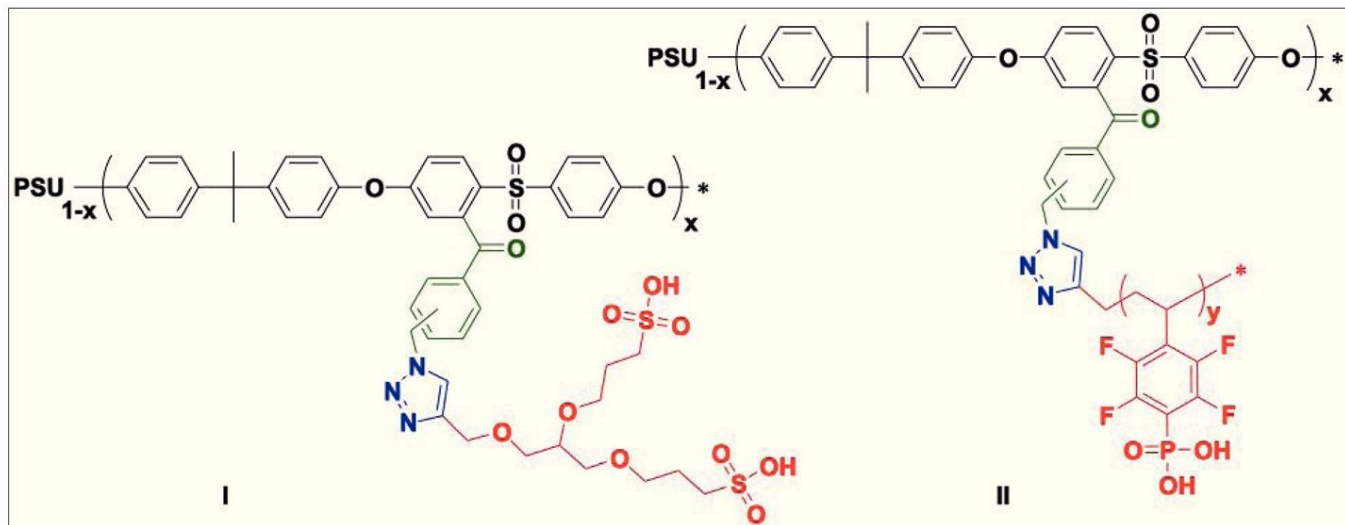
Figur 6. Produkter fremstillet gennem modificering (grøn), ATRP (kun **II**) og "click"-kemi.

(boks 4) modificeres polysulfonen til enten at få fleksible strukturer med parvist placerede sulfonsyregrupper eller længere delvist fluorerede sidekæder med fosfonsyre som protonledende gruppe (hhv. **I** og **II** i figur 6) [6]. Idéen med at benytte sidekæder med to sulfonsyregrupper er opstået ud fra forventningen om, at en højere lokal koncentration af protonledende grupper kan lede til forbedrede ionkanaler. Tilgangen med fosfonsyrefunktionaliseret delvist fluoreret polymer er med henblik på PEMFC drevet ved temperaturer over 100°C, hvor altså fosforsyre og ikke vand bidrager til protontransporten.

Uden nogen form for optimering af materialerne er der opnået lovende protonledningsevner for begge de nye membraner (se også *"Click" i polymerer 1* i september-nummeret [9]). Sandsynligvis kan begge strukturer optimeres yderligere, hvilket vi arbejder på nu. Det bliver spændende at se, om det så bliver på bekostning af andre afgørende egenskaber. Laboratoriearbejde fordrer ofte kompromiser.

Selvom tanken muligvis er let drejet til lejligheden, så er det sjovt at tænke på, hvor lang vejen har været, fra da Neil Armstrong med brændselsceller i sin rumraket satte kursen mod Månen, til vi i dag kan sætte kursen mod arbejde i en brændselscelledrevet bil. Sådan er forskning. Men vi kommer frem.

E-mail
Mads Møller Nielsen: mon@kt.dtu.dk
Søren Hvilsted: sh@kt.dtu.dk

Referencer:
1. http://www.ens.dk/da-DK/UndergrundOgForsyning/VedvarendeEnergi/ Vindkraft/Fakta/ Noegletal_statistik/Sider/Forside.aspx, 10.09.12.
2. M. Winter, R. J. Brodd (2004), What are batteries, fuel cells, and supercapacitors?, Chemical Reviews 104: 4245-4269.
3. K.-D. Kreuer, S. J. Paddison, E. Spohr, M. Schuster (2004), Transport in proton conductors for fuel-cell applications: simulations, elementary reactions, and phenomenology, Chemical Reviews 104: 4637-4678.
4. S. J. Osborn, M. K. Hassan, G. M. Divoux, D. W. Rhoades, K. A. Mauritz, R. B. Moore (2007), Glass transition temperature of perfluorosulfonic acid ionomers, Macromolecules 40: 3886-3890.
5. O. Savadogo (2004), Emerging membranes for electrochemical systems, Journal of Power Sources 127: 135-161.
6. I. Dimitrov, S. Takamuku, K. Jankova, P. Jannasch, S. Hvilsted (2012), Polysulfone functionalized with phosphonated poly(pentafluorostyrene) grafts for potential fuel cell applications, Macromolecular Rapid Communications 33: 1368-1374.
7. S. Hvilsted (2012), Facile design of biomaterials by "click" chemistry, Polymer International 61: 485-494.
8. K. Matyjaszewski, J. Xia (2001), Atom transfer radical polymerization, Chemical Reviews 101: 2921-2990.
9. S. Hvilsted (2012), "Click" i polymerer 1, Dansk Kemi 93 (9): 44-46.

Nyt om …

… Frit difluor F₂ i naturen

Fluor, det mest elektronegative grundstof, har hidtil været antaget ikke at findes frit i naturen, da det straks ville reagere med alt. Det er nu blevet påvist, at det findes indesluttet i mineralet antozonit, der er en form af fluorit eller flusspat CaF_2. Antozonit er også blevet kaldt stinkspat eller stinkende fluorit pga. en ubehagelig lugt, der fremkommer, når man knuser mineralet. Der har været mange forslag til, hvad lugten kunne skyldes: - der har været foreslået ozon og forskellige forbindelser af phosphor, arsen, svovl og selen. Henri Moissan der var den første, der fremstillede elementært fluor, foreslog allerede i 1891, at lugten skyldtes fluor; men først nu er det lykkedes at bevise dette.

Man har nu undersøgt antozonit med faststof-NMR og har iagttaget et højtopløst spektrum af ^{19}F, som svarer til spektret af F_2. Man har ud fra spektret kunne udelukke andre oxiderende fluorforbindelser. Og man har ud fra NMR-spektret beregnet, at antozoniten indeholder ca. 0,4 mg F_2 pr. gram mineral. Man har sammenlignet lugten af det knuste mineral med lugten af autentisk F_2 og konkluderer, at de to entydigt har samme lugt.

Nu melder spørgsmålet sig, hvor F_2 kommer fra. Rent CaF_2 er farveløst; bestråles det imidlertid med - eller -stråling bliver det mørkt violet, og antozonit er blåt/violet. Der findes uran og thorium i antozonit; man forestiller sig, at det er strålingen fra spaltningen af ^{238}U og ^{235}U samt -stråling fra deres henfaldsprodukter ^{234}Th, ^{214}Pb, ^{214}Bi, ^{210}Pb, og ^{210}Bi, der spalter CaF_2 og giver anledning til dannelse af F_2.

Carl Th.

III

Dendronised Polymer Architectures for Fuel Cell Membranes

M. M. Nielsen, I. Dimitrov, S. Takamuku, P. Jannasch, K. Jankova, S. Hvilsted

Dendronised Polymer Architectures for Fuel Cell Membranes

Mads M. Nielsen[1], Ivaylo Dimitrov[1], Shogo Takamuku[2], Patric Jannasch[2], Katja Jankova[1] and Søren Hvilsted[1,*]

[1]Danish Polymer Centre, Department of Chemical and Biochemical Engineering, Technical University of Denmark, Søltofts Plads, Building 227, DK-2800 Kgs. Lyngby, Denmark
[2]Department of Chemistry, Polymer and Materials Chemistry, Lund University, P.O. Box 124, SE-22 100 Lund, Sweden

*Corresponding author. E-mail sh@kt.dtu.dk.

Abstract

Multi-step synthetic pathways to low-ion exchange capacity (IEC) polysulfone (PSU) with sulfonic acid functionalized aliphatic dendrons and sulfonated comb-type PSU structures are developed and investigated in a comparative study as non-fluorinated proton exchange membrane (PEM) candidates. In each case the side chains are synthesized and introduced in their sulfonated form onto an azide-functionalized PSU via click chemistry. Three degrees of substitution of each architecture were prepared in order to evaluate the dependence on number of sulfonated side chains. Solution cast membranes were evaluated as PEMs for use in fuel cells by proton conductivity measurements, and in the case of dendronised architectures: thermal stability. The proposed synthetic strategy facilitates exploration of a non-fluorous system with various flexible side chains where IEC is tunable by the degree of substitution.

Keywords: Click Chemistry, Fuel Cells, Polysulfone, Proton Conductivity, Sulfonic Acid.

1 Introduction

Proton exchange membrane fuel cells (PEMFC) and direct methanol fuel cells (DMFC) are attractive power sources for especially the automotive industry as they convert chemical energy to electricity in an environmentally benign way [1]. They can be refueled rather than recharged and the potential in operating lifetime is promising, hence, fuel cells in the automotive industry are facing scheduled commercial upscaling in 2015 [2]. The heart of such fuel cells is the proton exchange membrane (PEM). General requirements to PEMs comprise: proton conductivity, (chemical, mechanical and thermal) stability, fuel (hydrogen or methanol) and oxygen impermeability, and they must be electronically insulating. PEM candidates are designed to meet these criteria by tuning an amphiphilic system, typically constructed from a hydrophobic backbone, that provides support, with hydrophilic moieties. It is through ionic water channels that proton conduction occurs [3, 4]. Being able to control the hydrophilicity/hydrophobicity induced phase-segregation is thus an important tool in the PEM optimization process. The targeted operating conditions are also important to keep in mind as the choice of protogenic group depends on this. Due to their acidity and thermostabilities, sulfonic acid is the best choice at high humidification and low temperature, whereas phosphonic acid usually performs better at a higher temperature and lower humidification [5]. PEMFCs are typically operated at varying humidification levels at 60 - 100 °C [6], which is partly due to the limited properties of current benchmark perfluorosulfonic acid (PFSA) membranes [7], e.g. Nafion[®]. PFSAs suffer from drawbacks like low conductivity at low humidification, relatively low mechanical strength at elevated temperatures and high cost [8-10]. Owing to its superiority over current commercial alternatives, Nafion[®] is a constant subject of study and inspiration as the quest for its successor proceeds. Attempts that address the aforementioned limitations of Nafion[®] include the insertion of hydrophilic inorganic particles into the ionomer [6] and analogue short-side-chain PFSA ionomers [11]. Approaches to non-PFSA polymer designs include partially fluorinated graft copolymers [12], aromatic hydrocarbons [13, 14], blocks [15], acid-base blends [16] and polybenzimidazoles (PBI) or benzimidazole(s) tethered onto polysulfone (PSU) as high-temperature membranes [17-19]. Some of the systems that have been studied extensively are early version candidates with a commercial perspective, whereas others are merely model systems for investigation of structure-property relationships. The latter is usually done through systematic alterations of single parameters, e.g. choice of backbone, degree of sulfonation (DS), chemical architecture etc. Another factor is the positioning of the acid group. For instance, ionomers with sulfonic acid groups covalently linked to the backbone are reported to result in increased membrane water swelling [20]. Examples of common spacers for separating the sulfonic acid group from the main chain are: 1) shorter aliphatic side chains (these could also be used for cross-linking [21]), 2) sulfonated grafts [12], 3) aromatic linear side chains [13], and 4) aromatic dendritic side chains [13]. However, it appears that little – if any – work is published on aliphatic dendritic side chains though such a system intuitively seems promising. The introduction of flexible aliphatic chains is believed to facilitate phase segregation and hydrophilic domain connectivity, which are known to provide good proton conductivity and less dependence on hygroscopy [22].

The present work is based on this concept, applying non-fluorous commercially available PSU (T_g = 189 °C) as backbone. PSUs have previously proven good film forming properties [21] and show high thermal and chemical resistance and stability under steam oxygen and steam hydrogen atmospheres up to 200 °C [23]. Dendrons are introduced onto the azide-functionalized PSU (**PSU-N**) by copper-catalyzed azide-alkyne cycloaddition (CuAAC) (click chemistry) [24], thus enabling an enhanced phase segregation due to acid-base interactions between the resulting Brønsted base 1,2,3-triazole (pK_B = 0 - 1) [25] and neighboring –SO_3H groups. For comparison two linear monosulfonated side chains of different length are clicked onto **PSU-N**, resulting in different comb-type architectures. Recently phosphonated grafts were clicked onto a similar system by our group [26], and it was shown that introduction of this spacer did not reduce thermal stability. Lithiation chemistry was used for this introduction as earlier studies proved ortho-sulfone substituted PSU to be more stable than meta-sulfone substituted PSU [27]. To evaluate the influence of graft length two different spacers between –SO_3H and the 1,2,3-triazole ring are investigated. Keeping the backbone length fixed three different degrees of substitution are applied in the evaluation of the effect thereof. An analogue use of click chemistry directly from a PSU backbone followed by cross-linking is reported to reduce methanol crossover and give proton conductivities comparable to Nafion[®] [21]. The same group recorded low conductivities when omitting cross-linking and using linear chains, thus the present system is incorporating a spacer between the azide and the PSU backbone. Huang et al. published on non-covalent acid-base interactions to mediate physical cross linking of sulfonated polytriazole with resulting well-connected ion channels, suppressed membrane swelling and improved proton conductivity [28]. Furthermore, click chemistry with PSU has previously shown promising results for bioapplications [29]. In addition to this, imidazoles are described as proton conductivity enhancers by blending with sulfonated poly(ether ether ketone) [16].

The present work is intended as a proof-of-concept study of such a non-fluorous architecture. Consequently, sulfonated hydrocarbon dendrons are used, and not fluoroalkylsulfonic acids (super acids), although they are known to generate higher proton conductivities [3].

2 Experimental Section

2.1 Materials

The chemicals were purchased from Aldrich unless otherwise stated and used as received: *n*-butyllithium (BuLi, in hexanes, 2.5 M, Acros), 3-(chloromethyl)benzoyl chloride (3-cmbc, Acros, 98%), 4-(chloromethyl)benzoyl chloride (4-cmbc, Acros, 97%), sodium sulfite (anhydrous, Merck), sodium azide (NaN$_3$, 99%), propargyl bromide (in toluene, 80%), propargyl alcohol (99%), sodium hydride (NaH, dry, 95%), 1,3-propanesultone (98%), copper(I)bromide (CuBr, 98%), Dowex$^®$ (H) resin (DR-G8, dry), 3-bromopropane-1,2-diol (97%), 2,2-dimethoxypropane (98%), DL-1,2-isopropylideneglycerol (98%), Merrifield's peptide resin (1.0-1.5 mmol/g Cl$^-$ loading), Dialysis tubing (benzoylated, cut off 1,200 Da), toluene-4-sulfonic acid monohydrate (Fluka), sulfuric acid (H$_2$SO$_4$, 96%, chemically pure), magnesium sulfate (MgSO$_4$, anhydrous), 2-propanol (IPA, Honeywell), methanol (MeOH >99.9%), acetone (>99%), *N,N*-dimethylformamide (DMF, anhydrous, 99.8%), methylsulfoxide (DMSO ≥99%), dichloromethane (DCM >99.8%), chloroform-*d* (CDCl$_3$, 99.8%) and deuterium oxide (D$_2$O, 99.9 atom% D). Tetrahydrofuran (THF, Fisher Scientific) and DMSO-*d$_6$* (99.9 atom% D) were

dried on 4 Å molecular sieves prior to use. PSU (Udel P-3500 LCD MB8, $\overline{M}_n$ = 40,000 Da, PDI = 1.95, Solvay Advanced Polymers) was dried in oven before use.

2.2 Polysulfone with pendant chloromethylbenzoyl groups (PSU-Cl)

PSU was functionalized with chloromethylbenzoyl side groups by a previously reported method [26]. 7 g of pre-dried Udel$^®$ was dissolved in 350 mL dry THF overnight and placed in a round-bottom glass reactor equipped with a stirring bar, a thermometer, a rubber septum and a gas inlet. A blanket of argon was applied during cooling to -60 °C, then 7 degassing cycles were carried out and BuLi (1.2 eq of the desired degree of substitution (DS)) was added still under argon with a gas tight syringe to activate the ortho position to the SO$_2$ group [30]. After 1 hour the colorless solution changed via green to light brown. Chloromethylbenzoyl chloride was added with a gas tight syringe. Both meta and para substituted versions were used. Due to different melting points the liquid meta form was degassed directly, whereas the solid para form was diluted in THF first. The lithiated sites were thereby quenched over 30 min. (color change via orange to yellow). After heating to room temperature (RT) the modified polymer was precipitated and purified in IPA for several hours, then filtered and stirred in demineralized water overnight, filtered again, then dried, stirred in methanol overnight, filtered and dried in vacuum oven at 60 °C overnight. The resulting white solid **PSU-Cl** precursors carried on average 18, 25, 54 or 67 chloromethyl groups per 100 repeat units respectively. Table 1 summarizes the reaction ratios. ^{1}H NMR (300 MHz, chloroform-*d*, δ (ppm)): 8.05-6.80 (Ar *H, PSU* + substituted PSU), 4.61-4.56 (Ar-C*H$_2$*-Cl), 1.79-1.59 ppm (C-(C*H$_3$*)$_2$). FTIR (cm^{-1}): 1674 (C=O), 1583 and 1488 (Ar C=C), 1445 and 1364 (CH$_3$), 1237 (C-O-C), 1169 and 1151 (O=S=O), 1103, 1082 and 1012 (Ar ring).

Table 1 Chemical compositions of the click precursors.

Sample	PSU:BuLi:(electrophile)	DS$_{actual}$ %	Electrophile
PSU-Cl$_{0.18}$	1:0.5:0.6	18	3-cmbc
PSU-Cl$_{0.25}$	1:0.5:0.6	25	4-cmbc
PSU-Cl$_{0.54}$	1:1.2:1.2	54	4-cmbc
PSU-Cl$_{0.67}$	1:1.2:1.2	67	3-cmbc

2.3 Polysulfone with pendant azidomethylbenzoyl groups (PSU-N)

PSU-N was prepared according to literature [26]. **PSU-Cl** was stirred in a round-bottomed flask with 15 times (wt.) DMF, under nitrogen at RT. 2 eq NaN$_3$ were added and the reaction proceeded as the color changed from brown over orange to yellow/white. The mixture was poured into demineralized water and stirred for at least 1 h. After decantation the white precipitate was stirred in water for 1 h. This procedure was repeated twice before filtration and drying in vacuum oven at 80 ^{o}C. ^{1}H NMR spectroscopy (300 MHz, chloroform-*d*, δ (ppm)): 8.05-6.80 (Ar *H*, PSU + substituted PSU), 4.45-4.25 (Ar-C*H$_2$*-N$_3$), 1.79-1.59 ppm (C-(C*H$_3$*)$_2$). FTIR (cm^{-1}): 2097 (N$_3$), 1678 (C=O), 1585 and 1488 (Ar C=C), 1445 and 1364 (CH$_3$), 1228 (C-O-C), 1168 and 1151 (O=S=O), 1106, 1088 and 1014 (Ar ring).

2.4 Synthesis of sodium prop-2-yne-1-sulfonate [HC≡CCH$_2$SO$_3^-$Na$^+$] (1fS)

The short monosulfonated linear side chain, **1fS** (1-functional Short), was prepared according to literature [31]. 1 eq propargyl bromide solution and 1.25 eq sodium sulfite in (methanol/deionized water = 1:1) = 1:3 (vol.) were stirred overnight in a round bottom flask at 65 ^{o}C with a condenser, then the temperature was decreased to RT and the reaction mixture stirred overnight. The reaction mixture was then poured into methanol under stirring, filtered and concentrated on rotary evaporator. By addition of acetone white particles precipitated, and further cooling in a fridge enhanced the precipitation. The mixture was filtered and dried in vacuum oven at RT overnight. ^{1}H NMR (300 MHz, DMSO-d_6, δ (ppm)): 3.75 (CH_2-SO$_3^-$Na$^+$), 2.62 (*H*-C≡C). FT-IR (cm^{-1}): 3281 (C≡C), 1039 and 1178 (O=S=O).

2.5 Synthesis of 3-(prop-2-ynyloxy)propane-1-sulfonate [HC≡CCH₂O(CH₂)₃SO₃⁻Na⁺] (1fL)

The long monosulfonated linear side chain, **1fL** (1-functional Long), was prepared by the Williamson ether synthesis, using conditions similar to previously reported sulfopropylation of poly(2,3,5,6-tetrafluoro-4-hydroxystyrene) [32]. Propargyl alcohol was activated with NaH in DMF at 0°C followed by nucleophilic ring-opening of cyclic sulfonate (1,3-propanesultone) at RT. ^{1}H NMR (300 MHz, D$_2$O, δ (ppm)): 4.25 (O-CH_2-CH$_2$), 3.74 (C≡C-CH_2-O), 3.00 (*H*-C≡C + CH_2-SO$_3^-$Na$^+$), 2.06 (CH$_2$-CH_2-CH$_2$). FTIR (cm^{-1}): 3287 (C≡C), 1048 and 1182 (O=S=O).

2.6 Synthesis of 2f

The bisulfonated first generation (1G) dendron, 2f (2-functional), was prepared according to Scheme 1.
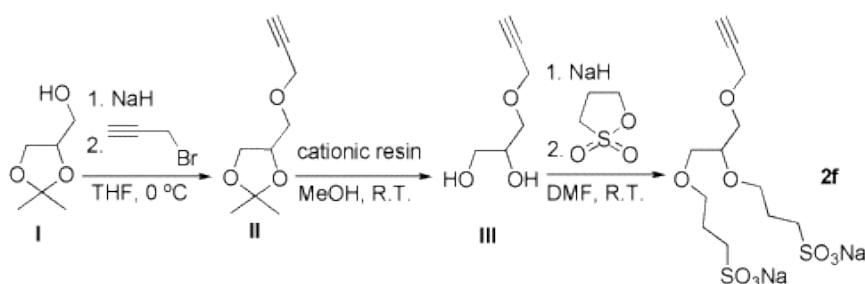
Scheme 1 Synthesis of the bisulfonated dendron.

2.6.1 Synthesis of II

DL-1,2-isopropylideneglycerol was activated with 1.7 eq NaH in dry THF = 1:5 (vol.) at 0 ^{o}C by drop wise addition over 30 min under nitrogen in a round-bottom flask on an ice/water bath. The color changed from sand over orange to light brown. The mixture was stirred for 50 min., and then 2 eq propargyl bromide was added to the addition funnel with a nitrogen purged syringe facilitating dropwise addition without admitting deactivating air to the system. Stirring for at least 1 h followed, and the color changed to dark brown. The reaction mixture was quenched with ultrapure water, and then THF was removed by rotary evaporation. After addition of DCM the solution was extracted with 2 times (vol.) saturated aqueous NaCl and 3 times (vol.) ultrapure water. The organic phase was then dried with MgSO$_4$ and concentrated on rotary evaporator. ^{1}H NMR (300 MHz, chloroform-d, δ(ppm)): 4.33 (CH$_2$-CH-O), 4.25-4.24 (C≡C-CH_2-O), 4.13-4.08 and 3.80-3.75 (CH$_2$-O-CH_2-CH), 3.63-3.61 (CH-CH_2-O-C), 2.50 (*H*-C≡C), 1.46 and 1.40 (C-(CH_3)$_2$). FTIR (cm^{-1}): 3273 (C≡C), 1456 (CH$_2$), 1371 (CH$_3$), 1213 (C-O-C).

2.6.2 Synthesis of III

In the typical case deprotection was done by stirring **II** overnight in methanol with a cationic resin under nitrogen at 45 °C. The product after rotary evaporation was a yellow oil (see assigned ^{1}H NMR spectrum in Fig. S3 in the Supporting Information). ^{1}H NMR (300 MHz, DMSO-d_6, δ (ppm)): 4.72-4.70 (CH-OH), 4.53 (CH$_2$-OH), 4.13-4.12 (O-CH_2-C≡C), 3.56 (CH-OH), 3.39 and 3.48-3.43 (CH_2-OH), 3.35-3.31 (O-CH_2-CH + H$_2$O) 3.29 (*H*-C≡C). FTIR (cm^{-1}): 3376 (OH, H-bonded), 3287 (C≡C), 1211 (C-O-C).

2.6.3 Sulfopropylation of III

The diol, **III**, was activated with 1.9 eq NaH in DMF at 0 °C, then 1,3-propanesultone in a few mL DMF was added drop wise to control the nucleophilic ring-opening. The mixture was heated to RT and stirred overnight. The resulting gel was dissolved in MeOH, whereupon the mixture was filtered and the filtrate concentrated on a rotary evaporator, before being poured into hot acetone. Hot suction filtration and drying in vacuum oven overnight at 50 °C followed. Analyses showed solvent residues in the orange solid, hence an excess of **2f** was used in the following click reactions. ^{1}H NMR (300 MHz, DMSO-d_6, δ (ppm)): 4.14 (C≡C-CH_2), 3.70-3.27 (C≡C-CH$_2$-O-CH_2-CH, CH-O, CH-CH_2-O-(CH$_2$)$_3$, O-CH_2-CH$_2$-CH$_2$ + H$_2$O), 2.57-2.38 (H-C≡C, O-CH$_2$-CH_2-CH$_2$, CH_2-SO$_3$Na + DMSO), 1.83-1.67 (O-CH$_2$-CH_2-CH$_2$, CH_2-SO$_3^-$Na$^+$). Solvent peaks appeared at 3.20 (MeOH), 2.89 and 2.73 (DMF), 2.09 (acetone). FTIR (cm^{-1}): 3274 (C≡C), 1443 (CH$_2$), 1183 and 1043 (O=S=O).

Tetrasulfonated second generation (2G) dendrons were prepared by similar chemistry (see Scheme S2 in the Supporting Information). Preliminary results from the synthesis are included in the Supporting Information.

2.7 Synthesis of comb-shaped architectures

Comb-shaped architectures were prepared according to Scheme 2. In a typical click reaction **PSU-N** was stirred with 5 eq **1fS** / 3 eq **1fL**, 0.4 eq CuBr in DMF whilst purging with nitrogen for 30 min. The reaction mixture was then left at 60 °C overnight. The color changed from green to brown as the reaction mixture partially turned into a gel. The polymers were precipitated from and purified in demineralized water and then dried in vacuum oven at 50 °C overnight. A higher purity product was obtained when dialyzing against demineralized water. Freeze-drying the product resulted in a fluffy, slightly colored powder. ^{1}H NMR (300 MHz, DMSO-d_6, δ (ppm)): 8.11 (N-CH=C), 7.89-6.80 (H Ar), 5.67 (N-CH_2-Ar), 4.44 (C=C-CH_2-O), 3.48 (O-CH_2-CH$_2$), 2.25 (CH$_2$-SO$_3^-$Na$^+$), 1.80 (CH$_2$-CH_2-CH$_2$), 1.64 (C-(CH$_3$)$_2$). FTIR (cm^{-1}): 1679 (C=O), 1585, 1503 and 1488 (C=C Ar), 1364 (CH$_3$), 1227 (C-O-C), 1188 and 1044 (O=S=O acid), 1168 and 1151 (O=S=O PSU).
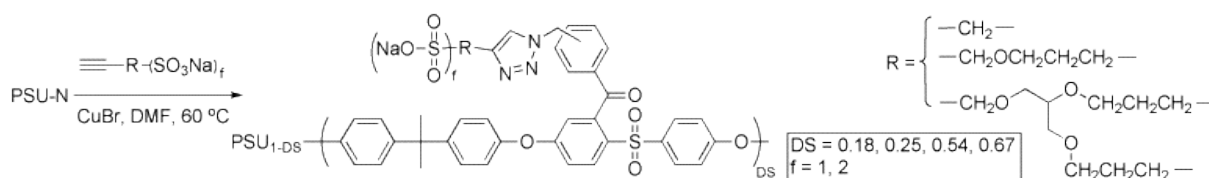
Scheme 2 The general case of click reactions with pre-sulfonated side chains.

2.8 Synthesis of bisulfonated dendronised architectures (PSU-2f)

Two different synthetic routes to **PSU-2f** are applied, 1) clicking **2f** onto **PSU-N** in a pre-sulfonated approach, and 2) clicking **III** onto **PSU-N** followed by post-sulfonation.

2.8.1 Synthesis by pre-sulfonation

Bisulfonated 1G dendronised architectures were prepared according to Scheme 2. The typical click reaction was performed under similar conditions to those described for the comb-shaped structures but with 2.5 eq **2f**. The color changed from yellow to orange as the reaction proceeded. In the typical case azide functionalized Merrifield's resin [33] was added towards the end of the click reaction between **PSU-N** and **2f** to react with excess **2f** overnight, still at 60 °C. The slightly colored compounds were isolated by dialysis against demineralized water and subsequently freeze-dried to a fluffy powder. ^{1}H NMR (300 MHz, DMSO-d_6, δ (ppm)): 8.12 (N-CH=C), 7.90-6.60 (H Ar), 5.60 (N-CH_2-Ar), 4.50 (C=C-CH_2-O), 3.95-2.95 (O-CH_2-CH$_2$, O-CH_2-CH-O, CH$_2$-CH-CH$_2$, CH-CH_2-O-CH$_2$-CH$_2$), 2.38 (CH_2-SO$_3$Na), 1.83 (CH$_2$-CH_2-CH$_2$), 1.64 (C-(CH$_3$)$_2$). FTIR (cm^{-1}): 1679 (C=O), 1586, 1504 and 1489 (C=C Ar), 1229 (C-O-C), 1168 and 1151 (O=S=O PSU), 1039 (O=S=O acid).

2.8.2 Synthesis by post-sulfonation

The approach of clicking before sulfonating was attempted by similar chemistry as previously stated by first clicking **III** onto **PSU-N** and then ring-opening of the 1,3-propanesultone. The diol dendronised PSU was successfully synthesized: ^{1}H NMR (300 MHz, DMSO-d_6, δ (ppm)): 5.67 (Ar-CH_2-N), 4.64 (OH), 4.49 (C=C-CH2-O). FTIR (cm^{-1}): 3431 (OH H-bonded), no azide signal. ^{1}H NMR (300 MHz, DMSO-d_6) of the sulfonated product was similar to that obtained by pre-sulfonation (a full NMR spectrum is included as Fig. S6 in the Supporting Information). FTIR (cm-1): 1678 (C=O), 1585, 1504 and 1489 (C=C Ar), 1226 (C-O-C), 1168 and 1151 (O=S=O PSU), 1040 (O=S=O acid).

2.9 Membrane preparation

An amount of 30 mg click product was dissolved in 5-10 mL of DMSO under heating and subsequently concentrated to the appropriate viscosity for solvent casting on two leveled 4 cm x 1 cm glass slides at ~80 °C. When all solvent had evaporated the membranes were dried overnight in a vacuum oven at 80 °C. Detachment of membranes from the glass substrate proceeded easily by immersion in demineralized water. Acidification of the sodium salt membranes was done by stirring for 1 h in 1M aqueous H_2SO_4, followed by stirring for 1 h in demineralized water - both at 80 °C. Subsequently the water was changed several times until neutral pH. The membranes were stored in demineralized water until conductivity measurements were carried out shortly after. The obtained wet film thicknesses ranged from 11 to 118 μm (the wet thickness of internal reference, Nafion® 212 [**N212**], was 7 μm).

2.10 Measurements

NMR spectra were recorded in chloroform-d or DMSO-d_6 using a Bruker spectrometer at a resonance frequency of 300 MHz. Reference signals in ^{1}H NMR were 2.50 ppm of DMSO-d_6, 7.26 ppm of chloroform-d and 4.79 ppm of D_2O. When solubility was poor ultrasonication and moderate heating was applied.

FT-IR analyses were conducted on a Perkin-Elmer Spectrum One instrument in the range of 4000-650 cm^{-1} and 16 scans were used.

The thermal stability was studied by thermogravimetric analysis (TGA) with a heating speed of 20 °C/min from RT to 650 °C under nitrogen on a TA Instruments TGA Q500. Before commencing analyses the membranes in acidic form were kept under vacuum at 90 °C for one hour and then 60 °C overnight to remove solvent residues. The degradation temperature was noted at 10% weight loss ($T_{d\ 10\%}$).

Differential scanning calorimetry (DSC) was conducted on the acidic membranes with a heating speed of 10 °C/min from RT to 220 °C under nitrogen on a TA Instruments DSC Q1000. Data collection was performed during the third heating cycle from RT to 220 °C. Thermal responses, including glass transition temperatures (T_g) were calculated from the third heating cycle.

Proton conductivities of the membranes were measured by use of a homemade bench with two electrodes for in-plane conductivity measurements, a GW Instek laboratory DC power supply, model GPS-3030DD and two Fluke True RMS Multimeter 189.

For the water uptake measurements each membrane was dried in vacuum oven overnight at 80 °C and subsequently stored in desiccator for half a day at RT before obtaining the dry weight. After overnight soaking in water careful removal of surface water with lense paper the wet weight was recorded.

The film thickness was measured with a Mitutoyo Digimatic Micrometer.

2.11 Calculations

The DS is calculated from the ^{1}H NMR of **PSU-Cl** by dividing half the integral value of the introduced CH_2Cl by one sixth of that of C(CH_3)$_2$ from the backbone.

The IEC, i.e. the inverse equivalent weight (EW^{-1}) [meq g^{-1}], of the membranes was calculated from from Eq. (1), where DP$_{\textbf{PSU}}$ is the degree of polymerization of **PSU** ($\overline{M}_{n\ PSU}$ = 40 kDa, determined by gel permeation chromatography (in CHCl$_3$)), DS is the degree of sulfonation of the side chains (assumed to be 100%) and f is the number of –SO$_3$H groups of the side chain:

$$IEC = EW^{-1} = \frac{DP_{PSU} \times DS \times f}{\overline{M}_{n\ (incl.-SO_3H)}} \times 1000$$

(1)

The water uptake [wt%] is calculated from Eq. (2) as the weight gain of a dry film after immersion in water, where m$_{wet}$ is the wet weight and m$_{dry}$ is the dry weight:

$$Water\ uptake = \frac{m_{wet} - m_{dry}}{m_{dry}} \times 100$$

(2)

3 Results and Discussion

The structure relationship between the various synthesized architectures is showed in Scheme 3. **PSU** is modified to four degrees of azide-content (or DS). Series of three different DS are applied in the click reaction with two different lengths of sulfonated linear side chains and a bisulfonated dendron. **PSU-2f** prepared by

sulfonation before and after the click reaction are compared. Due to generally reduced resolution in NMR yields are not stated.
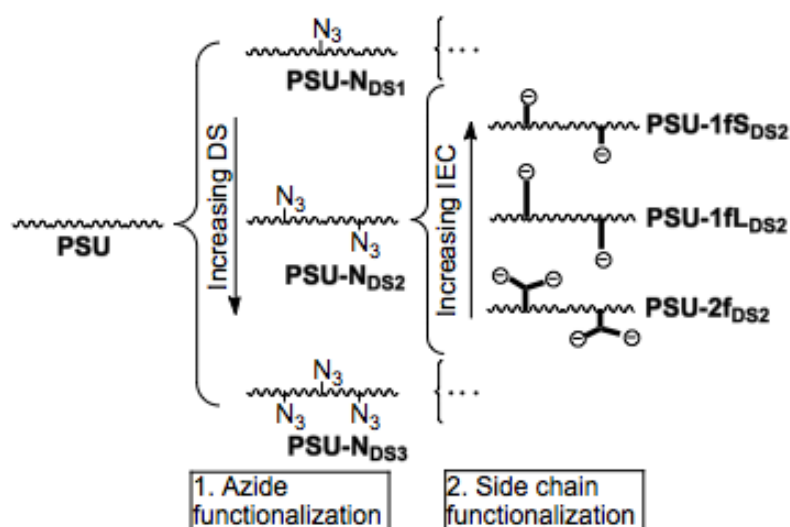
Scheme 3 The structure relationship between the various synthesized architectures.

3.1 Polysulfone with pendant azidomethylbenzoyl groups (PSU-N)

The PSU backbone was lithiated and reacted with 3-cmbc or 4-cmbc. Four different DS were obtained: 18%, 25%, 54% and 67% (digital number 0.18, 0.25, 0.54 and 0.67 are used in the following). Table 1 summarizes these along with the used stoichiometries. 4-cmbc as side group was originally chosen due to its symmetry but was later abandoned for 3-cmbc that was easier to work with, due to a lower melting point. No remarkable differences were observed between products made from these different compounds. DS was calculated from the main chain methyl protons at 1.79-1.59 ppm and the chloromethyl protons of the spacer at 4.61 ppm in 1D ^{1}H NMR. The chlorine was easily and quantitatively substituted by azide during the overnight reaction with NaN_3 at RT, as the methylene peak shifted upfield to 4.40-4.30 ppm by azide-functionalization, leaving no signal of its precursor. It was noted that when carrying out the reaction at elevated temperatures (80 °C) an insoluble product was formed. A stacked view of ^{1}H NMR spectra of **PSU**, **PSU-Cl**, **PSU-N** is provided in the Supporting Information (Fig. S2).

3.2 Syntheses of linear side chains 1fS and 1f L

The substitution of bromine with $-SO_3^-Na^+$ to give **1fS** and the sulfopropylation of propargyl bromide to resulting **1fL** were proved by FTIR and ^{1}H NMR.

3.3 Synthesis of bisulfonated 1G dendron, 2f

Activation of DL-1,2-isopropylideneglycerol, introduction of triple bond functionality and subsequent deprotection of diol proceeded successfully (see Fig. S3 in the Supporting Information for assigned ^{1}H NMR spectrum). Activation and ring-opening of the 1,3-propanesultone was performed near-quantitatively. Fig. 1 shows the assigned ^{1}H NMR spectrum with identified solvent residues based on values from literature [34]. The multiplets at 3.70-3.27 ppm and 2.57-2.38 are overlapping with H_2O and DMSO, thus the C≡C-CH_2-O protons at

4.14 ppm and the CH_2-$SO_3^-Na^+$ and CH_2-CH_2-CH_2 at 1.83-1.67 ppm are used in the calculations.
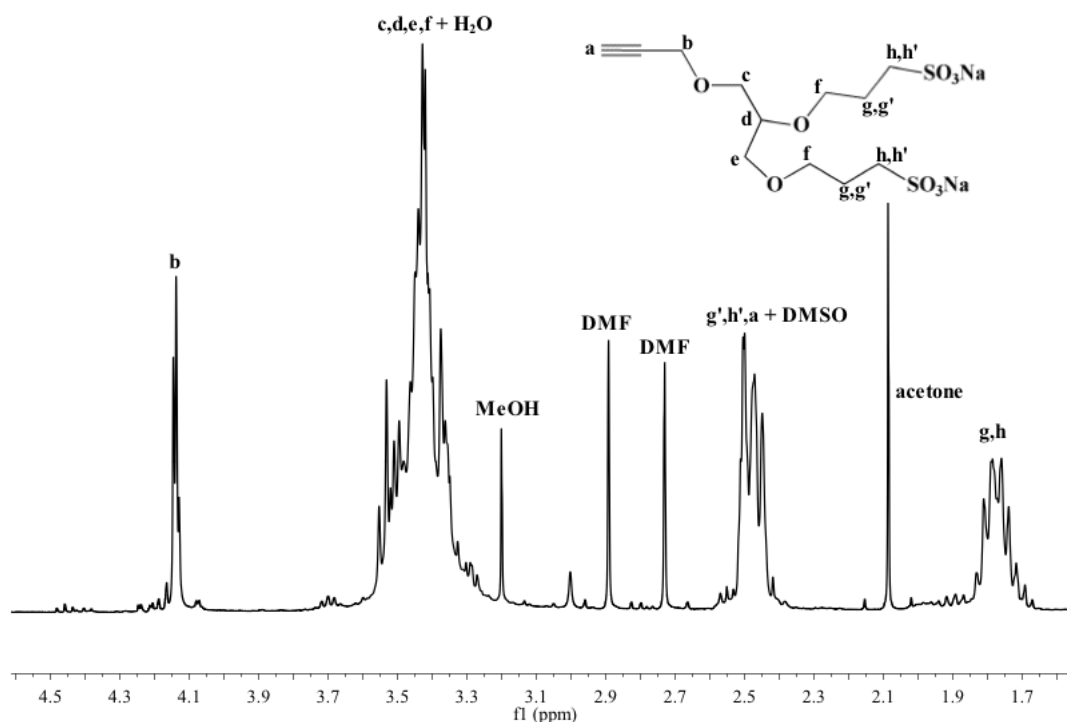

Fig. 1 ^{1}H NMR spectrum of **2f** in sodium form.

3.4 Synthesis of sulfonated click products

Fig. 2 shows an overlay of partial IR spectra of **PSU-Cl**, **PSU-N**, **PSU-1fS**, **PSU-1fL** and **PSU-2f**, all at DS = 0.67. The characteristic peak of -N_3 around 2097 cm^{-1} has disappeared for all click products, which indicates full conversion. Moreover, the band characteristic for the O=S=O of the attached sulfonates appeared at 1044-1040 cm^{-1}.
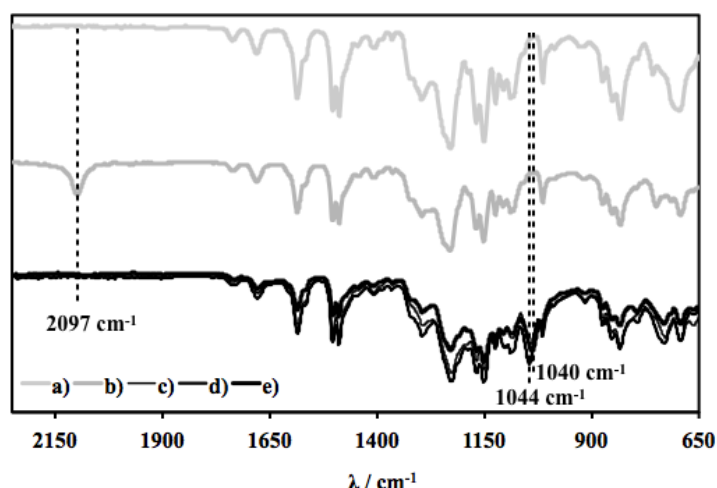
Fig. 2 Overlay of partial IR of a) **PSU-Cl$_{0.67}$**, b) **PSU-N$_{0.67}$**, c) **PSU-1fS$_{0.67}$**, d) **PSU-1fL$_{0.67}$**, e) **PSU-2f$_{0.67}$**.

3.4.1 Comb-type PSU architectures

Comb-type PSU architectures were prepared successfully from **PSU-N** (DS = 0.25, 0.54 and 0.67). In NMR the methylene peak of the benzoyl spacer shifted to 5.67 ppm; the 1,2,3-triazole proton appears at 8.11 ppm. Furthermore, the C=C-$CH_2SO_3^-Na^+$ of **PSU-1fS** appears at 2.25 ppm and C=C-CH_2-O of **PSU-1fL** at 4.44 ppm (assigned ^{1}H NMR spectra are included in the Supporting Information in Fig. S4 and Fig. S5).

8

3.4.2 Dendronised PSU architectures, PSU-2f

Dendronised PSU architectures were successfully synthesized from **PSU-N** (DS = 0.18, 0.54 and 0.67). 18% DS was used instead of 25% (used with comb-type architectures) for practical reasons. ^{1}H NMR showed a shift of the methylene peak next to the benzoyl spacer from 4.4-4.3 ppm to 5.6 ppm, as the azide was turned into a 1,2,3-triazole. **PSU-2f** prepared by the pre-sulfonation and post-sulfonation routes showed only minor differences in NMR that can probably be ascribed to the imperfect solubility caused by the amphiphilic nature of the compounds. An overlay of both compounds is included as Fig. S6 in the Supporting Information.

3.5 Thermal properties

The thermal properties of the sulfonated dendronised structures, along with precursor **PSU** and **N212** for comparison, were quantified by glass transition temperatures (T_g)/exothermal responses (T_{exo}) and decomposition temperatures at 10% ($T_{d\ 10\%}$) as summarized in Table 2. The TGA curves of the sulfonated dendrons and reference **PSU** are shown in Fig. 3A. The weight losses from RT up to 150 °C are attributed to solvent residues in the polymer as previously described [26] thus 100 wt% is defined at this temperature. The observed initial weight losses up to 370 °C are attributed to the decomposition of the dendrons, whereas the main degradation hereafter is related to that of the backbone. As expected the trend is that the more dendrons are attached to the backbone the larger the ratio of initial loss to main loss. The DSC curves of the sulfonated dendrons are shown in Fig. 3B. There appears to be two exothermal responses that are almost identical for the three different DS of **PSU-2f**. Furthermore there is an exothermal response at 162 °C for **PSU-2f$_{0.18}$** that might be hidden in the curves of the higher DS systems. The peak maximum at 188-191 °C suggests a relation to the T_g of the PSU backbone. From literature it is known that sulfonation of PSU induces an increase in Tg as the ionic concentration is enhanced [35, 36]. However, situations where T_g is lowered upon sulfonation include: when residual solvent serves as plasticizer in the membrane and increases chain mobility or in the case of sulfonation of polycarbonate and polystyrene [35, 37] or upon introduction of aliphatic side chains [38]. The change from the classical S-shape that is observed with **PSU** is attributed to annealing effects, possibly including a degree of cross-linking of the –SO$_3$H groups. A similar effect is described in literature [37], and furthermore the curve shape of **N212** is similar to that of the **PSU-2f** samples, and thus different from unannealed Nafion® [38]. The smaller peak at 85-86 °C is also observed when analyzing the isolated dendrons, indicating that this is a transition temperature of the dendritic side chains. As the thermal stability of the dendronised structures is reduced by the introduction of aliphatic dendrons this system will not be suited for operation at higher temperatures, but with offset in the operating range of Nafion® in humidified systems below 100 °C a T_g of 85-86 °C is not enough to rule out this candidate.

Table 2 Properties of selected membranes.

Sample	T_{peak} / °C			$T_{d\ 10\%}$ / °C	IEC$_{NMR}$[c] / meq g^{-1}	σ / mS cm^{-1}	WU / wt%
PSU-1fS$_{0.25}$	-			-	0.49	<1	7
PSU-1fS$_{0.54}$	-			-	0.91	<1	12
PSU-1fS$_{0.67}$	-			-	1.06	1	14
PSU-1fL$_{0.18}$	-			-	0.47	<1	5
PSU-1fL$_{0.54}$	-			-	0.86	2	11
PSU-1fL$_{0.67}$	-			-	1.00	2	28
PSU-2f$_{0.18}$	86	162	188	340	0.33	12	19
PSU-2f$_{0.54}$	86		191	307	0.74	24	25
PSU-2f$_{0.67}$	85		190	292	0.84	62	141
PSU		189[a]		527	-	-	-
N212		120[a,b]		352	0.91[d]	92	19

[a]T_g.; [b]Nafion® NRE 212 value from literature [26]; [c]calculated values assuming complete click reaction and 100% sulfonation; [d]Product specifications.
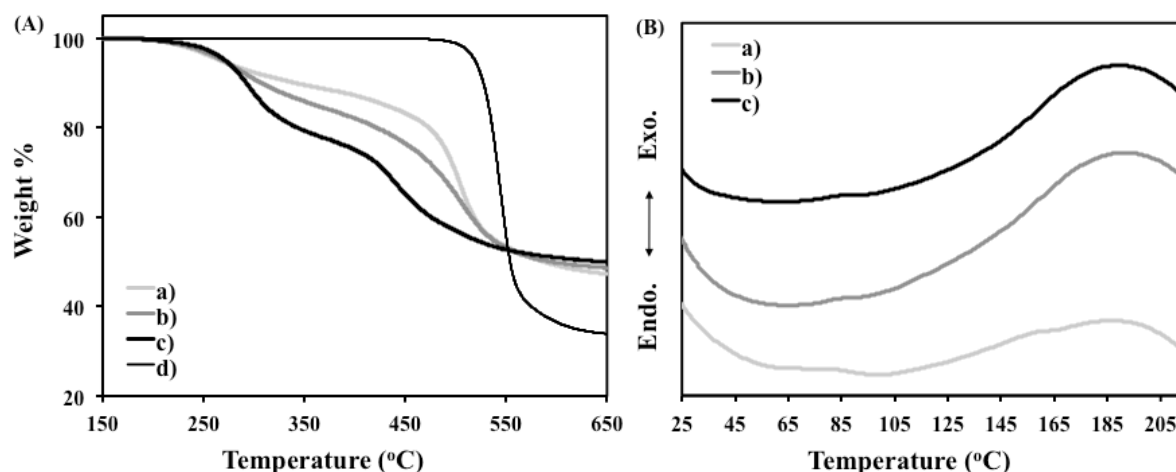
Fig. 3 (A) TGA curves and (B) DSC curves. a) **PSU-2f$_{0.18}$**; b) **PSU-2f$_{0.54}$**; c) **PSU-2f$_{0.67}$**; d) **PSU**.

3.6 Membrane properties.

The sulfonated click products showed low solubility in DMSO at room temperature, so the temperature was increased to ~80 °C, which resulted in slightly colored (comb-type: yellow, and dendronised: red) clear solutions. Homogenous films were obtained when solution casting from concentrated solutions, still at 80 °C, whereas room temperature cast films were visibly inhomogeneous. A previously used way to cast the films under a blanket of nitrogen [36] was applied with no remarkable difference in membrane performance from when cast in air. Therefore this procedure was adapted. During the membrane acidification in 1M H_2SO_4 followed by demineralized H_2O, both for 1 h at 80 °C the membranes changed color to various shades of brown. Membranes prepared by postsulfonation fell apart during this treatment; meanwhile presulfonated comb-type structures and dendronised structures were strong enough to withstand both acidification and proton conductivity measurements.

Fig. 4A shows the proton conductivity-dependency under fully immersed conditions at room temperature on ionic content for the sulfonated archtectures, including **N212** for comparison. Table 2 contains a membrane property summary. The proton conductivities of comb-type architectures **PSU-1fS** and **PSU-1fL** range from 0 to 2 mS cm^{-1}, which is the same order of magnitude as those of resembling architectures (same backbone, no aromatic spacer and two short side chains on the same repeat unit) presented by Bielawski and coworkers [21]. The obtained values of the linear side chain products were too low to consider a trend in the influence of chain length. Likewise, there was no clear trend in the contribution of ionic content, e.g. **PSU-1fS$_{0.25}$** and **PSU-1fS$_{0.54}$** showed similar conductivities (0.3 mS cm^{-1}). The main reason for these low conductivities is believed to be the low IEC values - as is also the case for poly(arylene ether) sulfonated directly to the backbone in ortho position [27] - and poor phase segregation as a result thereof. The water uptake study is shown in Fig. 4B. A linear trend in water uptake by increasing the IEC is indicated for **PSU-1fS**, and - except **PSU-1fL$_{0.67}$** - equally low values are obtained for the longer side chains **PSU-1fL**. This observation supports the low proton conductivities.

The dendronised architectures show a rather different behavior. At IEC = 0.33 meq g^{-1} the conductivity of **PSU-2f$_{0.18}$** is 12 mS cm^{-1}, and at IEC = 0.74 meq g^{-1} the conductivity of **PSU-2f$_{0.54}$** is 24 mS cm^{-1}. However, when further increasing the ionic content to IEC = 0.84 meq g^{-1} the proton conductivity of **PSU-2f$_{0.67}$** reaches 62 mS cm^{-1}, i.e. five times higher than at one third the IEC, and a factor of 30 higher than the equivalent comb-type architectures. Due to the contribution of the large dendritic spacer to the IEC calculations this is even obtained at a lower IEC than of the comb-type architectures. A similar trend in the water uptake is observed, with a remarkable increase happening from sample **PSU-2f$_{0.54}$** to **PSU-2f$_{0.67}$**, i.e. 25 wt% vs 141 wt%. This suggests that an increased percolation of the proton conducting water system is occurring around these compositions. The dendronised architectures show much higher conductivities but also at much higher water sorption. The higher water uptake and conductivities of the dendronised system are believed to be caused by the increased flexibility of the groups separating the sulfonic acid groups.

From the observations of increased conductivity by introduction of ionic groups plus the postulated change in connectivity between the ionic groups over a short IEC-interval, it seems feasible that higher conductivities of both dendronised and comb-type architectures can be reached by tuning the ionic content.
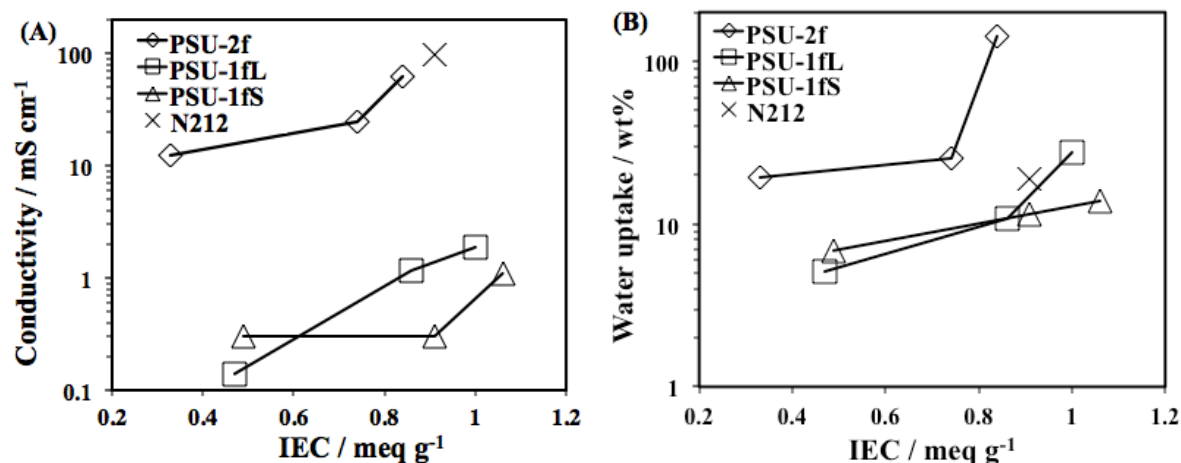
10

Fig. 4 (A) Proton conductivity and (B) water uptake plotted against calculated IEC values.

4 Conclusions

Novel, non-fluorous architectures of PSU tethered with bisulfonated aliphatic dendrons were synthesized and evaluated in a comparative study with monosulfonated aliphatic comb-type PSU structures, in a range of low IEC values (0.33-1.06 mS cm^{-1}). All polymer systems were synthesized in a combination of polymer modifications and click chemistry. Due to the high efficiency of the click reaction, DS is controlled through the degree of lithiation of the pristine PSU. Films were solvent cast from DMSO at 80 °C, and whereas membranes of dendronised structures prepared prior to sulfonation disintegrated during the protonation treatment, membranes prepared by clicking presulfonated side chains onto the PSU backbone withstood protonation as well as proton conductivity measurements. Proton conductivity at room temperature under fully hydrated conditions differed by a factor of 30 for dendronised architectures and comb-type architectures of comparable IEC values. Similarly the water uptake of the dendronised system was higher, especially after what appears to be a change in connectivity between the sulfonic acid groups of **PSU-2f** taking place between IEC = 0.74 and 0.84 meq g^{-1}. There was a non-linear trend in increasing conductivity by number of dendrons on the backbone, whereas even the highest number of linear side chains appeared to have too low ionic content to provide sufficient proton conductivity. This suggests a different structure-property relationship of sulfonated aliphatic dendronised PSU compared to the comb-type analogue. In the dendronised architectures percolation of the conducting water system occurs within the investigated IEC-range, probably also partially due to noncovalent acid-base interactions. It is expected that the trend in proton conductivity by number of sulfonated dendrons is followed at higher IEC, so that even higher proton conductivities can be obtained, however water uptakes are believed to follow the same trend.

Acknowledgements

Supporting information available

^{1}H NMR of intermediates and a conceptual strategy for obtaining higher generation dendrons are available free of charge via the internet or from the author.

References

[1] M. Winter, R. J. Brodd, Chem. Rev. 2004, 104, 4245–4269.
[2] Y. Wang, K. S. Chen, J. Mishler, S. C. Cho, X. C. Adroher, Appl. Energy 2011, 88, 981–1007.
[3] K.-D. Kreuer, S. J. Paddison, E. Spohr, M. Schuster, Chem. Rev. 2004, 104, 4637–4678.
[4] K. Schmidt-Rohr, Q. Chen, Nat. Mater. 2008, 7, 75–83.
[5] M. Schuster, T. Rager, A. Noda, K. D. Kreuer, J. Maier, Fuel Cells 2005, 5, 355–365.
[6] L. Gubler, G. G. Scherer, Desalination 2010, 250, 1034–1037.
[7] S. J. Osborn, M. K. Hassan, G. M. Divoux, D. W. Rhoades, K. A. Mauritz, R. B. Moore, Macromolecules 2007, 40, 3886–3890.
[8] K. A. Mauritz, R. B. Moore, Chem. Rev. 2004, 104, 4535–4585.
[9] M. A. Hickner, H. Ghassemi, Y. S. Kim, B. R. Einsla, J. E. McGrath, Chem. Rev. 2004, 104, 4587–4612.
[10] K. E. Martin, J. P. Kopasz, K. W. McMurphy, Am. Chem. Soc. 2010, 1–13.
[11] K. D. Kreuer, M. Schuster, B. Obliers, O. Diat, U. Traub, A. Fuchs, U. Klock, S. J. Paddison, J. Maier, J. Pow. Sour. 2008, 178, 499–509.
[12] E. M. W. Tsang, Z. Zhang, A. C. C. Yang, Z. Shi, T. J. Peckham, R. Narimani, B. J. Frisken, S. Holdcroft, Macromolecules 2009, 42, 9467–9480.
[13] C. H. Park, C. H. Lee, M. D. Guiver, Y. M. Lee, Prog. Polym. Sci. 2011, 36, 1443–1498.
[14] Y. Chikashige, Y. Chikyu, K. Miyatake, M. Watanabe, Macromolecules 2005, 38, 7121–7126.
[15] Y. A. Elabd, M. A. Hickner, Macromolecules 2011, 44, 1–11.
[16] W. Li, B. C. Norris, P. Snodgrass, K. Prasad, A. S. Stockett, V. Pryamitsyn, V. Ganesan, C. W. Bielawski, A. Manthiram, J. Phys. Chem. B 2009, 113, 10063–10067.
[17] J. Mader, L. Xiao, T. J. Schmidt, B. C. Benicewicz, Adv. Polym. Sci. 2008, 216, 63–124.
[18] Y. Fu, A. Manthiram, M. D. Guiver, Electrochem. Commun. 2006, 8, 1386–1390.
[19] W. Li, A. Manthiram, M. D. Guiver, J. Membr. Sci. 2010, 362, 289–297.
[20] D. S. Kim, G. P. Robertson, Y. S. Kim, M. D. Guiver, Macromolecules 2009, 42, 957–963.
[21] B. C. Norris, W. Li, E. Lee, A. Manthiram, C. W. Bielawski, Polymer 2010, 51, 5352–5358.
[22] M. L. Einsla, Y. S. Kim, M. Hawley, H.-S. Lee, J. E. McGrath, B. Liu, M. D. Guiver, B. S. Pivovar, Chem. Mater. 2008, 20, 5636–5642.
[23] O. Savadogo, J. Pow. Sour. 2004, 127, 135–161.
[24] W. H. Binder, R. Sachsenhofer, Macromol. Rapid Commun. 2007, 28, 15–54.
[25] J.-L. M. Abboud, C. Foces-Foces, R. Notario, R. E. Trifonov, A. P. Volovodenko, V. A. Ostrovskii, I. Alkorta, J. Elguero, Eur. J. Org. Chem. 2001, 3013–3024.
[26] I. Dimitrov, S. Takamuku, K. Jankova, P. Jannasch, S. Hvilsted, Macromol. Rapid Commun. 2012, 33, 1368–1374.
[27] S. Takamuku, P. Jannasch, Polym. Chem. 2012, 3, 1202–1214.
[28] Y. J. Huang, Y. S. Ye, Y. C. Yen, L. D. Tsai, B. J. Hwang, F. C. Chang, Int. J. Hydrogen Energy 2011, 36, 15333–15343.
[29] M. Karadag, G. Yilmaz, H. Toiserkani, D. O. Demirkol, S. Sakarya, L. Torun, S. Timur, Y. Yagci, Macromol. Biosci. 2011, 11, 1235–1243.
[30] L. E. Karlsson, P. Jannasch, J. Membr. Sci. 2004, 230, 61–70.
[31] E.-H. Ryu, Y. Zhao, Org. lett. 2005, 7, 1035–1037.
[32] I. Dimitrov, K. Jankova, S. Hvilsted, J. Polym. Sci. Part A: Polym. Chem. 2008, 46, 7827–7834.
[33] J. A. Opsteen, J. C. M. van Hest, Chem. Commun. 2005, 57–59.
[34] H. E. Gottlieb, V. Kotlyar, A. Nudelman, J. Org. Chem. 1997, 62, 7512–7515.
[35] C. H. Lee, K.-S. Lee, O. Lane, J. E. McGrath, Y. Chen, S. Wi, S. Y. Lee, Y. M. Lee, RSC Adv. 2012, 2, 1025.
[36] B. Lafitte, M. Puchner, P. Jannasch, Macromol. Rapid Commun. 2005, 26, 1464–1468.
[37] B. Smitha, S. Sridhar, A. A. Khan, J. Membr. Sci. 2003, 225, 63–76.
[38] S. Borkar, K. Jankova, H. W. Siesler, S. Hvilsted, Macromolecules 2004, 37, 788–794.
[39] M. Laporta, M. Pegoraro, L. Zanderighi, Phys. Chem. Chem. Phys. 1999, 1, 4619–4628.

Supporting information

Dendronised Polymer Architectures for Fuel Cell Membranes

Mads M. Nielsen[1], Ivaylo Dimitrov[1], Shogo Takamuku[2], Patric Jannasch[2], Katja Jankova[1] and Søren Hvilsted[1,*]

[1]Danish Polymer Centre, Department of Chemical and Biochemical Engineering, Technical University of Denmark, Søltofts Plads, Building 227, DK-2800 Kgs. Lyngby, Denmark
[2]Department of Chemistry, Polymer and Materials Chemistry, Lund University, P.O. Box 124, SE-22 100 Lund, Sweden

*Corresponding author. E-mail sh@kt.dtu.dk.

A conceptual strategy to obtain higher generation dendrons analogue with the bisulfonated 1G dendronised structure was developed but not further optimized. Section A) covers the synthetic pathway to a tetrasulfonated 2G dendron along with preliminary characterization data from FTIR.

Section B) comprises selected ^{1}H NMR spectra to clarify the determination of the degree of substitution and subsequent azide-functionalization (Fig. S2), the purity of key compound **III** (Fig. S3), efficiency of the click reaction (Fig. S4 and Fig S5) and to elucidate the relationship between the pre- and postsulfonation approaches (Fig. S6).

A. Synthetic pathway to 2G tetrasulfonated aliphatic dendrons

Preliminary results from a conceptual synthetic approach to obtaining a second generation tetrafunctionalized dendron, **4f**, based on similar chemistry and nature of side chains (see Schemes S1 and S2) is reported in the following.
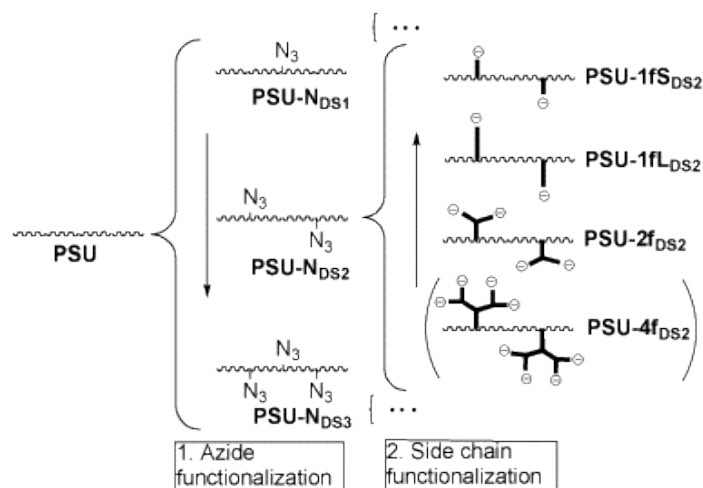
Scheme S1 The structure relationship between the various synthesized architectures, and the visions for a 2G dendronised structure.
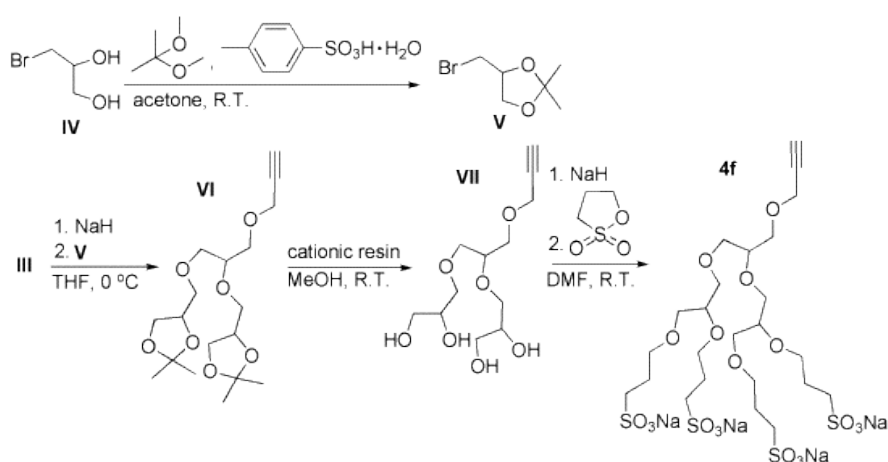
Scheme S2 Synthesis of tetrasulfonated 2G dendrons.

Protection of IV to V

3-bromo-1,2-propanediol was protected by stirring with 1.5 eq 2,2-dimethoxypropane and 0.05 eq p-toluene-sulfonic acid monohydrate in dry acetone = 1:10 (vol.) under nitrogen for 2 h at room temperature (RT). The catalyst was neutralized with aqueous ammonia before filtration and concentration on rotary evaporator. Dichloromethane was added and extraction was performed with 2 times demineralized water, then drying with $MgSO_4$, filtration and concentration, which resulted in a light yellow oil. ^{1}H NMR (300 MHz, chloroform-d, δ (ppm)): 4.33 (CH), 4.12 and 3.86 (O-CH_2), 3.41 and 3.30 (Br-CH_2), 1.44 and 1.35 (C-(CH_3)$_2$). FTIR (cm^{-1}): 1479, 1455 and 1436 (CH$_2$), 1212 (CH$_2$-Br), 1055 (C-O).

Sythesis of VI

III prepared as previously described was activated with 2 eq NaH in dry THF = 1:20 (vol.) at 0 ^{o}C under nitrogen. Color: orange. Drop wise addition of 4 eq **V** in dry DMF = 1:2 (vol.) followed, and after 2 h the color had changed to brown. Demineralized water was added, the mixture was transferred to an evaporation flask, and concentrated until only water/DMF phase was left. Again demineralized water was added and the solution was extracted by ethyl acetate = 1:7 (vol.), then dried with $MgSO_4$ and concentrated to a brown oil. FTIR (cm^{-1}): 1438 and 1384 (CH$_3$), 1090 and 1056 (C-O).

Deprotection of VI to VII

Deprotection of **VI** was performed by the same approach as previously described. The product was a brown oil. FTIR (cm^{-1}): 3370 (C≡C + OH H-bonded), 1097 and 1062 (C-O ether), 1031 (C-O alcohol).

Synthesis of 4f.

4f was accomplished by the same approach as previously described. The product appeared as light yellow sticky flakes, probably due to imperfect isolation. FTIR (cm^{-1}): 3315 (C≡C), 1439 (CH$_2$), 1183 and 1048 (O=S=O), 1107 (C-O). See Fig. S1.
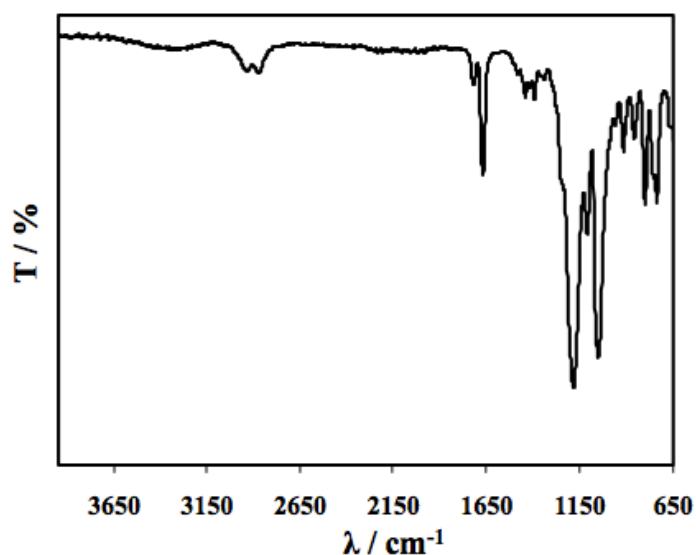
Fig. S1. FTIR spectrum of **4f**.

B. Selected ^{1}H NMR spectra
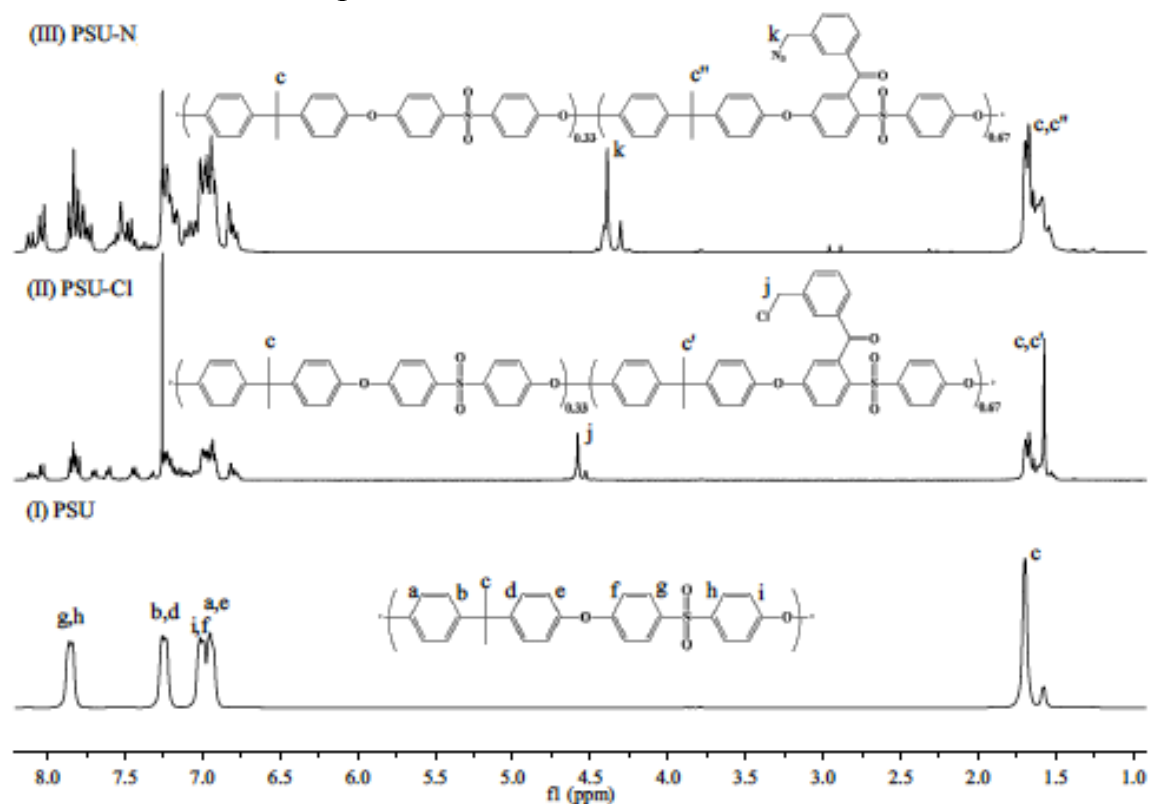
Fig. S2 ^{1}H NMR spectra of **PSU, PSU-Cl$_{0.67}$** and **PSU-N$_{0.67}$** (CDCl$_3$-*d*).
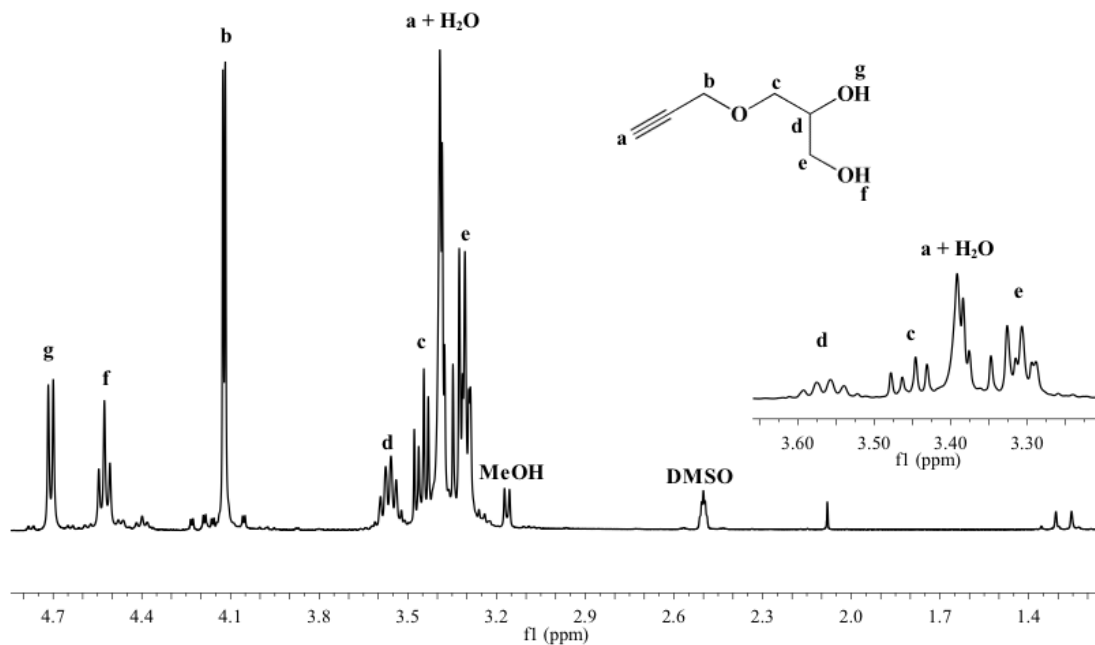
Fig. S3 ^{1}H NMR spectrum of **III** (DMSO-d_6).
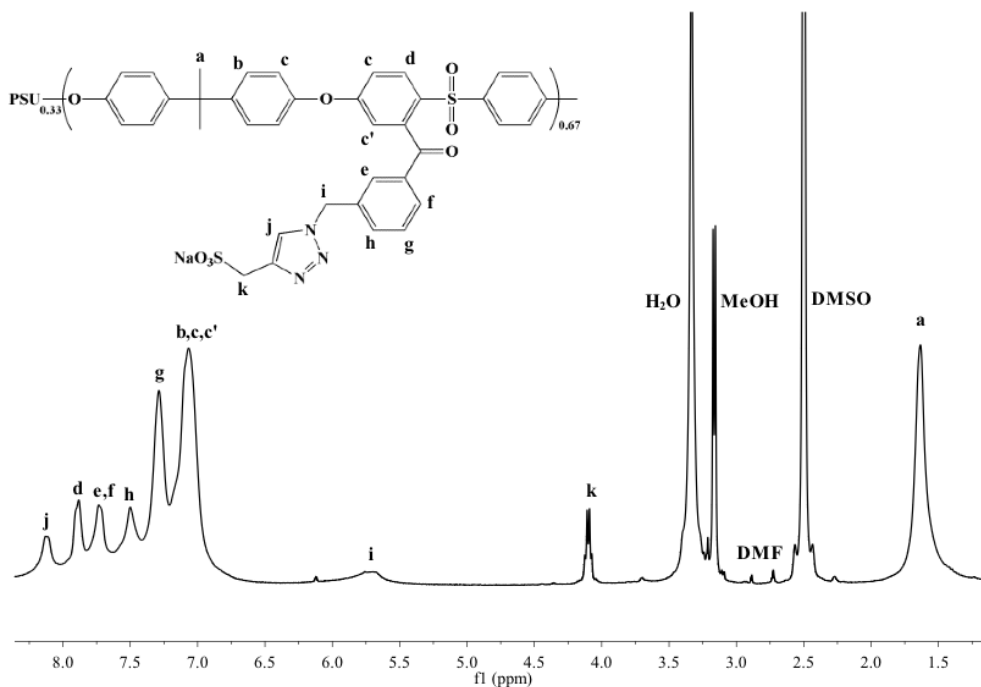
Fig. S4 ^{1}H NMR spectrum of **PSU-1fS$_{0.67}$** (DMSO-d_6).
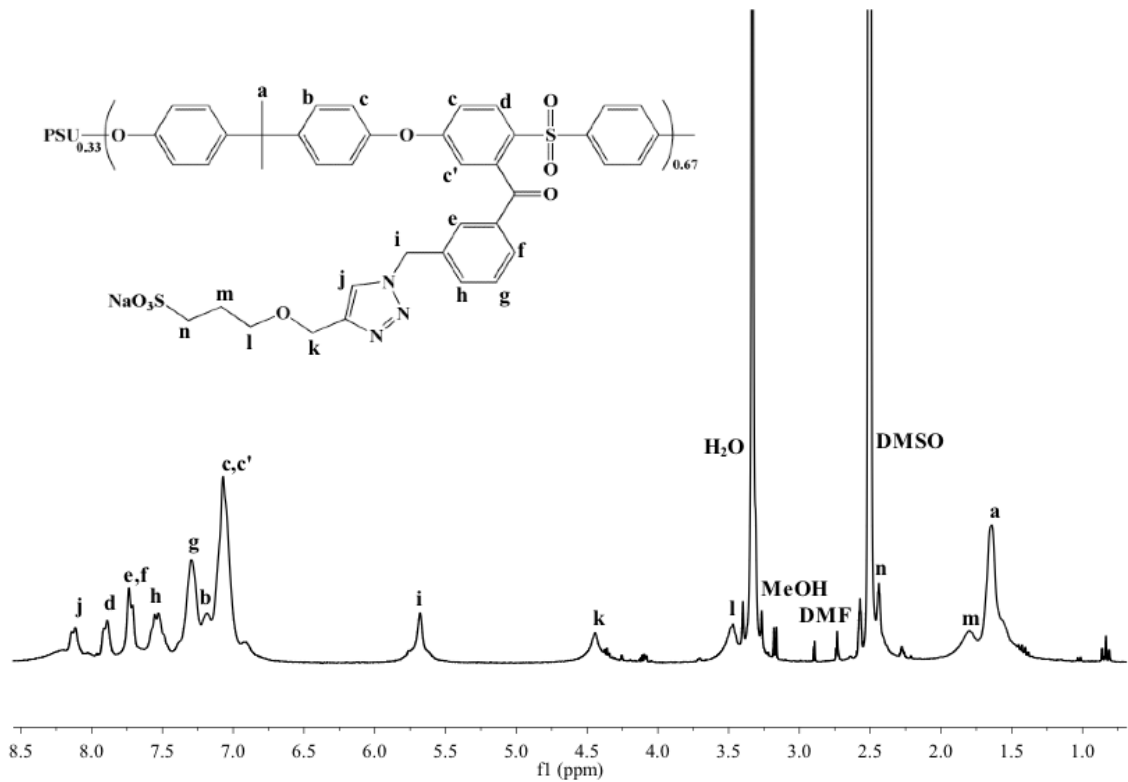
Fig. S5 ^{1}H NMR spectrum of **PSU-1fL$_{0.67}$** (DMSO-d_6).
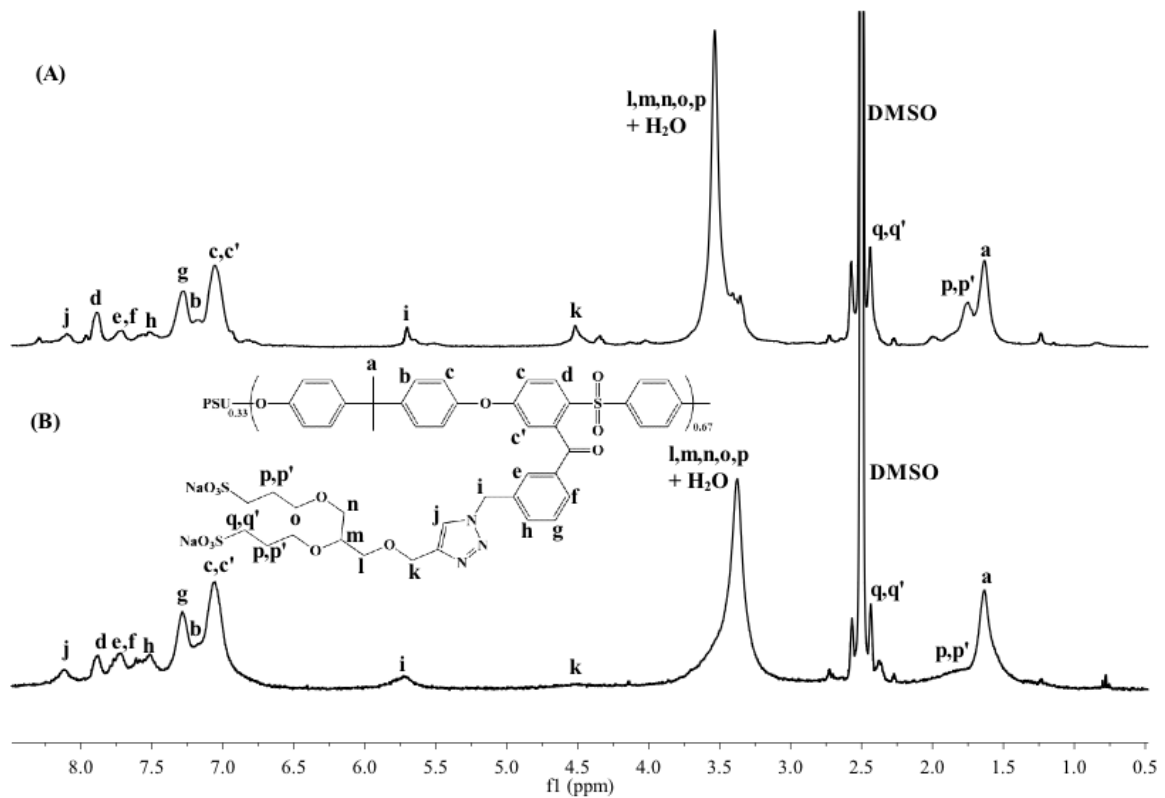
Fig. S6 ^{1}H NMR spectra of **PSU-2f$_{0.67}$** prepared by (A) post-sulfonation, and (B) pre-sulfonation (both DMSO-d_6).

IV

Sulfonated Hydrocarbon Graft Architectures for Cation Exchange Membranes

M. M. Nielsen, K. Jankova, S. Hvilsted
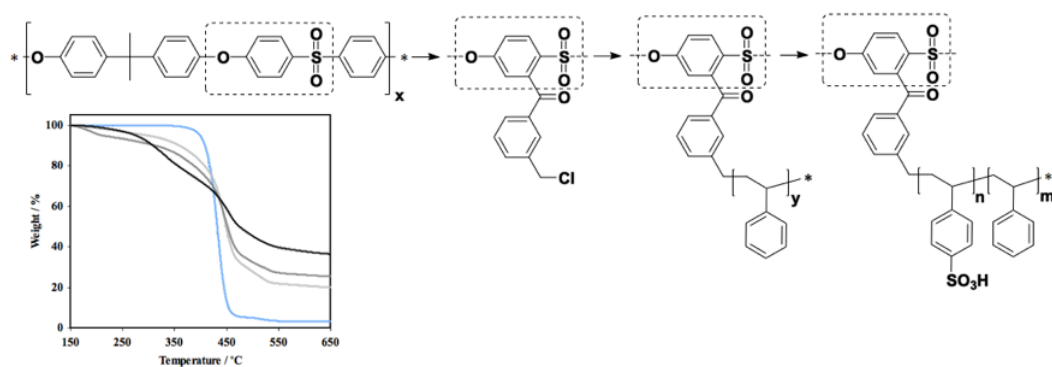
Sulfonated Hydrocarbon Graft Architectures for Cation Exchange Membranes

Mads M. Nielsen[a], Katja Jankova[a], Søren Hvilsted[a,*]

[a] Danish Polymer Centre, Department of Chemical and Biochemical Engineering, Technical University of Denmark, Søltofts Plads, Building 227, DK-2800 Kgs. Lyngby, Denmark
* Corresponding author at: Danish Polymer Centre, Department of Chemical and Biochemical Engineering, Technical University of Denmark, Søltofts Plads, Building 227, DK-2800 Kgs. Lyngby, Denmark. Tel.: +45 4525 2965. E-mail address: sh@kt.dtu.dk (S. Hvilsted).

 ABSTRACT

A synthetic strategy to hydrocarbon graft architectures prepared from a commercial polysulfone and aimed as ion exchange membrane material is proposed. Polystyrene is grafted from a polysulfone macroinitiator by atom transfer radical polymerization, and subsequently sulfonated with acetyl sulfate to various degrees. Series of grafting densities and graft lengths are prepared, and membranes are solvent cast from DMSO. The membrane properties in aqueous environments are evaluated from their water swelling behavior, and their thermal properties and stability are investigated by thermogravimetric analysis and differential scanning calorimetry.

1. Introduction

Cation exchange membranes have widespread uses, mainly within separation and power generation devices. More specifically, the amphiphilic polymers are applied for electrodialysis, desalination, water purification, sensors and fuel cells [1-4]. Depending on the application, hydrophobic polymers are functionalized with carboxylic acid, phosphonic acid or sulfonic acid [1,5]. Research drivers are ways either to improve the ion exchange properties or the lifetime of the membranes, or to come up with cheaper alternatives to the well established membranes such as DuPont's Nafion®. Perfluorosulfonic acid membranes (PFSA) are vastly used as cation exchange membranes [2,6,7]. Currently, a trend is to investigate hydrocarbon-based cation exchange membranes as it can be argued that the advantages of such materials can make up for limitations like lower performance and shorter lifetime compared to PFSA's [2,8]. Advantages include lower price of raw materials, easier processing due to the eliminated fluorination step, and a reduced negative environmental impact [2]. For fuel cell applications, the membranes must be tailored to facilitate migration of protons from the anode to the cathode in the proton exchange membrane fuel cell (PEMFC) *via* percolated ionic channels [9-12]. The interplay between hydrophilic and hydrophobic domains is vital for the creation of a phase-separation that enables the passage between ionic sites [13-15]. Upon humidification the acidic groups dissociate, allowing for proton conduction [5]. Despite outstanding overall properties PFSAs suffer from limitations at elevated temperatures especially above 100 °C and at lower relative humidities [6,8,13]. Alternative systems are continuously being investigated, e.g. PFSA/inorganic composites [16], partially fluorinated ionomers [17], poly(arylene ethers) [4,18,19], polybenzimidazoles [20], polystyrene based copolymers [21,22] and blends [23-25]. When designing the proton exchange membrane (PEM) a compromise must be made when settling on an ion exchange capacity (IEC) as the presence of acidic groups is related to both proton conductivity and water uptake. It is desirable that the membrane retains its dimensions and does not swell or even dissolve when it gets in contact with water. Block copolymers and graft copolymers are especially suited for this purpose due to the inherent phase-separation of incompatible components of which either a block or

the grafts contain e.g. sulfonic acid groups [21,22]. Previous studies on block and graft structures have shown how grafts at low degree of grafting (DG) exhibit lower water uptakes without negatively affecting the conductivity [22,26].

Previous investigations of PEM systems based on the commercial polysulfone (PSU) Udel[®] as backbone have shown promising results, both with sulfonated aliphatic side chains [27] and phosphonated, partially fluorinated grafts [28]. Durability studies of an analogue, directly sulfonated PSU (with a biphenyl rather than bisphenol A segment) suggested that the stability was higher when sulfonated PSU copolymers had the acidic groups in the *ortho*-position to the SO_2 group [19]. In addressing the aim of a hydrocarbon structure with sulfonic acid sites, the polysulfone is modified to contain a chloromethyl group. In previous studies of partially fluorinated graft structures, the chlorine was substituted by an azide, thereby enabling the use of click chemistry [27-29]. However, styrene can be grafted directly from the macroinitiator by ATRP [30]. The polystyrene component is widely used in cation exchange membranes [1,2,21,31], and is established as sulfonated graft in various partially fluorinated PEM systems [24,25,32]. Handles in the partially sulfonated polysulfone-*g*-polystyrene (PSU-*g*-SPS) system are thus *i)* DG, *ii)* graft length, and *iii)* degree of sulfonation (DS). Incomplete initiating efficiency (*f*) is a common issue when grafting from e.g. chlorotrifluoroethylene [26] that might be of little significance of model compounds, but more so in final applications. From a synthetic point of view it is therefore desirable to obtain complete *f* when developing a new macroinitiator. The aromatic spacer in the modified PSU is expected to reduce incomplete initiation caused by steric hindrance. The aim with the present study of the PSU-*g*-SPS system is to pursue a synthetic approach to cheaper cation exchange membrane materials, and - through tuning of the handles of the system and by performing preliminary studies of its water sorption and thermal properties - to evaluate its potential for this application.

2. Experimental

2.1 Materials

The materials were purchased from Aldrich unless otherwise stated and used as received: copper(I)bromide (CuBr, 98%), *N,N,N'N'',N''*-pentamethyldiethylenetriamine (PMDETA, 99%), *n*-butyllithium (BuLi, in hexanes, 2.5M, Acros), 3-(chloromethyl)benzoyl chloride (3-cmbc, Acros, 97%), acetic anhydride (AA, Bie & Berntsen A/S), sulfuric acid (H_2SO_4, 96%, chemically pure), methanol (MeOH, >99.9%), dichloroethane (DCE >99%, Bie & Berntsen A/S), propan-2-ol (IPA, Honeywell), dimethylsulfoxide (DMSO ≥ 99%), chloroform-*d* ($CDCl_3$, 99.8%), dimethylsulfoxide-d_6 (DMSO, 99.9 atom% D). Styrene (St ≥99%, ReagentPlus®, 4-tert-butylcatechol stabilized), was passed through a column of activated basic aluminum oxide (Al_2O_3, activated, basic, Brockmann I) and subsequently dried over calcium hydride (CaH_2, reagent grade, 90-95%) and distilled under reduced pressure. Tetrahydrofuran (THF, Fisher Scientific, 99.9%) was distilled and dried on 4 Å molecular sieves prior to use. PSU (Udel® P-3500 LCD MB8, $\overline{M}_n$ = 40 kDa, 195, Solvay Advanced Polymers) was dried in oven prior to use. Dialysis tubing of regenerated cellulose (cut off 12,000-14,000 Da, Membrane Filtration Products Inc.), dialysis tubing benzoylated (cut off 1,200 Da).

2.2 Polysulfone with Pendant (chloromethyl)benzoyl groups (PSU-Cl)

PSU was functionalized according to a previously reported method [27,28]. In the typical reaction 7 g pre-dried PSU was dissolved in 350 mL dry THF and placed under argon in a glass reactor equipped with a magnetic stirring bar, a thermometer, a septum and a connection to a vacuum line. The mixture was cooled down to -65 °C on dry ice/IPA and degassed by first applying vacuum on the system, then putting it under a blanket of argon; This was repeated seven times. BuLi (20% excess of targeted degree of substitution) was added with a gas tight syringe to activate the *ortho* position to SO_2 of PSU [18,19,33,34]. After 1 hour a 3-cmbc amount of 20% excess relative to BuLi was added with a gas tight syringe and the lithiated sites were quenched over 30 min. At RT the resulting **PSU-Cl** was precipitated in IPA, filtered, washed with water, filtered again and dried before stirring in MeOH, filtered once more and dried at 60 °C in vacuum oven overnight. **PSU-Cl** precursors bearing 3 and 18 chloromethyl groups per 100 repeat units were obtained, and they are referred to as **PSU-Cl-3** and **PSU-Cl-18**. ^{1}H NMR (300 MHz,

CDCl$_3$, δ (ppm)): 8.05-6.80 (Ar H, PSU + substituted PSU), 4.66-4.56 (Ar-CH_2-Cl), 1.79-1.56 (C-(CH_3)$_2$). FTIR (cm^{-1}): 1683 (C=O), 1585 (Ar C=C), 1487 (CH$_3$), 1237 (C-O-C), 1169 and 1149 (O=S=O), 1105, 1081 and 1014 (Ar ring). Size exclusion chromatography (SEC) (DMF, Da) of **PSU-Cl-3** and **PSU-Cl-18**: $\overline{M}_p$ = 60,000 and 61,000, and polydispersity index (PDI$_{\textbf{PSU-Cl}}$): 1.64 and 3.59 respectively.

2.3 Polysulfone Grafted with Polystyrene Side Chains (PSU-g-PS)

Graft copolymers were made according to Scheme 1. In the typical case, 100 mg **PSU-Cl** and 4 eq CuBr were mixed with 5,000 eq St in a Schlenk tube and purged with nitrogen. The reaction mixture was degassed by employing three freeze-thaw cycles, then 4.1 eqs PMDETA were added and the mixture was degassed again before starting the bulk polymerization at 110 °C until the reaction mixture became too viscous to stir, after approximately 2 hours. Chain propagation was followed by ^{1}H NMR and SEC (THF). See the supporting information for more details. The reaction mixture was then dissolved in THF and precipitated from MeOH, washed with fresh MeOH twice and then dried in vacuum oven at 80 °C overnight. Three graft copolymers were prepared: an average of 47 styrenic units per site (*g3-47*) was grafted from **PSU-Cl-3** at almost complete *f*, and from **PSU-Cl-18** 10 and 8 styrenic units per site respectively (*g18-10* and *g 18-8*) were grafted at almost complete and 75% *f*. Yield (*g3-47* / *g18-10* / *g18-8*): 0.706 g / 2.021 g/ 1.154 g. ^{1}H NMR (300 MHz, CDCl$_3$, δ(ppm)): 7.86-7.83 (Ar *H,* PSU), 7.23-6.95 (*meta*/*para H*, PS + Ar *H*, PSU), 6.58-6.40 (*ortho H*, PS), 2.25-1.25 (Aliphatic *H*, PSU/PS). FTIR (cm^{-1}): 1493 and 1452 (Ar C=C), 1601 and 1583 (Ar C=C), 1178 and 1154 (O=S=O), 1106, 1070 and 1028 (Ar ring).
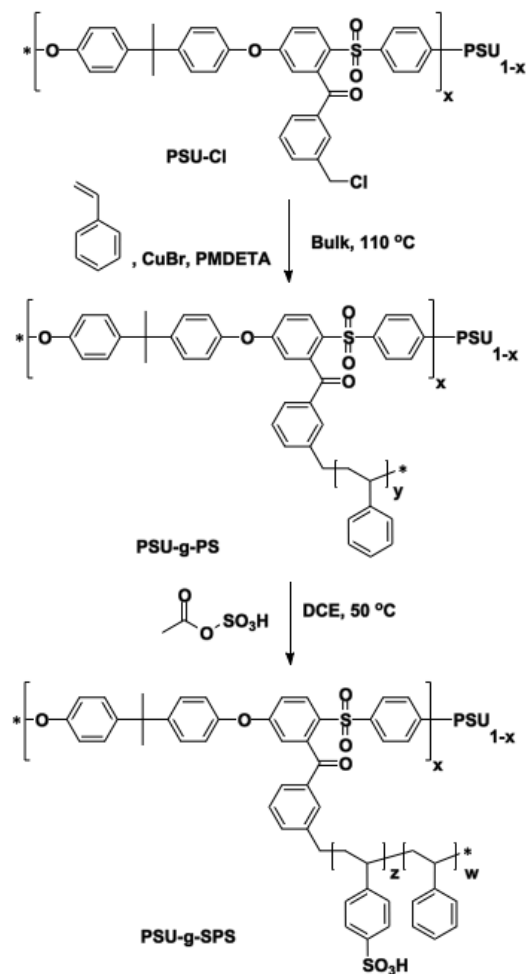
Scheme 1. Synthetic pathway from macroinitiator **PSU-Cl** over graft copolymer PSU-*g*-PS to sulfonated PSU-g-SPS.

2.4 Sulfonation of PS grafts (PSU-g-SPS)

In the typical case, 200 mg PSU-*g*-PS was dissolved in 5 mL DCE under a blanket of nitrogen at 50 °C in a 50 mL two neck round bottom reactor equipped with a condenser and a rubber septum. Acetyl sulfate was simultaneously prepared in an Erlenmeyer flask on an ice bath by mixing 3.4 eqs AA and 5 mL DCE whilst purging with nitrogen, and after a few minutes 2 eqs H_2SO_4 were added. The acetyl sulfate was immediately transferred to an addition funnel and drop-wise introduced to the polymer solution. The reaction proceeded from 2 to 42 hours (see Table 1 for the exact reaction times) at 50 °C

during which the colorless solution turned to various shades of brown. The mixture was quenched with 10 mL IPA, air stripped and stirred with 30 mL deionized water for an hour, all at elevated temperature. Thereafter dialysis of the mostly gelled solution was performed against deionized water for several days, followed by freeze drying. Samples were named with prefix S for sulfonated, and suffixes according to DS, from S = small, M = medium, L = large – i.e. **Sg3-47-S** for sulfonated **g3-47** with lowest DS.

Yields are stated in Table 1. ^{1}H NMR (300 MHz, DMSO-*d*, δ(ppm)): 7.88 (Ar *H*, PSU), 7.50-7.25 (Ar *ortho-H* to SO$_3$H), 7.25-6.75 (Ar *meta/para-H*, PS), 6.75-6.20 (Ar, *ortho-H*), 2.08-0.85 (Aliphatic *H*, PSU/PS/SPS). FTIR: 1598 (Ar C=C), 1143 (O=S=O), 1123, 1027 and 1001 (Ar ring).

Characteristic signals in ^{1}H NMR of **S-PSU-Cl-18** (300 MHz, DMSO-*d*, δ(ppm)): 7.90-7.88 (Ar *H*, PSU), 7.83-7.80 + 7.70 (Ar *H*, sulfonated PSU-Cl) 7.27 + 6.93 (Ar *H*, PSU), 6.93-6.88 (Ar *H*, sulfonated PSU-Cl).

2.5 Membrane preparation

Membranes were solvent cast according to a previously described method [27]. In the typical case, 50 mg PSU-*g*-SPS were dissolved in DMSO under heating and stirring, whereupon the mixture was concentrated to a viscosity allowing for full coverage of a 4 x 1 cm glass substrate, placed on a hot plate. The solvent evaporated over few hours at approximately 80 °C. The films were dried to completion in vacuum oven at 80 °C overnight. In some cases the films easily let go of the glass when using a razor blade, in other cases they stuck to the glass and had to be detached by immersion into deionized water.

2.6 Analytical techniques

The polymerizations were followed by SEC (data presented in the supporting information) on a Viscotek 200 instrument using two PLgel mixed-D columns (Polymer Laboratories, PL) assembled in series and a refractive index (RI) detector. Samples were run in THF at RT (1 mL min^{-1}). Calculations were performed from a polystyrene (PS)

standard calibration. The molecular weights and PDI values stated in the main text were obtained by a Tosoh Corporation Bioscience Division HLC-8320GPC equipped with three PFG micro columns (100 Å, 1000 Å, and 4000 Å) from Polymer Standards Service (PSS), with an RI detector. The samples were run in DMF (with 5 mM LiCl) at 50 °C (0.3 mL min^{-1}). Molecular weights were calculated using WinGPC Unity 7.4.0 software and PMMA standards from PSS.

NMR analyses were conducted in CDCl$_3$ or DMSO-d_6 using a Bruker spectrometer at a resonance frequency of 300 MHz. FT-IR spectra were recorded on a Perkin-Elmer Spectrum One instrument in the 4000-650 cm^{-1} operating range over 16 scans. Thermal stabilities were investigated by thermogravimetric analysis (TGA) with a TA Instruments TGA Q500 under nitrogen from RT to 650 °C at a heating rate of 20 °C min^{-1}. The degradation temperature was recorded as the 10% weight loss ($T_{d\ 10\%}$) of the dry weight, taking the weight at 150 °C to be 100% weight. Differential scanning calorimetry (DSC) was conducted with a TA Instruments DSC Q1000. Data collection was performed over three heating cycles from RT to 220 °C. Thermal responses, including estimated glass transition temperatures (T_g) were determined from the second heating cycle. Prior to running DSC all samples were stored in vacuum oven at RT overnight as PSU-g-SPS absorbs moisture when stored in a vial at atmospheric pressure.

In the investigation of water swelling behavior, the membranes were dried in vacuum oven at 80°C overnight and then stored in a vacuum oven at RT until the dry weight, m$_{dry}$, was obtained, then the membranes were immersed in deionized water overnight. Before the wet weights, m$_{wet}$, were obtained excess water was wiped off the surface with lens paper.

2.7 Calculations

Prior to deciding which DG, DP$_{PS}$ and DS to aim for, theoretical IEC (IEC$_{th}$) [meq g^{-1}] values were calculated from Eqn. (2). Here, DP$_{PSU}$ is the degree of polymerization of the backbone, DS is the degree of sulfonation of PS grafts, f is the initiator efficiency, DP$_{PS}$ is the degree of polymerization of St grafts, and $\overline{M}_{n\ (incl.\ SO_3H)}$ is the molecular weight of the amphiphilic polymer.

$$IEC_{th} = \frac{DP_{PSU} \times DS \times f \times DP_{PS}}{\overline{M}_{n\,(incl.\ SO_3H)}} \times 1000 \qquad (1)$$

E.g., from Equation 1, **g3-47** series with grafts sulfonated to completion has $IEC_{th} = 2$ meq g^{-1}, and under the same conditions IEC_{th} (**g18-10**) = 2.25 meq g^{-1}. The GD is calculated from the ^{1}H NMR spectra of **PSU-Cl** by dividing the normalized CH_2Cl signal of the *meta* (chloromethyl)benzoyl group by that of C(CH_3)$_2$ of the PSU backbone. f is determined from ^{1}H NMR as the ratio between the peak corresponding to CH_2Cl at 4.58 ppm and the one corresponding to Ar H PSU at 7.86-7.83 ppm. In polymerizations where the protons characteristic of the macroinitiator disappear, f is considered complete. DP_{PS} is calculated from the ^{1}H NMR spectra of the three PSU-*g*-PS samples: the normalized protons *ortho* to SO$_2$ at 7.86-7.83 ppm corrected for GD and the normalized alkyl protons corresponding to the PS backbone corrected for contribution of the CH$_3$ of the bisphenol A segment of PSU as these overlap (2.08-0.85 ppm).

DS is calculated from the ^{1}H NMR spectra as the ratio between the peak corresponding to protons *ortho* to SO$_3$H on the grafts (7.50-7.25 ppm) and the *ortho* protons of PS (6.75-6.20 ppm). Here actually the peak at 7.50-7.25 ppm overlaps with that corresponding to the *para* peaks in PS at 7.25-6.75 ppm. This is a source of error. The same applies for the sulfonation of the PSU backbone, which will contribute with peaks overlapping with others. In the following, DS is for simplicity treated as if only the grafts are sulfonated. However, during the TGA data discussion, the ratio between sulfonation of the grafts and the backbone is estimated.

The water uptake is calculated from Equation 2.

$$Water\ uptake = \frac{m_{wet} - m_{dry}}{m_{dry}} \times 100 \qquad (2)$$

3. Results and Discussion

3.1 Synthesis of Polysulfone with Polystyrene Side Chains (PSU-g-PS)

The commercial PSU was modified through lithiation and electrophilic attack of (chloromethyl)benzoyl chloride to contain 3 or 18 chloromethyl sites per 100 repeat units (DG = 0.03 and 0.18). From **PSU-Cl-3** was grafted an average of 47 styrenic repeat units per initiating site (**g3-47**) and from **PSU-Cl-18** were grafted an average of 10 and 8 repeat units respectively (**g18-10** and **g18-8**). 100% initiating efficiency was obtained with both macroinitiators, yet in the synthesis of **g18-8**, f = 75%. ^{1}H NMR spectra of **PSU-Cl-18** and **g18-10** are shown in Figure 1. Here it can be seen how the "j" resonance has disappeared upon polymerization.

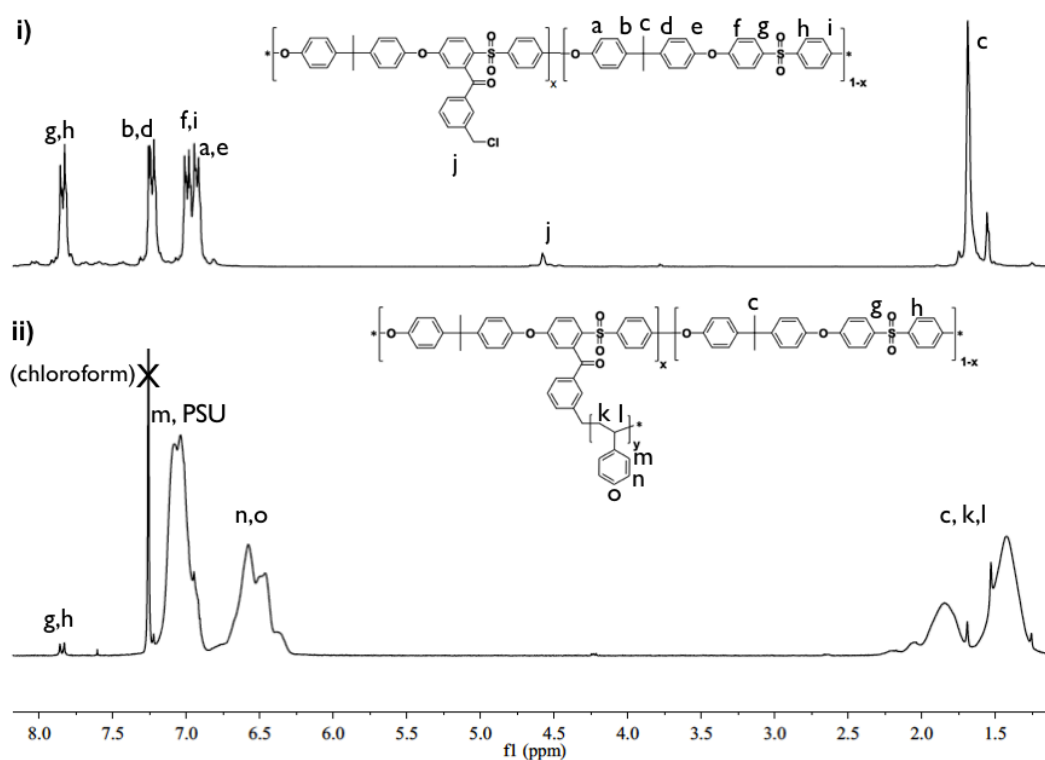Figure 1. ^{1}H NMR spectra of i) **PSU-Cl-18** and ii) **g18-10**.

GD, f and DP$_{PS}$ per chain are listed in Table 1. Normalized SEC (DMF) traces of PSU (red), **PSU-Cl-3** (black) and **g3-47** (green) are shown in Figure 2. A slightly lower retention volume (RV) is recorded of the macroinitiator, and the RV of the graft copolymer is much lower. The absence of shoulders or other indicators of uneven chain

10

growth suggests that symmetric propagation is obtained when grafting St from PSU-Cl including almost complete f. A SEC trace from the chain extension is provided in the supporting information. **g18-10** showed resembling traces but with a shoulder at high RV and f. This shoulder can be explained by the lower DP_{PS} of **PSU-Cl-18.** The apparent incomplete initiation experienced in **g18-10-8** could be due to a small amount of unreacted **PSU-Cl-18** that escaped the polymerization reaction by sticking to the Schlenk tube wall. The solubility of PSU in St is not complete, as a small gel like particle was observed for all polymerizations. FTIR spectra had some overlapping characteristic peaks, but support ^{1}H NMR and SEC, especially with the peak around 1029 cm^{-1} from the aromatic C=C stretch in PS.

Table 1. Selected graft copolymer properties.

Sample	GD / %	f / %	DP_{PS} / no. St units	t / hrs	Yield / mg	DS[3] / %
S**g3-47-S**	3	100	47	2	36[2]	34
S**g3-47-M**	3	100	47	6	248	51
S**g3-47-L**[1]	3	100	47	42	234	60
S**g18-8-S**	18	75	8	2	311	40
S**g18-8-L**	18	75	8	16.6	333	56
S**g18-10-S**	18	100	10	2	244	38
S**g18-10-M**	18	100	10	4.5	299	46
S**g18-10-L**[1]	18	100	10	23	315	85

[1] 50-50 wt.% PSU-g-SPS – PSU blends were prepared with no remarkable influence on water swelling.

[2] Prepared from 75 mg **g3-47**. [3] Based on the assumption that only the grafts are sulfonated.
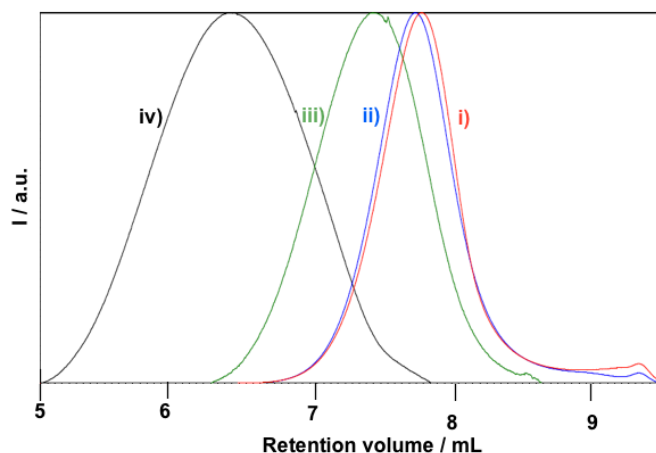
Figure 2. Normalized SEC (DMF) trace of i) PSU, ii) **PSU-Cl-3**, iii) *g***3-47** and iv) **S***g***3-47-S**.

3.2 Sulfonation of PS grafts

The three graft copolymers, *g***3-47**, *g***18-10** and *g***18-8** were sulfonated to various degrees by varying the reaction time, keeping the other reaction conditions constant, according to a modified version of a previously reported method originally applied on non-aromatic backbones with styrenic grafts [26,35]. This was chosen over sulfonation conditions conventionally known to sulfonate PSU quantitatively [19] in an attempt to restrict sulfonation to the PS grafts. Details are provided in Table 1. Figure 3 shows the aromatic region of **S***g***18-10-S**, **S***g***18-10-M** and **S***g***18-10-L** ^{1}H NMR spectra, from which DS is calculated, assuming sulfonation solely of the styrenic units. In parallel with the graft copolymer sulfonation, the unmodified macroinitiator, **PSU-Cl-18**, was treated with the sulfonating agent in the evaluation of whether the backbone and/or the (chloromethyl)benzoyl group were sulfonated as well and not just the PS grafts. SEC (DMF) showed a 2-4 fold $\overline{M}_p$ increase from the pristine samples to the samples after the sulfonation reaction, i.e. from 53,800 Da to 200,000 Da of PSU and from 61,400 Da to 144,600 Da of **PSU-Cl-18**. This indicates a change of the compound that is even more pronounced as the reaction proceeds. The approximately two-fold increase of **PSU-Cl-18** occurred over 2 hours' reaction time, while the four-fold increase of PSU occurred of an overnight reaction. Contrary to the grafts, these reference samples were insoluble in water

12

after the air stripping, yet both were difficult to dissolve in chloroform and much more easily soluble in DMSO for the NMR characterization. As only one peak appeared in the SEC plot it can be concluded that no chain scission takes place. ^{1}H NMR showed a peak position shift, and particularly the peak integral ratios between the one at 7.70 ppm corresponding to modified **PSU-Cl-18** relative to that of the benzoyl segment at 8.13-8.14 ppm indicated that the modification that takes place is mainly due to the backbone itself being sulfonated. The peak pattern appears to be similar to that of *ortho*-to the SO$_2$ segment in an analogue PSU consisting of a biphenyl rather than bisphenol A. SEC (DMF) showed increasing retention volumes upon sulfonation. Gravimetric data supported this observation (see Table 1).
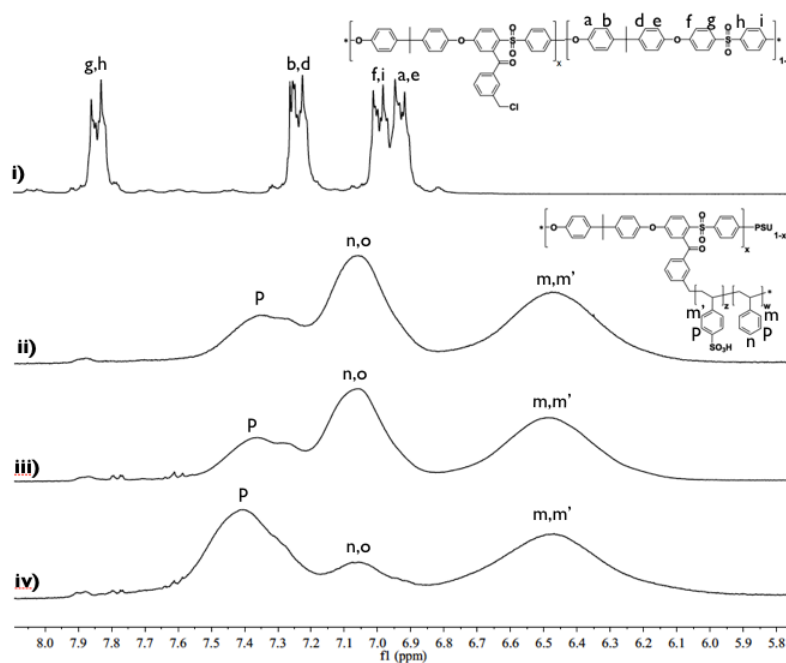

Figure 3. Aromatic region ^{1}H NMR spectra of i) **PSU-Cl-18** (in chloroform-*d*), ii) **S*g*18-10-S**, iii) **S*g*18-10-M**, and iv) **S*g*18-10-L** (all three in DMSO-*d*$_6$)**. The resonances "m,m'" and "p" are used in the calculation of DS.

3.3 Thermal Properties

13

The thermal stabilities of the graft copolymers and their precursors were quantified by TGA as $T_{d\ 10\%}$. These values are listed in Table 2 along with T_g obtained by DSC, including data of pristine PSU, the macroinitiators **PSU-Cl-3** and **PSU-Cl-18**, the reference sulfonated macroinitiator **S-PSU-Cl-18** and a SPS (Na form) (polymerization details are stated in the supporting information). For visualization, the TGA curves of **g18-10** and the three sulfonated graft copolymers made from it are shown in Figure 4. The unsulfonated graft copolymer **g18-10** degrades almost entirely (down to 3.3 wt%) between 360 °C and 480 °C in one major degradation step followed by a smaller one from 480 °C to 530 °C. The thermal stability of the unsulfonated graft copolymers is decreased by more than 110 °C relative to pure PSU. The sulfonated grafts exhibit weight losses in two similar steps, and in addition they undergo weight losses from around 150 °C and until the degradation observed for **g18-10** begins. The higher the DS the more is lost until the deflection tangent of the **g18-10** curve after which the trend inverses and the **Sg18-10** curves even out at 650 °C at the weight percentages 20.1, 25.5 and 36.6 in order of increasing DS. This is not observed with sulfonated polysulfone with no grafts [36], indicating that the grafts play a role in this phenomenon. The decreasing weight loss upon introduction of SO_3H indicates that crosslinking with the acidic groups playing a key role occurs. The same trend is observed between pristine **PSU-Cl-18** and the sulfonated version. Comparing **S-PSU-Cl-18** and **Sg18-10-L**, the former has lost 12 wt.% at 375 °C, whereas the latter has lost 35 wt.%. This suggests that approximately one third of the sulfonation observed of the graft copolymers can be attributed to sulfonation of the PSU backbone, and two thirds correspond to the sulfonated PS grafts. TGA plots of the **Sg3-47** and **Sg18-8** series are included in the supporting information. It is noted how T_d $_{10\%}$ decreases upon introduction of the (chloromethyl)benzoyl group from 527 °C to 496 °C of **PSU-Cl-18**. Between the two graft copolymers of different graft length (**Sg18-10** and **Sg18-8**), the longer graft has a slightly lower $T_{d\ 10\%}$, 408 °C vs. 413 °C. No real trend is observed within the sulfonated graft copolymer series. Hence, **Sg3-47-S** and **Sg3-47-L** have $T_{d\ 10\%}$ of 350 °C while $T_{d\ 10\%}$ of **Sg3-47-M** is 368 °C. Similarly **Sg18-10-M** and **Sg18-10-L** have $T_{d\ 10\%}$'s of 309 °C while that of **Sg18-10-S** is 358 °C. **Sg18-8-S** and **Sg18-8-L** both have a $T_{d\ 10\%}$ of 259 °C. For the shortest sulfonated grafts, e.g. **Sg18-10-S**, the degradation temperature is almost 50 °C higher than for the two analogue graft

structures with higher DS. Another tendency is that the higher graft density series (**S*g*18**) exerts lower $T_{d\,10\%}$. Besides **S*g*18-10-S**, whose $T_{d\,10\%}$ seems high compared to **S*g*18-10-M** and **S*g*18-10-L**, the trend shows that $T_{d\,10\%}$ is decreased by increasing DG and decreasing graft length. **S-PSU-Cl-18** reaches a $T_{d\,10\%}$ of 397 °C, which is approximately 100 °C lower than for the backbone (**PSU-Cl-18**) before the sulfonation reaction has been performed. In this context it should be noted that the $T_{d\,10\%}$ relates to a point where the loss of SO_3H has begun, and in reality this loss is undesired. This suggests that the thermal stability of the graft copolymer structures could be improved by preventing this reaction from taking place. However, this has not been further investigated in the present paper.

Table 2. Thermal properties of the investigated polymers.

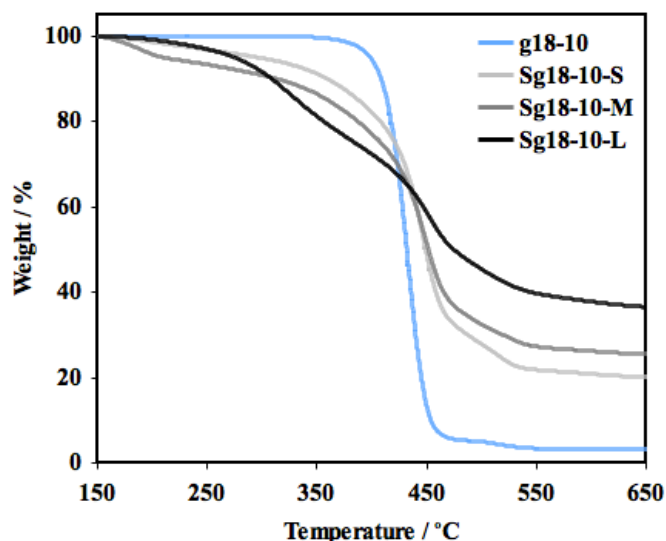| Sample	$T_{d\,10\%}$ / °C	T_g / °C	Water uptake
PSU	527	189	-
PSU-Cl-3	524	183	-
PSU-Cl-18	496	181	-
***g*3-47**	NA[1]	NA[1]	-
***g*18-10**	408	109	-
***g*18-8**	413	110	-
S*g*3-47-S	350	177	62%
S*g*3-47-M	368	85 / 191	NA[2]
S*g*3-47-L	350	99 / 201	NA[2]
S*g*18-8-S	259	150	NA[3]
S*g*18-8-L	259	109 / 206	NA[2]
S*g*18-10-S	358	188	NA[2]
S*g*18-10-M	309	152	NA[2]
S*g*18-10-L	309	210	NA[2]
S-PSU-Cl-18	397	171	-
SPS Na salt	496	134	-

Figure 4. TGA data for the S*g*-18-10 series.

Regarding T_g, the introduction of (chloromethyl)benzoyl-functionality leads to a reduction of T_g from 189 °C to 183 °C for **PSU-Cl-3** and to 181 °C for **PSU-Cl-18**. The graft copolymers contain a lot of PS, which, depending on the molecular weight, typically has T_g around 100°C [37], while SPS which is determined to have a T_g of 134 °C. Hence T_g's of 109-110 °C of the graft copolymers made from **PSU-Cl-18** sounds reasonable. Regarding the effect of sulfonation, **S-PSU-Cl-18** shows a T_g of 171 °C, i.e. 10 °C lower than before the sulfonation. This tendency supports the observation from $T_{d\ 10\%}$, that thermal stability is lowered upon sulfonation of the backbone. In **S*g*3-47-S** T_g is 177 °C, a number that increases upon increasing DS, but at the same time **S*g*3-47-M** and **S*g*3-47-L** show an additional exothermal response in the region of PS, namely 85 °C and 99 °C. A similar trend of increasing T_g is observed for **S*g*18-8-S** and **S*g*18-8-L**, and again the higher DS graft copolymer exhibits two responses. The lower temperature here is 109 °C, i.e. the T_g of the unsulfonated graft copolymer *g*18-8. The trend of increasing T_g by DS is also valid for the **S*g*18-10** series, even though **S*g*18-10-S** does not fit into the pattern with 188 °C against 152 °C and 210 °C respectively. Annealing of the polymer chains could

arguably play a role but hardly represent the full contribution. A possible explanation for the high T_g's at high DS might be found in a crosslinking taking place across the SO_3H groups, e.g. anhydride formation. Figure 5 shows the third cycle of the DSC curve of **Sg18-8-S** when the cycle goes between RT and 220 °C and RT and 250 °C respectively. When applying a higher temperature the observed T_g shifts from 150 °C to 209 °C, an indication that the sample is physically altered during the process.
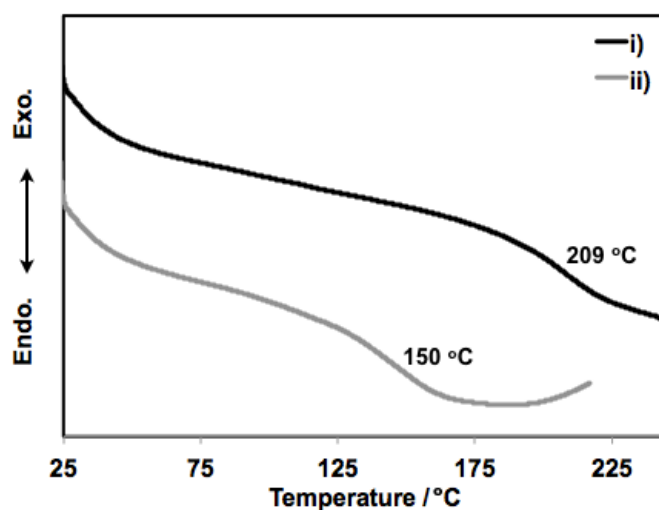
Figure 5. DSC curves from the third cycle of **Sg18-8-S** when cycled between i) RT and 250 °C, and ii) between RT and 220 °C, where thermal decomposition is more pronounced.

3.4 Water sorption

An overview of the water swelling behavior of the membranes is provided in Table 2. The **Sg3-47-S** membrane showed a water uptake of 62% and seemingly maintained mechanical integrity upon swelling. **Sg18-8-S** could not be detached from the glass substrate and was therefore immersed in water still attached to the slide. The film showed moderate swelling behavior, but during detachment of the wetted membrane mechanical integrity was lost. **Sg18-10-S** swelled to such an extent that the film would not endure transfer out of the liquid. All other sulfonated graft copolymer membranes experienced multiple time dimensional increase. The water sorption observation warrants further

investigation of the influence of IEC, ideally in a system with a 100% non-sulfonated backbone and reduced GD/graft length/DS.

4. Conclusion

A novel macroinitiator for non-fluorous graft copolymer architectures proved efficient for bulk ATRP-grafting of styrene onto PSU. DG of 3% and 18% were applied in obtaining up to 47 and 10 repeat units per graft site on average in polymerizations that experienced high initiating efficiency. The graft copolymers were sulfonated under conditions known to sulfonate PS in approaching structures intended for cation exchange membrane applications. SEC showed that no chain scission of PSU takes place. ^{1}H NMR, SEC and TGA indicated that the backbone is also being sulfonated during the reaction, likely in the *ortho*-position to the SO_2 group of PSU, the same place as the (chloromethyl)benzoyl functionality is incorporated. As a consequence, the phase separation potential is reduced, and overall poor mechanical integrity upon immersion in water warrants alterations for the structure to become viable as cation exchange membranes. TGA showed that the thermal stability decreases by DG as well as DS, a feature mainly related to the increased content of sulfonic acid groups. DSC showed increasing exothermal responses equivalent to T_g's, which increased by DS, possibly partly due to crosslinking between the degrading sulfonic acid groups, e.g. in the formation of anhydrides.

Supporting information available: Supporting Information is available from the internet or from the author.

References

[1] Xu T. J Membr Sci 2005;263: 1–29.
[2] Yee RSL, Rozendal RA, Zhang K, Ladewig BP. Chem Eng Res Des 2012;90:950–959.
[3] Kreuer KD. Solid State Ionics 1997;97:1–15.
[4] Park CH, Lee CH, Guiver MD, Lee YM. Prog Polym Sci 2011;36:1443–1498.
[5] Schuster M, Rager T, Noda A, Kreuer KD, Maier J. Fuel Cells 2005;5:355–365.
[6] Martin KE, Kopasz JP, McMurphy KW. Am Chem Soc 2010:1–13.
[7] Spendelow JS, Papageorgopoulos DC. Fuel Cells 2011;11:775–786.
[8] Hickner MA, Ghassemi H, Kim YS, Einsla BR, McGrath JE. Chem Rev 2004;104:4587–4612.
[9] Kreuer KD. J Membr Sci 2001;185:29–39.
[10] Schmidt-Rohr K, Chen Q. Nat Mater 2008;7:75–83.
[11] Eikerling M, Kornyshev AA, Stimming U. J Phys Chem B 1997;101:10807–10820.
[12] Malek K, Eikerling M, Wang Q, Liu Z, Otsuka S, Akizuki K, Abe M. J Chem Phys 2008;129(20):204702.
[13] Mauritz KA, Moore RB. Chem Rev 2004;104:4535–4585.
[14] Smitha B, Sridhar S, Khan AA. J Membr Sci 2005;259:10–26.
[15] Hickner MA. J Polym Sci Part B: Polym Phys 2012;50:9–20.
[16] Nørgaard CF, Nielsen UG, Skou EM. Solid State Ionics 2012;213:76–82.
[17] Li Y, Roy A, Badami AS, Hill M, Yang J, Dunn S, McGrath JE. J Pow Sour 2007;172:30–38.
[18] Takamuku S, Jannasch P. Macromolecules 2012;45:6538–6546.
[19] Takamuku S, Jannasch P. Polym Chem 2012;3:1202–1214.
[20] Li Q, Jensen JO, Savinell RF, Bjerrum NJ. Prog Polym Sci 2009;34:449–477.
[21] Elabd YA, Hickner MA. Macromolecules 2011;44:1–11.
[22] Tsang EMW, Zhang Z, Shi Z, Soboleva T, Holdcroft S. J Am Chem Soc 2007;129:15106–15107.
[23] Kerres JA. Fuel Cells 2005;5:230–247.
[24] Weissbach T, Tsang EMW, Yang ACC, Narimani R, Frisken BJ, Holdcroft S. J Mater Chem 2012;22:24348–24355.
[25] Nielsen MM, Yang ACC, Jankova K, Hvilsted S, Holdcroft S. Submitted.
[26] Tsang EMW, Zhang Z, Yang ACC, Shi Z, Peckham TJ, Narimani R, Frisken BJ, Holdcroft S. Macromolecules 2009;42:9467–9480.
[27] Nielsen MM, Dimitrov I, Takamuku S, Jannasch P, Jankova K, Hvilsted S. Submitted.
[28] Dimitrov I, Takamuku S, Jankova K, Jannasch P, Hvilsted S. Macromol Rapid Commun 2012;33:1368–1374.
[29] Hvilsted S. Polym Int 2012;61:485–494.
[30] Matyjaszewski K, Xia J. Chem Rev 2001;101:2921–2990.
[31] Horsfall JA, Lovell KV. Eur Polym J 2002;38:1671-1682.
[32] Tsang EMW, Shi Z, Holdcroft S. Macromolecules 2011;44:8845–8857.
[33] Karlsson LE, Jannasch P. J Membr Sci 2004;230:61–70.
[34] Lafitte B, Puchner M, Jannasch P. Macromol Rapid Commun 2005;26:1464–1468.
[35] Weiss RA, Sen A, Willis CL, Pottick LA. Polymer 1991;32:1867–1874.

[36] Park HB, Shin HS, Lee YM, Rhim JW. J Membr Sci 2005;247(1-2):103-110.
[37] Plackett D, Jankova K, Egsgaard H, Hvilsted S. Biomacromolecules 2005;6:2474-2484.

Sulfonated Hydrocarbon Graft Architectures for Cation Exchange Membranes

Mads M. Nielsen[1], Katja Jankova[1], Søren Hvilsted[1,]*

[1]Danish Polymer Centre, Department of Chemical and Biochemical Engineering, Technical University of Denmark, Søltofts Plads, Building 227, DK-2800 Kgs. Lyngby, Denmark
*Corresponding author. E-mail sh@kt.dtu.dk.

S1. Kinetics

A kinetic study of the polymerization was performed until the reaction mixture started gelling. Samples for SEC (THF) were withdrawn after 15, 30, 45, 60, 120 and 140 min. in the case of **PSU-Cl-3**, and after 2, 15, 30, 45, 60, 120 min. in the case of **PSU-Cl-18**. The SEC traces of **PSU-Cl-3** are shown in Figure S1.
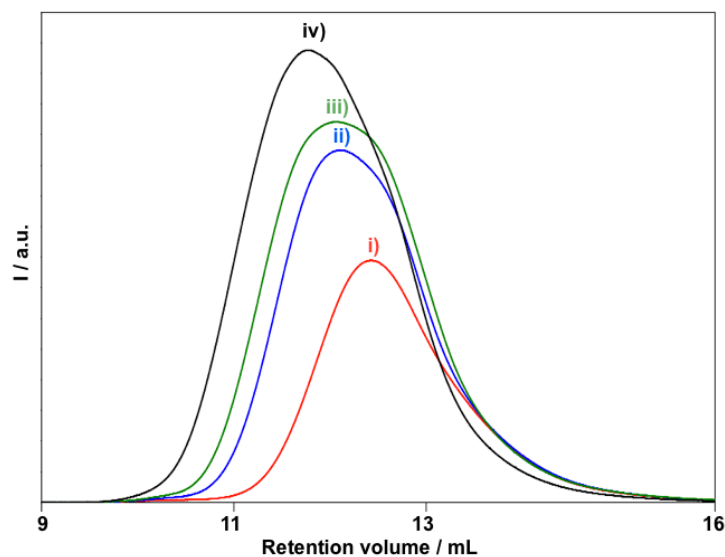

Figure S1. SEC (THF) trace of **PSU-Cl-3** from samples withdrawn after i) 15 min., ii) 30 min., iii) 45 min. and iv) 120 min.

In evaluating the sulfonation step a reference sulfonation reaction is run with **PSU-Cl-18**. Figure S2 contains ^{1}H NMR spectra of treated and untreated sample.
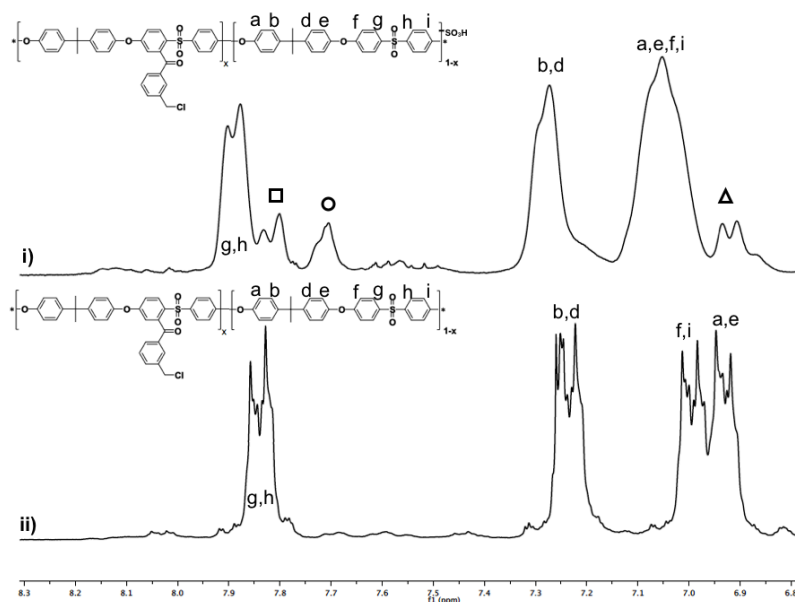
Figure S2. Aromatic region ^{1}H NMR spectra of i) **S-PSU-Cl-18** and ii) **PSU-Cl-18**. The quadrant, circle and triangle represent peaks appearing after the sulfonation reaction.

S2. Synthesis of poly(styrene sulfonic acid sodium salt) (SPS (Na form))

All reagents were purchased from Aldrich and used as received. In a 40 mL Schlenk was placed 2.188 g sodium styrene sulfonic acid hydrate (SSS), 5.6 mg L-ascorbic acid (AA) and 33 mL DMSO and the solution was purged with N_2 under stirring. In a separate 10 mL Schlenk was placed 13.8 mg copper(II)chloride (CuCl$_2$), 7 μL ethyl 2-bromoisobutyrate (EBiB), 15.4 mg bpy and 2 mL DMSO, the mixture was purged with N_2 under stirring. Three freeze-pump-thaw cycles were carried out with both reactors, then the content of small Schlenk was transferred to the monomer mixture and yet a degassing was performed. The reaction was quenched after 2 hours at 60 °C, then the mixture was concentrated and dialyzed (cutoff 1,200 Da, benzoylated tubes) against deionized water for a week to get rid of excess monomer, and subsequently it was filtered and thereafter freeze dried.

^{1}H NMR (300 MHz, D$_2$O, δ(ppm)): 7.66 (Ar *H ortho* to SO$_3^-$Na$^+$), 6.79 (Ar *H meta* to SO$_3^-$Na$^+$), no peaks at 6.0.5.0 ppm indicative of C=C*H$_2$* indicates the pure polymer.

S3. Thermal analysis

TGA plots of **S*g*3-47-S**, **S*g*3-47-M**, **S*g*3-47**-L, **S*g*18-8**, **S*g*18-8-L** and ***g*18-8** are shown in Figure S3. The same trend as that of the **S*g*18-10** series is observed: higher the DS the more material is still left at 650 °C.
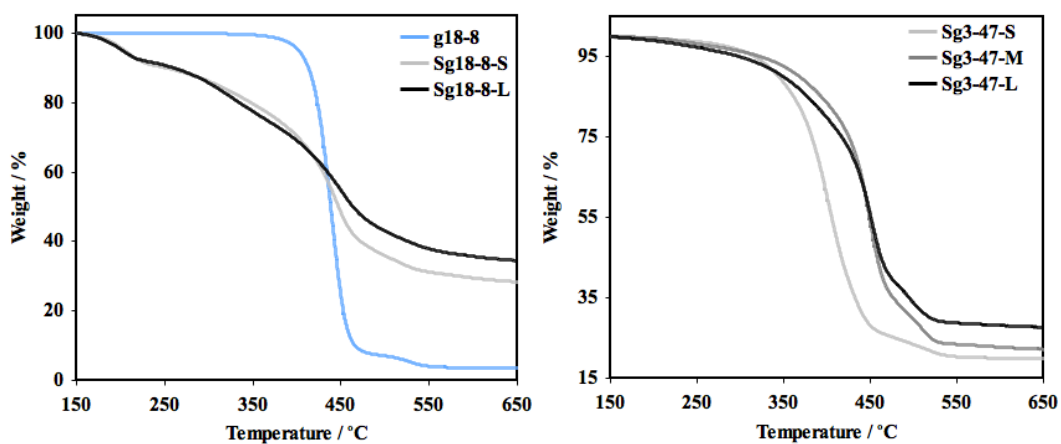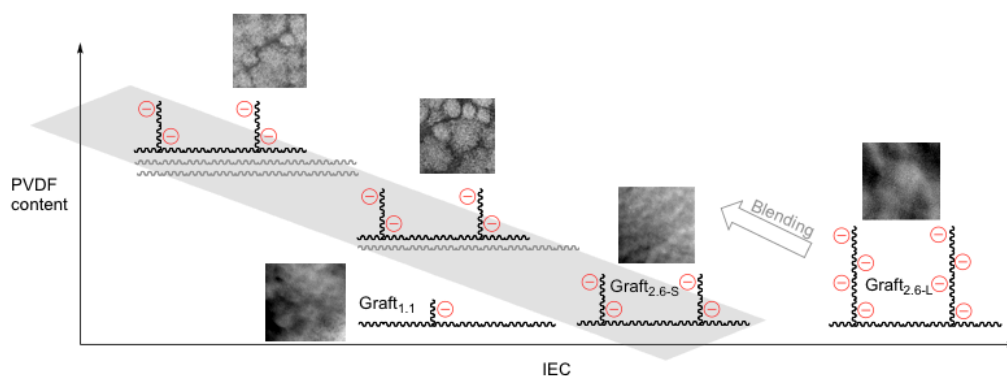

Figure S3. TGA curves of ***g*18-8, S*g*18-8** and **S*g*18-8-L** (left), and **S*g*3-47-S**, **S*g*3-47-M** and **S*g*3-47-L** (right).

V

Enhancing the Ionic Purity of Hydrophilic Channels by Blending Fully Sulfonated Graft Copolymers with PVDF Homopolymer

M. M. Nielsen, A. C. C.Yang, K. Jankova, S. Hvilsted, S. Holdcroft

Enhancing the Ionic Purity of Hydrophilic Channels by Blending Fully Sulfonated Graft Copolymers with PVDF Homopolymer

Mads Møller Nielsen[1,2], Ami Ching-Ching Yang[1], Katja Jankova[1], Søren Hvilsted[1,*], Steven Holdcroft[2,*]

[1]Department of Chemistry, Simon Fraser University, 8888 University Drive, Burnaby, British Columbia, Canada V5A 1S6
[2]Department of Chemical and Biochemical Engineering, Danish Polymer Centre, Technical University of Denmark, Søltofts Plads 227, DK-2800 Kgs. Lyngby, Denmark

* Correspondence to: Steven Holdcroft (E-mail: _holdcrof@sfu.ca_), Søren Hvilsted (E-mail: _sh@kt.dtu.dk_)

Additional Supporting Information may be found in the online version of this article.

ABSTRACT

Membranes of fully sulfonated poly(vinylidene fluoride-_co_-chlorotrifluoroethylene)-_g_-poly(styrene sulfonic acid) blended with PVDF were prepared and investigated for morphology, water sorption, and proton transport properties. The influence of tuning the ionic content of membranes by blending, as opposed to varying the degree of sulfonation, is evaluated. The blend membranes exhibit conductivities superior to pure graft copolymers under fully humidified conditions despite their lower water uptake. Transmission electron microscopy images of the blends reveal the membranes comprise of a combination of macro-phase segregated regions of ion-rich and PVDF-rich domains, and, at higher PVDF contents, a seemingly repetitive pattern of ion-rich nano-scale domains in the PVDF-rich domains.

KEYWORDS: Dynamic vapour sorption, Fuel cells, Morphology, Partially fluorinated, Proton conductivity, Proton exchange membrane, Sulfonic acid, Water sorption

INTRODUCTION

Benchmark proton exchange membranes (PEMs) are based on perfluorosulfonic acid (PFSA) ionomers,[1] e.g., Nafion®. PFSAs show high mechanical and chemical stability, and high proton conductivities under fully humidified conditions but suffer from reduced conductivity at lower humidification, insufficient fuel barrier properties, costly production, and the high fluorine content disfavours them in an environmental context.[2-7] Potentially alternative PEMs include partially fluorinated ionomers,[8-10] and non-fluorinated systems like poly(arylene ether)s,[11-13] polybenzimidazoles[14-18] and polystyrenes,[19] in the form of composites,[20] blocks,[6,21] grafts,[8,22] (acid-base) blends,[23-25] and short, multi-sulfonated side chains.[11,26] Common to these systems is that hydrophilic and hydrophobic domains phase segregate, which facilitates proton transfer. Hydrophobic domains contribute to the mechanical stability of the membrane and the hydrophilic moieties provide proton conductivity.

Understanding structure-property relationships in such systems is crucial for tailoring PEMs for specific applications; hence studies of model systems are essential. Investigating the relationship between polymer architecture, morphology, and transport properties has been a focus of our group.[8,21,27,28] In this context, we have studied partially fluorinated diblock and the graft copolymer systems sulfonated to various degrees.[8,29,30] The degree of sulfonation on the effect of ionic purity and connectivity of proton-

1

conducting channels in poly(vinyl fluoride-*co*-hexafluoropropane)-*b*-poly(styrene sulfonic acid) (P(VDF-*co*-HFP)-*b*-SPS) has been shown to have considerable impact on the size of ionic clusters.[8,29] Recent studies of the graft copolymers by small angle X-ray scattering (SAXS) and small angle neutron scattering (SANS) reveal that the ionic content is the major parameter influencing water uptake[31] when the PS content is >75 vol%[28], whereas other factors are predominant when the PS content is <75 vol%. From studies where the graft density is varied, it appears that the PVDF volume ratio and the degree of crystallinity also play a strong role on the morphological structure and resulting transport properties[28]. In follow-up work, a partially sulfonated P(VDF-*co*-CTFE)-*g*-SPS ionomer was blended with (i) a high m.wt. amorphous fluorous polymer that increased the entanglement of amorphous fluorous domains, (ii) a low m.wt. crystalline fluourous polymer that increased the fluorous crystallinity but did not enhance the connectivity of the fluorous crystalline domains, and (iii) a high m.wt crystalline fluorous polymer that increased both crystallinity and the connectivity of crystalline domains.[31] Separately increasing the crystallinity and the connectivity of crystalline domains resulted in a resistance to excessive swelling in water. Recently, work on PVDF blends with partially sulfonated systems proved graft copolymers better suited for blending than block copolymers due to its nanostructured morphology.[27] A common message has emerged in all of this work: the ionic rich regions observed by TEM analysis are compromised by the presence of non-sulfonated polymer in the graft chains, and that high ionic purity of the ionic-rich domains facilitates phase-segregation, restricts water swelling, and enhances proton transport.

In the present study four fully sulfonated poly(vinylidene fluoride-co-chlorotrifluoroethylene)-graft-poly(styrene sulfonic acid) [P(VDF-*co*-CTFE)-*g*-SPS] were prepared to investigate ionic channel formation and proton transport. These graft copolymers consist of a hydrophobic fluorous backbone and fully sulfonated polystyrene graft chains. The fluorous backbone provides mechanical integrity to the copolymers and the sulfonated graft side chains allow for proton conductivity. The graft copolymers were synthesized by atom transfer radical polymerization (ATRP) of styrene, followed by post-sulfonation. Two systems of graft copolymers comprising different graft density are studied here. The first series of graft copolymer comprises a backbone possessing 1.1 mol% of CTFE and a degree of polymerization of polystyrene (DP_{PS}) of 24 ($Graft_{1.1}$). The second series comprises of 2.6 mol% of CTFE in the backbone and a DP_{PS} of 39, 62, and 79 ($Graft_{2.6}$). Blends $Graft_{2.6}$ with PVDF are prepared to contain a similar volumetric ratio of PS:PVDF as that calculated for the pure graft $Graft_{1.1}$. The fully sulfonated graft copolymer, $Graft_{1.1}$, and the three of $Graft_{2.6}$ – PVDF blends possess 40 vol% of sulfonated polystyrene (SPS) and 60 vol % of PVDF, thus allowing comparisons of the effect of blending while holding hydrophobic to hydrophilic volume contents constant. Another series of graft blends containing 25 vol% SPS and 75 vol% PVDF were also prepared to investigate the proton transport properties of low ion content polymers. A scheme illustrating the differences of these materials is provided in Figure 1. Here, IEC is tuned by either controlling the degree of sulfonation of the graft copolymer or by blending a fully sulfonated graft copolymer with PVDF. The advantage of blending a fully sulfonated graft copolymer to improve mechanical properties and reduce excessive swelling, rather than reducing the degree of sulfonation (DS) of the PS grafts, is that the volumetric SPS content can be lowered without isolating ionic domains by non-sulfonated PS.
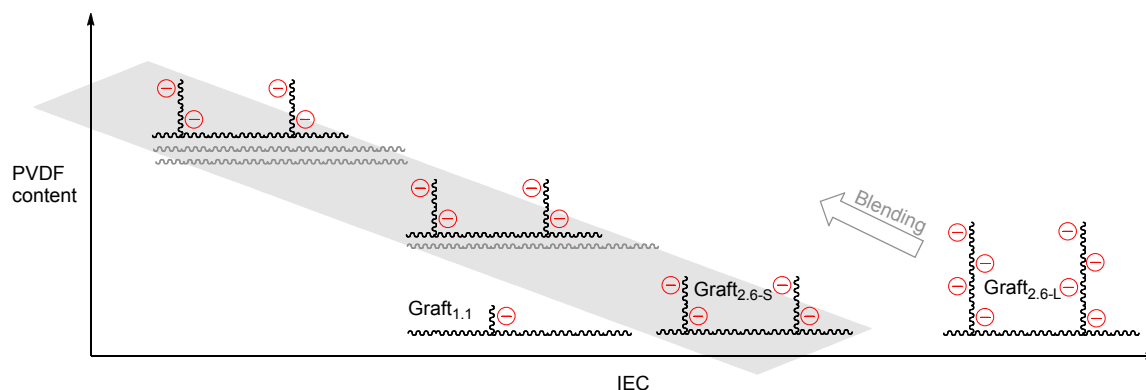
FIGURE 1 Illustration of the relationship between PVDF homopolymer content and IEC for [P(VDF-co-CTFE)-g-SPS] and their blends with PVDF. Where Graft$_{1.1}$, Graft$_{2.6}$, and Graft$_{2.6L}$ represent pure graft copolymers. The grey area represents the Graft$_{2.6-S}$ series. Similar-IEC blend series are made for Graft$_{2.6-M}$ (not shown) and Graft$_{2.6-L}$.

EXPERIMENTAL

Materials

The following chemicals were purchased from Aldrich and used as received unless otherwise stated: vinylidene fluoride (VDF, +99%), chlorotrifluoroethylene (CTFE, 98%), Acetic anhydride (AA, 99.5%), phenolphthalein, sodium hydroxide (NaOH), lead(II) acetate trihydrate (Pb(OAc)$_2 \cdot$ 3 H$_2$O), Spurr's epoxy resin, hexanes, ethanol, dimethyl acetamide (DMAc, anhydrous, 99.8%), calcium chloride (CaCl$_2$), acetone-d_6 (99.9 atom% D), potassium persulfate (KPS, Allied Chemical, reagent grade), 1,2-dichloroethane (DCE, Caledon, reagent grade), sulfuric acid (H$_2$SO$_4$, Anachemia, 95-98%, ACS reagent), poly(vinylidene fluoride) (PVDF, M$_w$ = 530 kDa, M$_n$ = 270 kDa). Copper(I) chloride (CuCl, 99%) and copper(II) chloride (CuCl$_2$, 99.999%) were purified according to literature.[32]

Synthesis

Synthesis of P(VDF-co-CTFE)-g-PS

P(VDF-*co*-CTFE) macroinitiators with molar percentages of ATRP-initiating CTFE units (X$_{CTFE}$) of 1.1% and 2.6% were prepared and styrene grafted from them as previously reported (details are provided in Table 1).[28] These series are referred to as Graft$_{1.1}$ and Graft$_{2.6}$. The degree of polymerization of PS for Graft$_{1.1}$ was 24 (DP$_{PS}$ = 24), and three graft lengths were grown from Graft$_{2.6}$: Graft$_{2.6-S}$ (DP$_{PS}$ = 39; $_S$ = short), Graft$_{2.6-M}$ (DP$_{PS}$ = 69; $_M$ = medium) and Graft$_{2.6-L}$; (DP$_{PS}$ = 79; $_L$ = Long). The synthesis and analysis of Graft$_{2.6}$, was recently reported.[28] Graft$_{1.1}$ were similarly prepared, see Supporting Information for further details. Graft copolymers were precipitated from MeOH, washed with cyclohexane, then filtered and dried under vacuum at 60 °C overnight. Characterization of the synthesized graft copolymers was performed using SEC analysis (using PS standards), and ^{19}F and ^{1}H NMR spectroscopy.[28]

Sulfonation of P(VDF-co-CTFE)-g-PS

In a typical sulfonation reaction, 0.2 g P(VDF-*co*-CTFE)-g-PS was stirred in 5 mL DCE under a blanket of argon at 40-50 °C in a 50 mL three neck round bottom flask equipped with a condenser. In a separate flask, 0.6 mL acetic anhydride was mixed with 1.0 mL DCE in a N$_2$-purged vial, cooled in a chilled 10%

CaCl$_2$ solution. 0.2 ml of 95 - 97 % sulphuric acid was added, and the resulting acetyl sulphate was immediately transferred to the polymer solution at 40 °C. The colour changed from yellowish to brown as the reaction proceeded over 24 hrs. The mixture was poured into 1:1 EtOH/hexanes (EtOH terminates the reaction and hexanes act as a non-solvent). The solvent was removed, then the precipitate was washed with Millipore water until neutral pH, and then dried under vacuum at 60 °C overnight. The DS of PS was determined from ^{1}H NMR spectra (acetone-d_6) recorded on a 400 MHz Varian MercuryPlus spectrometer. ^{1}H NMR (400 MHz, acetone-d_6, δ): 7.65 (2H, Ar H *ortho* to –SO$_3$H), 6.81 (2H, Ar H *meta* to –SO$_3$H), 2.96 + 2.35 (2H, CH$_2$-CF$_2$, PVDF), 1.89-1.64 (2H, CH$_2$-CH, PS), 1.44-1.27 (1H, CH-CH$_2$, PS). The complete sulfonation of the graft copolymers was confirmed as shown in the supporting information Figure 1S.

Blending and membrane preparation

The volumetric percentage of poly(styrene sulfonic acid) (vol% SPS) was calculated from the number average molecular weights ($\overline{M}$) and densities (ρ) of SPS, PVDF and the MI, according to Equation 1. Graft$_{1.1}$ contains 40 vol % SPS and 60 vol% PVDF. In order to prepare blends with similar SPS-PVDF ratios the Graft$_{2.6}$ series was blended with a commercially available high molecular weight PVDF to provide 40 vol % SPS and 60 vol% PVDF. These three blend membranes of varying graft length and equal targeted molar ionic content are abbreviated SB40-60, MB40-60, and LB40-60, for short, medium, and long graft lengths, respectively. To investigate the influence on Graft$_{2.6}$ upon blending with PVDF blending component, a second blend series was prepared by using half the graft copolymer weight percentage, resulting in a SPS: PVDF molar ratio of 25:75, abbreviated SB25-75, MB25-75 and LB25-75.

$$V_{SPS}(\%) = \frac{\dfrac{\overline{M}_{n\,SPS}}{\rho_{SPS}}}{\dfrac{\overline{M}_{n\,SPS}}{\rho_{SPS}} + \dfrac{\overline{M}_{n\,P(VDF-co-CTFE)}}{\rho_{P(VDF-co-CTFE)}} + \dfrac{\overline{M}_{n\,PVDF}}{\rho_{PVDF}}}$$

(1)

The polymers and blend mixtures were dissolved in DMAc, concentrated and cast on a levelled Teflon sheet at room temperature. The resulting polymer films were dried at 80 °C in vacuum oven overnight. Upon drying the membranes, 50-75 μm thick, were cut into rectangular shapes of typically 10 mm by 5 mm after which they were protonated by immersion in 2M HCl. The protonated membranes were washed multiple times with Millipore deionized water to remove excess acid, and then stored in Millipore deionized water between two glass microscope slides to prevent coiling, until use.

Measurements and calculations

Transmission electron microscopy (TEM) and ionic domain distribution

Small samples for TEM were stained with lead acetate by soaking in a 2M solution overnight, followed by Millipore water rinsing and drying at 80 °C in vacuum oven overnight. The films were embedded in Spurr's epoxy and cured overnight at 70 °C. The pure graft copolymers were microtomed at RT using a Leica UC6 ultramicrotome, and the slices were collected on a copper grid. Electron micrographs were obtained with a Hitachi H7600 TEM by applying an accelerating voltage of 100 keV. The blends were cryo-microtomed using a Leica Ultracut UCT with a Cryo 35° Waterblade. Electron micrographs were

obtained with a Tecnai T20 G^2 operated at an accelerating voltage of 200 keV. Determination of the ionic domain sizes was performed applying the software ImageJ, estimating the average size and standard deviation from 100 samples of each image. The 2D number density and standard deviations was determined from counting of three areas defined in ImageJ.

Water uptake and IEC

The water uptake was calculated as the percentage mass gain of the dry membrane after immersion in water, according to Equation 2, with m_{wet} and m_{dry} representing the wet and dry masses of the membrane.

$$Water\ uptake = \frac{m_{wet} - m_{dry}}{m_{dry}} \times 100\%$$

(2)

The ion exchange capacity (IEC) was determined by acid-base titration. Firstly, the acidified membranes were equilibrated in 2M NaCl for at least 4 hours to convert the SO_3^- groups to the Na^+ form. The deprotonated films were titrated with 1mM NaOH to a phenolphthalein end point. After titration the salt form membranes were immersed in 2M HCl for 5 hours. The re-protonated membranes were washed several times to remove excess acid from the surface and the bulk. The membranes were dried in vacuum oven at 70 °C overnight. IEC [mmol g^{-1}] was calculated using Equation 3, where V_{NaOH} and c_{NaOH} are the volume [L] and molar concentration [mol L^{-1}] of NaOH solution, respectively.

$$IEC = \frac{V_{NaOH} - c_{NaOH}}{m_{dry}} \times 100\%$$

(3)

The hydration number (or [H$_2$O]/[SO$_3^-$]), λ, indicates the amount of water molecules per sulfonic acid group and was calculated using Equation 4.

$$\lambda = \frac{[H_2O]}{[SO_3^-]} = \frac{water\ uptake \times 10}{18 \times IEC}$$

(4)

The stated water uptake, IEC and λ are average values from measurements on multiple membranes. The stated errors are the standard deviations of the data points. Nafion® 117 (N117) membranes were used as internal reference in all measurements. IEC values determined by titration are referred to as IEC$_{act}$ (actual IEC), whereas theoretical IEC values are referred to as IEC$_{th}$.

Dynamic water vapour sorption (DVS)

Gravimetric water vapour sorption technique was used to obtain the isothermal water vapour sorption at different relative humidities (RH). The instrument used was a DVS-1000 from Surface Measurement Systems, UK. The target RH was reached by using a mixed gas flow of fully saturated water vapour and dry nitrogen. RH was maintained and controlled by a dew-point sensor. Typically, the membranes were kept at 25 °C in an RH range of 0-98% with steps of 10% from 0 to 90%, then to 95% and finally 98%. The mass of the membrane was recorded *in situ* every 10 seconds and the stable masses of the membrane at each RH stage were used to calculate the water sorption. The slope of a linear fit to the data points is

a useful measure of the dependency of temperature and humidity respectively. Even when the fit is not perfectly linear the slope can be a useful indicator of the relative sensitivities of multiple membranes. In the ideal case the slope should be as small as possible, i.e. the membrane performance remains constant regardless of fluctuations in temperature and humidity.

Proton conductivity
In-plane proton conductivity was measured by AC impedance spectroscopy by using a Solartron 1260 frequency response analyzer (FRA) employing a two-electrode configuration, according to a previously described procedure.[33] In short, a membrane (typically 10 mm by 5 mm) was placed between two Pt electrodes in a Teflon conductivity cell, applying a 100 mV sinusoidal AC voltage over a frequency range of 10 MHz-100 Hz. The membrane resistance was determined by fitting the resulting Nyquist plots to the standard Randles equivalent circuit.[8] Proton conductivity (σ) [mS cm^{-1}] was calculated according to Equation 5, where L [cm] represents the length of the conducting matter (i.e. the distance between the two electrodes), A [cm^2] is the cross-sectional area of the membrane, and with R [Ω] being the electrical resistance of the membrane. The proton conductivity was calculated as the average of several measurements.

$$\sigma = \frac{L}{R \times A} \tag{5}$$

It is perceived that well-ordered networks lead to increased proton conductivity, which is why different structures of similar ionic content can exhibit diverse conductivities.[34] The analytical acid concentration [-SO$_3$H] (M) has a strong influence on proton conductivity, so knowledge on its dependency on acid and water content is valuable,[35] e.g. at elevated IEC water uptake may be high and consequently the acid is diluted, which has a subversive affect on the proton conductivity. [-SO$_3$H] in wet membranes was calculated according to Equation 6 using IEC values measured by titration, where V_{wet} is the volume of the wet membrane (cm^3).

$$\left[-SO_3H \right] = \frac{m_{dry}}{V_{wet}} \times IEC \tag{6}$$

The effective proton mobility, μ_{eff}, [cm^2 sV^{-1}] in the wet membrane was estimated using Equation 7, where σ represents proton conductivity [mS cm^{-1}], and F is the Faraday constant[33]. μ_{eff} is the proton conductivity "normalized" for the effects of acid concentration and provides information on acid dissociation, ionic channel tortuosity, and special proximity of neighbouring acid groups.[35] In the extreme case where no dissociation of the acid takes place, $\mu_{eff} = 0$.[35]

$$\mu_{eff} = \frac{\sigma}{F \times \left[-SO_3H \right]} \tag{7}$$

Conductivity as function of temperature and relative humidity
Conductivity measurements under varying temperature and RH were performed in an ESPEC SH-241 temperature/humidity chamber. Conductivity measurements were obtained *in situ* until at least three

successive measurements proved that equilibrium had been reached. Typically, this occurred after 5 hours. Membranes were re-cast and their proton conductivities measured multiple times.

RESULTS AND DISCUSSION

Synthesis of P(VDF-co-CTFE)-g-PS

Graft copolymers were synthesized successfully as previously reported[28] and further described in the supporting information. From P(VDF-*co*-CTFE) with X_{CTFE} = 1.1%, $Graft_{1.1}$ (DP_{PS} = 24) was synthesized. From P(VDF-*co*-CTFE) with X_{CTFE} = 2.6%, $Graft_{2.6-S}$ (DP_{PS} = 39), $Graft_{2.6-M}$ (DP_{PS} = 69) and $Graft_{2.6-L}$ (DP_{PS} = 79) were synthesized. Details on the $Graft_{2.6}$ series sulfonated to different degrees are included in Table S2 in the Supporting Information.

Sulfonation of polystyrene grafts

^{1}H NMR spectra were obtained for all polymers and confirmed sulfonation of the initially partially sulfonated graft chains. ^{1}H NMR spectra of pristine, partially and fully sulfonated $Graft_{2.6-L}$ are shown in Figure S1 in the Supporting Information as an example. The pristine copolymers exhibit polystyrenic *ortho*-H NMR peaks at δ = 6.8 - 6.5 ppm and *meta/para*-H NMR peaks at δ = 7.4 - 6.9 ppm. The partially sulfonated graft copolymers exhibit an additional peak at δ = 7.6 ppm, corresponding to the protons adjacent to the sulfonated group. The fully sulfonated $Graft_{2.6-L}$ has no remaining *meta/para* -H NMR peaks. The chemical composition of the fully sulfonated $Graft_{1.1}$ copolymer and the blends of $Graft_{2.6-S}$ $Graft_{2.6-M}$ and $Graft_{2.6-L}$ are shown in Table 1.

Due to the increased ionicity of $Graft_{2.6-M}$ (IEC_{th} = 4.05 mmol g^{-1}) and $Graft_{2.6-L}$ (IEC_{th} = 4.29 mmol g^{-1}) these two polymers partially dissolved when immersed in water, which precluded the determination of IEC by titration.

TABLE 1 Chemical composition of fully sulfonated graft copolymer and their blends.

Polymer	Blend	X_{CTFE}[a] (mol%)	GD[b] (mol%)	DP_{PS}[c]	$M_{n\ P(VDF-co-CTFE)}$[d] (kg mol^{-1})	$M_{n\ SPS}$[e] (kg mol^{-1})	Wt%$_{graft}$[f]	Wt%$_{PVDF}$[f]	SPS:PVDF[g] (membrane vol%)
$Graft_{2.6}$	SB40-60	2.6	1.68	39	120	230	48.3	51.7	40:60
$Graft_{2.6}$	MB40-60	2.6	1.68	62	120	370	42.0	58.0	40:60
$Graft_{2.6}$	LB40-60	2.6	1.72	79	120	480	39.7	60.3	40:60
$Graft_{2.6}$	SB25-75	2.6	1.68	39	120	230	24.0	76.0	25:75
$Graft_{2.6}$	MB25-75	2.6	1.68	62	120	370	21.0	79.0	25:75
$Graft_{2.6}$	LB25-75	2.6	1.72	79	120	480	19.7	80.3	25:75
$Graft_{1.1}$	$Graft_{1.1}$	1.1	0.68	24	150	70	100	0	40:60

[a] Measured by ^{19}F NMR; no. of PS grafts per 100 backbone repeat units, [b] calculated from X_{CTFE} multiplied by the macroinitiator efficiency. [c] Average number of repeat units per graft, calculated from the St:VDF ratio divided by GD. [d] Measured by SEC (DMF) calibrated with PS standards. [e] Calculated from $M_{n\ P(VDF-co-CTFE)}$ and the St:VDF ratio determined by ^{1}H NMR. [f] Calculated from the compositions of the pure graft copolymers and the densities of the component monomer. [g] Blend compositions were chosen to be equal to that of $Graft_{1.1}$, and half the wt%$_{graft}$ respectively.

TEM

TEM images of $Graft_{2.6}$ – PVDF blends are shown in Figure 2. Images of the pure graft copolymers are also shown for comparison. In Table 2, ion-rich domain sizes and 2D number densities of these

membranes are listed. The 25-75 series is difficult to quantify unambiguously and thus excluded from the table. For all membranes, a phase-separated morphology of ion-rich domains, appearing as dark areas, are randomly distributed in a fluorous matrix, appearing as bright areas. The ion-rich domains do not vary remarkably in size from $Graft_{1.1}$ to $Graft_{2.6}$ (3.7 ± 0.6 nm vs. 4.7 ± 0.6 nm of $Graft_{2.6-L}$) – arguably due to a higher degree of flexibility of the low graft density $Graft_{1.1}$. Neither is there any significant difference in size within the $Graft_{2.6}$ series (3.8 ± 0.6 nm to 4.7 ± 0.6 nm) – indicative of a negligible influence of graft length on the ion-domain size. The 2D number density of ion-rich domains is considerably lower for $Graft_{1.1}$ than the $Graft_{2.6}$ series, (40 per $10^4 nm^2$ vs. 53-56 per $10^4 nm^2$), which is attributed to its lower graft density and low SPS content resulting in low IEC. At low magnification (scale bar 200 nm) the 40-60 series exhibit continuous ion-rich domains separating PVDF-rich domains in the size order of hundreds of nm. This suggests that the ionomer and PVDF phases separate at macro level. At high magnification of the PVDF-rich domains (scale bar 20 nm) a repetitive pattern of ion-rich domains in a predominantly PVDF containing network is observed, reminiscent of disordered versions of the continuous morphology obtained with self-assembling copolymer systems.[36] This suggests that nano-phase segregation takes place as well. The sizes of the ion-rich domains are not significantly different from SB40-60 to LB40-60 (1.52 ± 0.31 nm vs. 1.74 ± 0.37 nm), but smaller than the ion-rich domains of the pure graft copolymers. Neither are the 2D number densities significantly different from SB40-60 to LB40-60 (17 ± 2 per 100 nm^2 vs. 12 ± 2 per 100 nm^2), however, they are considerably higher than those of the pure graft copolymers. The 25-75 series also macrophase-separate into ion-rich domains and PVDF-rich domains, as can be seen at low magnification. At high magnification of the PVDF-rich domains (20 nm scale bar) there is no distinct pattern for the ion-rich groups.
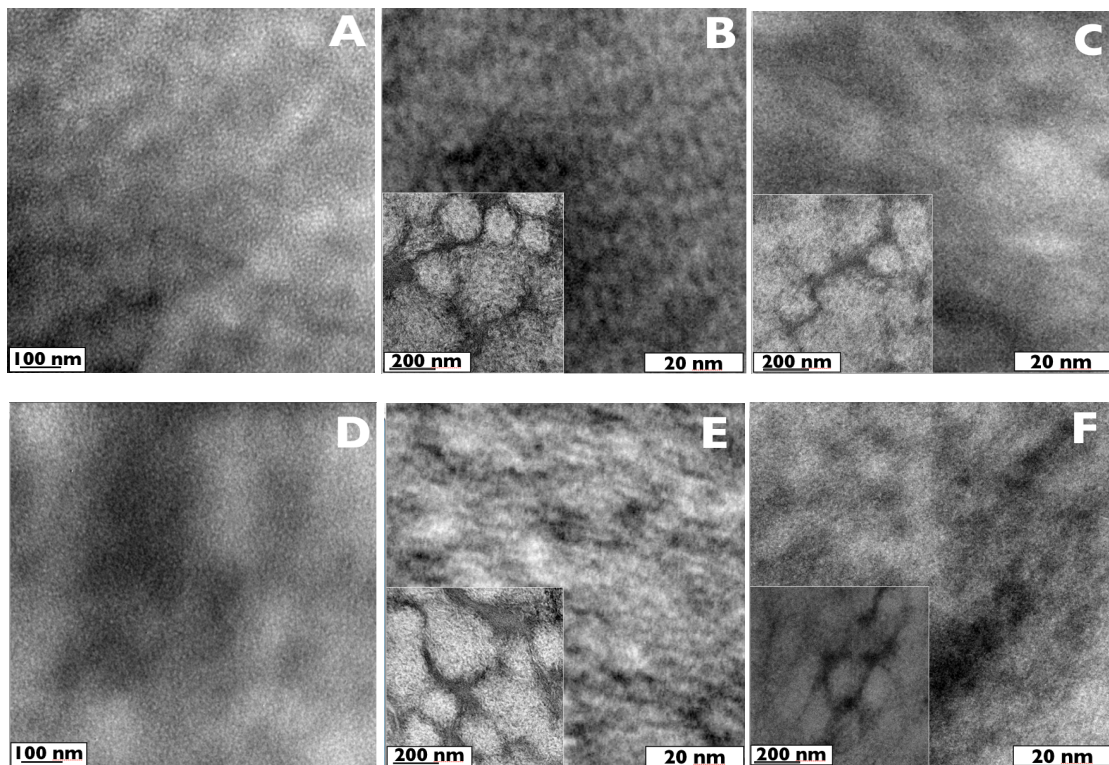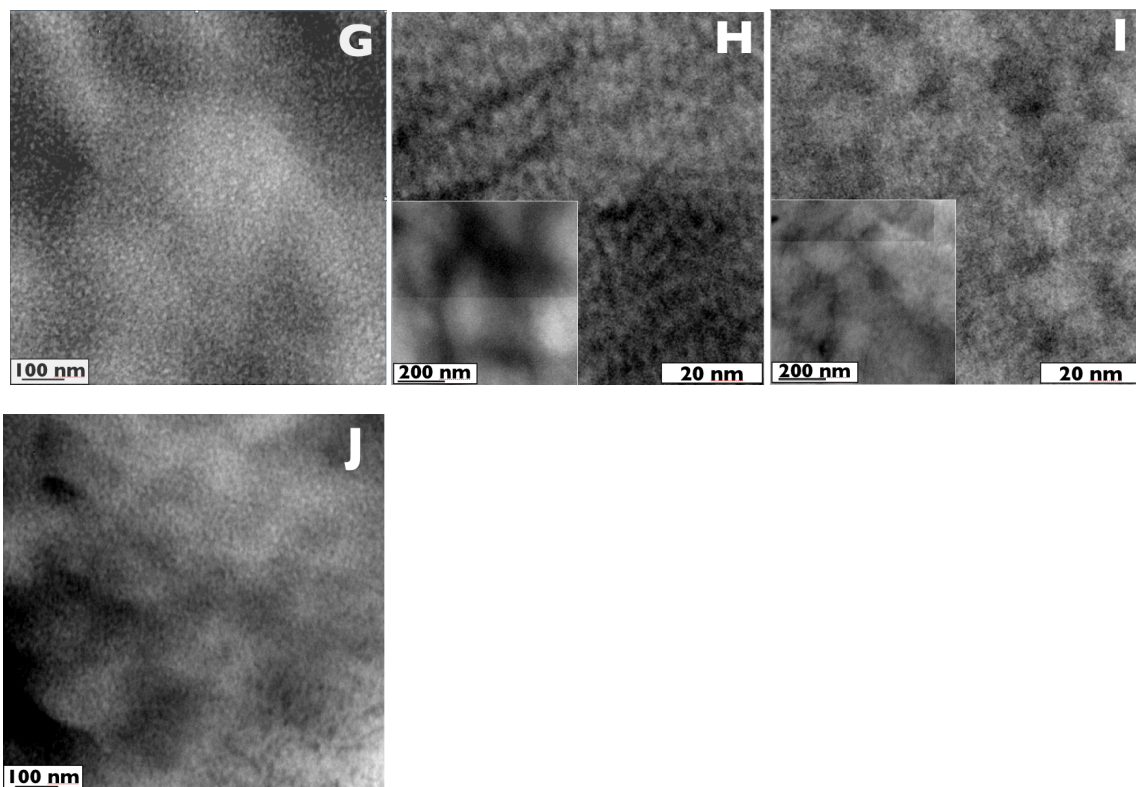
FIGURE 2 TEM images of (A) $Graft_{2.6-S}$, (B) SB40-60, (C) SB25-75, (D) $Graft_{2.6-M}$, (E) MB40-60, (F) MB25-75, (G) $Graft_{2.6-L}$, (H) LB40-60, (I) LB25-75 and (J) $Graft_{1.1}$. The bright domains are PVDF-rich and the dark domains ion-rich.

TABLE 2 Ion-rich domain sizes and number densities of pure graft copolymers and blends.

Polymer	IEC_{th} (mmol g^{-1})	IEC_{act} (mmol g^{-1})	DS (%)	Ion-rich domain size (nm)	2D number density
$Graft_{2.6-S}$ (A)	3.52	-[a]	99	3.8 ± 0.6	56 ± 3 [b]
SB40-60 (B)	1.72	1.22 ± 0.18	-	1.52 ± 0.31	17 ± 2 [c]
SB25-75 (C)	0.85	0.60 ± 0.02	-	-	-
$Graft_{2.6-M}$ (D)	4.05	-[a]	99	4.1 ± 0.7	55 ± 2 [b]
MB40-60 (E)	1.72	1.31 ± 0.10	-	1.59 ± 0.32	14 ± 2 [c]
MB25-75 (F)	0.85	0.75 ± 0.09	-	-	-
$Graft_{2.6-L}$ (G)	4.29	-[a]	99	4.7 ± 0.6	53 ± 1 [b]
LB40-60 (H)	1.72	1.15 ± 0.09	-	1.74 ± 0.37	12 ± 2 [c]
LB25-75 (I)	0.85	0.64 ± 0.02	-	-	-
$Graft_{1.1}$ (J)	1.72	1.10 ± 0.07	99	3.7 ± 0.6	40 ± 1 [b]

[a] Not available due to severe membrane swelling when immersed in water. [b] Per 10^4 nm^2. [c] Per 10^2 nm^2.

In Figure 3, TEM enlargement is used in explaining the phase separation taking place at two length scales in the 40-60 blend series. In the image to the left, primarily fluorous domains (bright) are surrounded by a seemingly continuous ion-rich phase (dark). At higher magnifications (red dotted box), dark areas appear in the bright domains. These can be either ion-rich domains within the otherwise predominantly fluorous domains, or primarily fluorous domains within the ion-rich domains. In the dark area, the sulfonated polystyrene grafts appear as the black domains, with the scattered bright area representing the fluorous nano-domains consisting of mainly the backbone, and possibly also smaller amounts of PVDF blending material. The blue dashed box shows the borderland between the ion-rich (left) and fluorous domains (right).
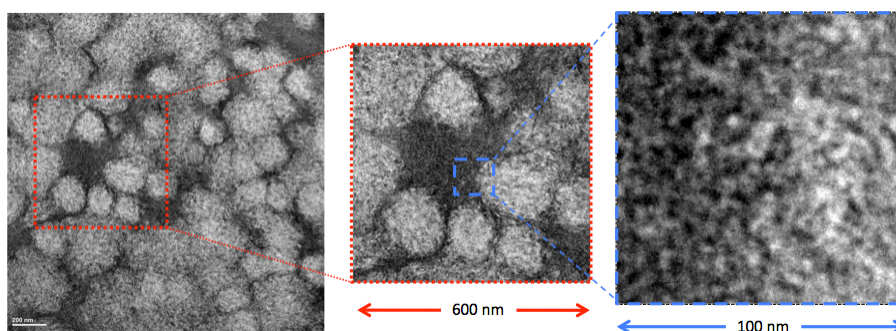

FIGURE 3 TEM images for interpretation of the phase separation taking place at two length scales.

IEC

IEC is lowered upon the addition of PVDF to the ionomer. Theoretical and actual IEC values of the pure graft copolymers and blends are listed in Table 2. Generally, IEC_{act} are lower than IEC_{th} by 10 - 35%, indicating partial inaccessibility to acidic groups in the fluorous matrix. Thus IEC_{th} of the 40-60 and 25-75 series are 1.72 mmol g^{-1} and 0.85 mmol g^{-1}, respectively, and IEC_{act} are in the range of 1.15 - 1.31 mmol g^{-1} and 0.60 - 0.75 mmol g^{-1}, respectively. The pure graft copolymer $Graft_{1.1}$ has a slightly lower IEC_{act} (1.10 mmol g^{-1}) than the similar-IEC_{th} 40-60 blend series.

Partial sulfonation vs. blending upon full sulfonation

Water sorption and proton transport properties under fully humidified conditions of the 40-60 blends and previously reported data for partially sulfonated graft[28] are plotted in Figure 4 (with N117 as reference) in order to evaluate the effect of varying IEC by blending or by changing the DS. Of particular interest is the performance at similar ionic content, at IEC ~ 1.0.

In Figure 4A, water uptake is plotted against IEC_{act}. The blends exhibit a factor 3 - 4 increase in water uptake relative to the partially sulfonated grafts (66 - 98 wt% vs. 18 - 29 wt%). The partially sulfonated grafts require twice as high an ionic content to obtain similar water uptake. Arguably, the blends allow for an increase in water percolation since the restricting effect of unsulfonated PS here is eliminated. Compared to N117, that takes up 33 wt% water, the blends take up 2 - 3 times more.
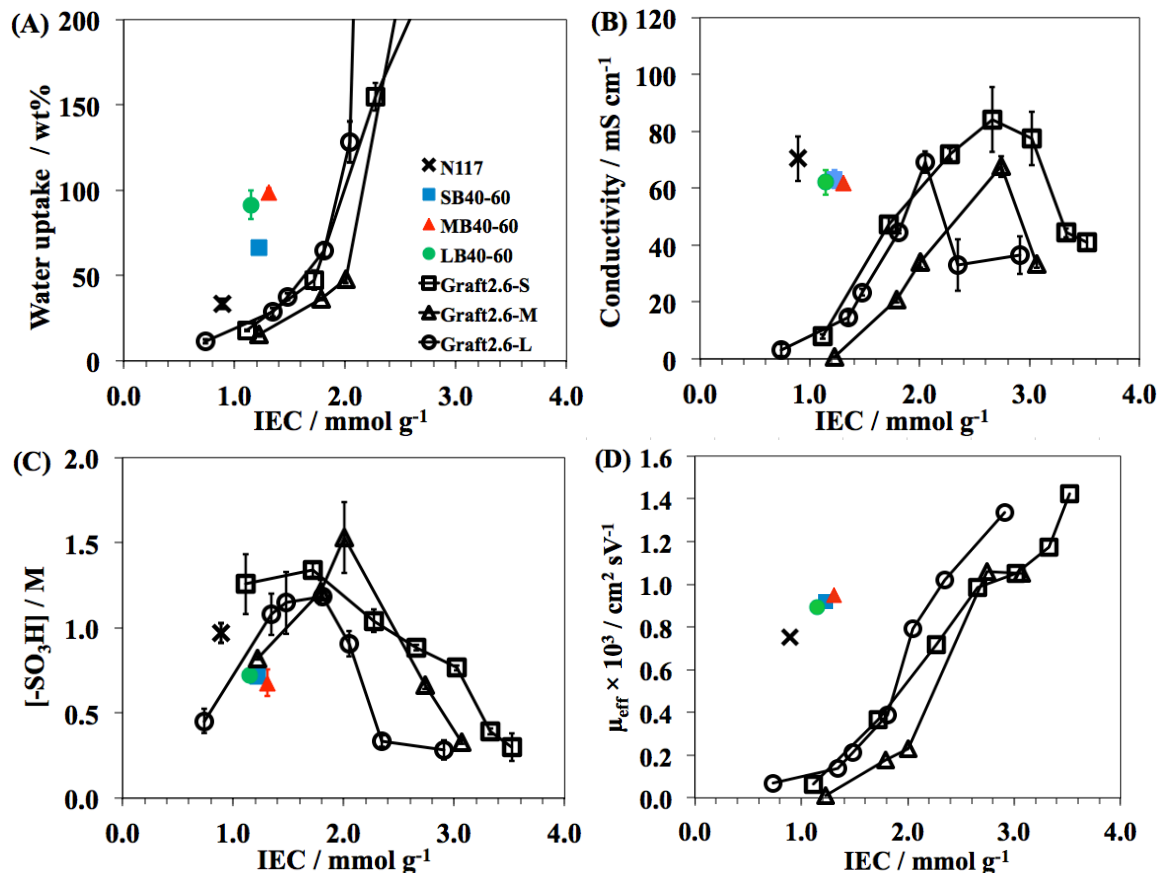
FIGURE 4 (A) Water uptake (data for the highest IEC values is not included due to excessive swelling), (B) proton conductivity, (C) analytical acid concentration and (D) *effective* proton mobility vs IEC for P(VDF-*co*-CTFE)-*g*-SPS at various DS (black)[28] and the 40:60 blend series.

In Figure 4B is shown the IEC_{act} dependency of the proton conductivity. The blends exhibit at least 4 times higher conductivities at IEC ~1.0 than partially sulfonated grafts (62 - 63 mS cm^{-1} vs. 1 - 15 mS cm^{-1}), approximately the same order of magnitude as observed for the water uptake. The partially sulfonated system requires 2 - 3 times the ionic content to obtain similar conductivities.

In Figure 4C, the analytical acid concentration,[$-SO_3H$], is plotted versus IEC_{act}. [$-SO_3H$] of the blends is similar to the partially sulfonated $Graft_{2.6-M}$ (0.68 - 0.72M vs. 0.82M) and half of partially sulfonated $Graft_{2.6-S}$ (1.26M). This deviance can be explained to a certain extent by the spread in IEC of the partially sulfonated $Graft_{2.6}$, leading to different water uptakes (18 - 29 wt%, as can be seen from Figure 4A). The [$-SO_3H$] of N117 is 0.97M, and thus closer in value to the blends than the factor 2 - 3 difference in water uptake that causes dilution of the acid.

In Figure 4D is shown the effective proton mobility, μ_{eff}, versus IEC_{act}. The blends exhibit μ_{eff} values that are several times larger than the partially sulfonated grafts (0.89 × 10^3 - 0.95 × 10^3 cm^2 sV^{-1} vs. 0.01 × 10^3 - 0.14 × 10^3 cm^2 sV^{-1}). This is more than they differ in conductivity, indicative of a morphological gain by

11

blending. As with conductivity, the partially sulfonated system requires 2 - 3 times the ionic content to obtain a similar μ_{eff}. The proton mobility in the blends is greater than N117 (0.75×10^3 cm^2 sV^{-1}) despite showing lower conductivities (Figure 4B). For comparison, the μ_{eff} of a free proton in water at infinite dilution is 3.623×10^{-3} cm^2 s^{-1} V^{-1} at 298 K.[37]

Figure 5 contains an illustration of the effects of changing the ion content by two different strategies: Changing the degree of sulfonation, DS (left) and blending with PVDF (right). The fully sulfonated graft membrane (Figure 5, center), which has high PS volumetric content and is completely sulfonated, possesses well connected ionic domains. However, it will lead to excessive water swelling and loss in mechanical integrity. If DS is decreased, thus allowing partially sulfonated grafts to exist, the unsulfonated PS may encapsulate ionic domains, causing poor connectivity between ionic domains (Figure 5, left). Therefore, partially sulfonated graft copolymers with low IEC's absorb low amount of water and their proton conductivity are expected to be low. Fully sulfonated blends, because of the absence of unsulfonated PS (Figure 5, right) promote and retain contiguous ionic domains for effective proton transport, thus higher ionic purity in the ionic channels. Furthermore, the PVDF homopolymer component helps reduce excessive water swelling and enhancing mechanical property.
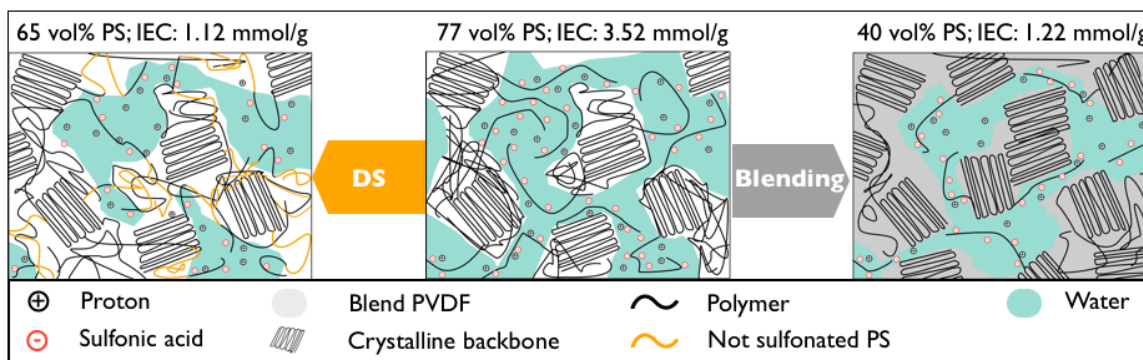

FIGURE 5 Schematic presentation of the effect of changing IEC by changing DS (left), and blending with PVDF (right). In the blending approach, the presence of unsulfonated PS, that restricts ionic domain growth, is mitigated.

Full sulfonation vs. blending
Water sorption and proton transport properties under fully humidified conditions of Graft$_{1.1}$, the 40:60 series and the 25:75 series are presented in Figure 6. In Figure 6A, water uptake is plotted against IEC$_{act}$. For a similar IEC, the 40-60 blend series show water uptakes of 66 - 98 wt%, i.e., 2 - 3 times less than Graft$_{1.1}$ at 192 wt%. When halving the IEC in the 25-75 blend series the water uptake is reduced proportionally to 25 - 40 wt%, which is close to N117 (33 wt%), but the IEC is also lower (0.60 - 0.75 mmol g^{-1} vs. 0.89 mmol g^{-1}).
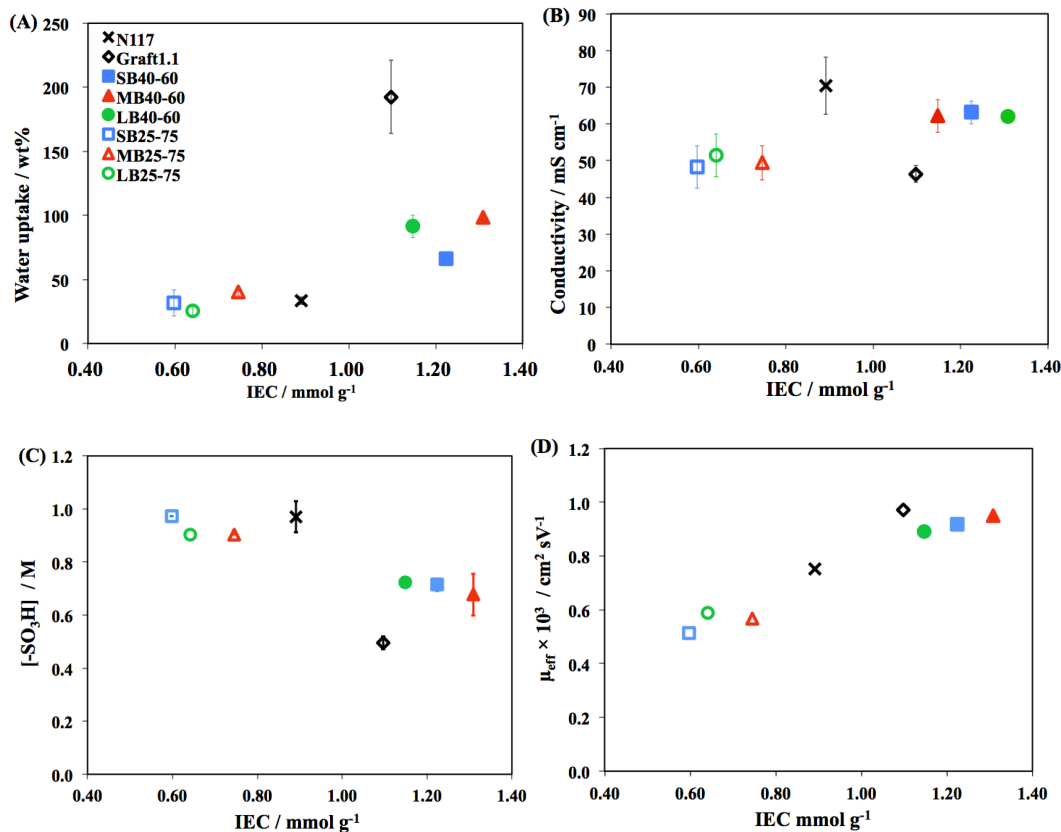
FIGURE 6 (A) Water uptake (fully hydrated), (B) proton conductivity (RT, wet conditions), (C) analytical acid concentration and (D) *effective* proton mobility vs IEC.

In Figure 6B, the relationship between proton conductivity and IEC_{act} is shown. For a similar IEC, the 40-60 blend series shows conductivities of 62 - 63 mS cm^{-1}, which is 35% higher than the 46 mS cm^{-1} of Graft$_{1.1}$. The 25-75 series has roughly half the IEC as Graft$_{1.1}$, yet the conductivities are similar: 48 - 51 mS cm^{-1}. Even though the ionic content is twice as high in the 40-60 series as it is in the 25 - 75 series, the conductivity is only ~ 30% higher. All blends show lower conductivities than N117 (70 mS cm^{-1}) but the 40-60 series is in the same order of magnitude.

In Figure 6C, the analytical acid concentration,[-SO$_3$H] - dependency on IEC_{act} is graphically depicted. The 40-60 blend series show concentrations of 0.68 - 0.72M, which is ~40% higher than Graft$_{1.1}$ at 0.49M – a difference that can be partially explained by the much higher water uptake of the pure graft copolymer. Interestingly, at least 25% higher concentrations (0.90 - 0.97M) are obtained for the 25-75 series, which is similar to N117 (0.97M).

In Figure 6D, the effective proton mobility, μ_{eff}, versus IEC_{act} is presented graphically. Blends and pure grafts behave similarly here: 0.89×10^3 cm^2 sV^{-1} - 0.95×10^3 cm^2 sV^{-1} versus 0.97×10^3 cm^2 sV^{-1}, and the effect of increasing the PVDF-content in the 25-75 series results in about half the μ_{eff}: 0.51×10^3 cm^2 sV^{-1}

- 0.59 × 10^3cm^2 sV^{-1}. N117 has an IEC between the two blend series and also exhibits a μ_{eff} value (0.75 × 10^3cm^2 sV^{-1}) between the two.

DVS and conductivity as function of RH and temperature

Water sorption behaviour at 25 °C and proton transport properties under different temperatures and relative humidity (RH) of the 40-60 series and Graft$_{1.1}$ are shown in Figure 7.
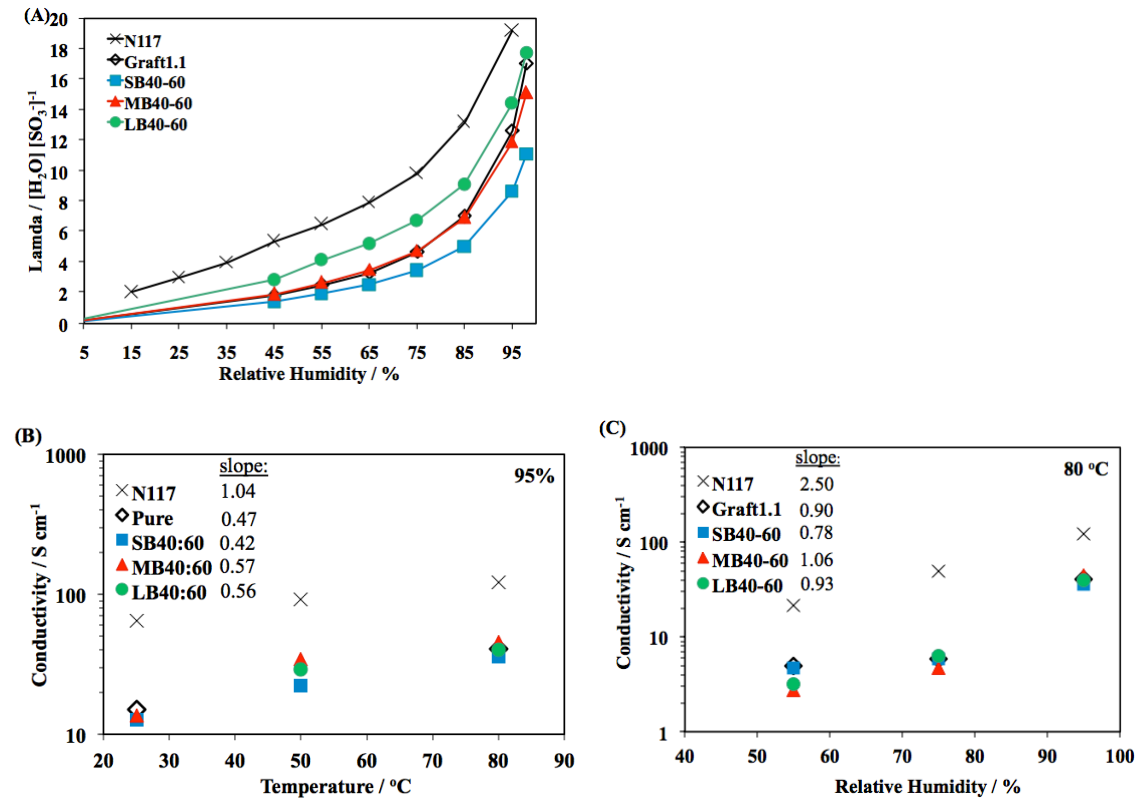

FIGURE 7 (A) Hydration number vs RH at 25 °C, (B) conductivity vs. temperature at RH = 95%, and (C) conductivity vs. RH at T = 80 °C of Graft$_{1.1}$ and 40:60 blends.

Hydration numbers, λ, determined by dynamic vapour sorption, are shown in Figure 7A. The 25:75 blend series is not included as it exhibited poor conductivities at reduced RH. At 45% RH the λ-values are in the range of 1-3 for both 40:60 blends and Graft$_{1.1}$, whereas N117 exhibits λ = 5. At 95% RH, the values are from 9 to 14 for the blends, 13 for Graft$_{1.1}$ and 19 for N117. The blends seem to follow a trend that longer grafts result in higher λ values, and Graft$_{1.1}$ exhibits similar values. Both blends and the pure graft copolymer take up less water molecules per acidic site than N117.

The conductivity is plotted against temperature (25 °C, 50 °C and 80 °C) at RH = 95% in Figure 7B and against RH (55%, 75% and 95%) at 25 °C in Figure 7C. The data are presented in a semi-logarithmic plot with linear fits and the slopes (in Figure 7B: [(S cm^{-1}) °C^{-1}] and in Figure 7C: [(S cm^{-1}) %RH^{-1}]) thereof listed in the legends. Graft$_{1.1}$ and the 40-60 series show similar dependencies on both temperature and

RH. At varying temperature (Figure 7B) the slope of Graft$_{1.1}$ is 0.47 while for the 40-60 series it spans the range 0.42 - 0.57. The slope of N117 is 1.04, twice as large as that of the blends. A similar trend is observed in Figure 7C, where RH is varied. The Graft$_{1.1}$ slope is 0.90 while the 40-60 series span 0.78 - 1.06. The slope of N117 is 2.50. However, the absolute conductivities of the blends are considerably lower than N117: at 80 °C N117 reaches 122 mS cm^{-1}, MB40-60 reaches 45 mS cm^{-1} and Graft$_{1.1}$ reaches 41 mS cm^{-1}.

CONCLUSIONS

Membranes of fully sulfonated graft copolymers blended with high molecular weight PVDF are different in morphology from pure graft copolymers as they macrophase separate into predominantly ion-rich and PVDF-rich domains. Blends with 40 vol% ionomer exhibit repetitive nano-scale ion-rich domains within the macro-scale PVDF-rich domains that are significantly smaller than the ion-rich domains found in the pure graft copolymer before blending. When diluting the ionomer content to 25 vol% by PVDF-addition, only macro-phase separation is observed. This implies that fully sulfonated P(VDF-*co*-CTFE)-*g*-SPS – PVDF blends, unlike their partially sulfonated counterparts blended with low molecular weight PVDF[27] are not morphologically resistant to blending. Compared to partially sulfonated pure P(VDF-*co*-CTFE)-*g*-SPS[8], unsulfonated styrenic moieties in the blends are avoided, which enables ionically pure grafts. Both blends and pure grafts are humidity-sensitive. At reduced water content they perform similar, and despite exhibiting lower absolute conductivities, the RH-dependency is lower than for N117. λ values are considerably higher of N117 than of the blends, so the trend in conductivity correlates well with reports of PFSAs exhibiting significant increases in conductivity at λ > 6[38]. A similar trend applies to the temperature sensitivity. When fully wetted the blends show conductivities superior to the pure grafts, reaching 63 mS cm^{-1} (vs. 46 mS cm^{-1}). Varying the graft length appears to have little, if any, effect on the blend system, whereas the ionomer content is of great significance, as exemplified by the increased analytical acid concentration of the blends with high PVDF content. Besides, IEC-tuning by blending helps maintaining the mechanical integrity of PEMs *via* reduced swelling. These findings will hopefully contribute to the tailoring of future generations of PEM to show improved conductivities at reduced water content.

REFERENCES AND NOTES

1. B. Smitha, S. Sridhar, A. A. Khan, *J. Membr. Sci.* **2005**, 259, 10–26.

2. M. A. Hickner, H. Ghassemi, Y. S. Kim, B. R. Einsla, J. E. McGrath, *Chem. Rev.* **2004**, 104, 4587–4612.

3. K. E. Martin, J. P. Kopasz, K. W. McMurphy, *Am. Chem. Soc.* **2010**, 1–13.

4. K. A. Mauritz, R. B. Moore, *Chem. Rev.* **2004**, 104, 4535–4585.

5. S. J. Osborn, M. K. Hassan, G. M. Divoux, D. W. Rhoades, K. A. Mauritz, R. B. Moore, *Macromolecules* **2007**, 40, 3886–3890.

6. Y. A. Elabd, M. A. Hickner, *Macromolecules* **2011**, 44, 1–11.

7. J. V. Gasa, R. A. Weiss, M. T. Shaw, *J. Membr. Sci*. **2008**, 320, 215–223.

8. E. M. W. Tsang, Z. Zhang, A. C. C. Yang, Z. Shi, T. J. Peckham, R. Narimani, B. J. Frisken, S. Holdcroft, *Macromolecules* **2009**, 42, 9467–9480.

9. I. Dimitrov, S. Takamuku, K. Jankova, P. Jannasch, S. Hvilsted, *Macromol. Rapid Commun.* **2012**, 33, 1368–1374.

10. H. Chang, H. Kim, Y. S. Choi, W. Lee, In Polymer Membranes for Fuel Cells; Javaid, Z.S.M.; Matsuura, T., Eds; Springer US, Boston, MA, 2009, pp 307–339.

11. C. H. Park, C. H. Lee, M. D. Guiver, Y. M. Lee, *Prog. Polym. Sci.* **2011**, 36, 1443–1498.

12. S. Takamuku, P. Jannasch, *Macromol. Rapid Commun.* **2011**, 32, 474–480.

13. Y. Chikashige, Y. Chikyu, K. Miyatake, M. Watanabe, *Macromolecules* **2005**, 38, 7121–7126.

14. Q. Li, J. O. Jensen, R. F. Savinell, N. J. Bjerrum, *Prog. Polym. Sci.* **2009**, 34, 449–477.

15. O. D. Thomas, T. J, Peckham, U. Thanganathan, Y. Yang, S. Holdcroft, *J. Polym. Sci. Part A: Polym. Chem.* **2010**, 48, 3640–3650.

16. J. Mader, L. Xiao, T. J. Schmidt, B. C. Benicewicz, *Adv. Polym. Sci.* **2008**, 216, 63–124.

17. Y. Fu, A. Manthiram, M. D. Guiver, *Electrochem. Commun*. **2006**, 8, 1386–1390.

18. W. Li, A. Manthiram, M. D. Guiver, *J. Membr. Sci.* **2010**, 362, 289–297.

19. Y. A. Elabd, E. Napadensky, C. W. Walker, K. I. Winey, *Macromolecules* **2006**, 39, 399–407.

20. S. J. Peighambardoust, S. Rowshanzamir, M. Amjadi, *Int. J. Hydrogen Energy* **2010**, 35, 9349–9384.

21. Z. Shi,; S. Holdcroft, *Macromolecules* **2004**, 37, 2084–2089.

22. T. Okayasu, K. Hirose, H. Nishide, *Polym. Adv. Technol.* **2011**, 22, 1229–1234.

23. J. A. Kerres, *Fuel Cells* **2005**, 5, 230–247.

24. N. Y. Arnett W. L. Harrison, A. S. Badami, A. Roy, O. Lane, F. Cromer, L. Dong, J. E. McGrath, *J. Pow. Sour.* **2007**, 172, 20–29.

25. F. A. Landis, R. B. Moore, *Macromolecules* **2000**, 33, 6031–6041.

26. M. M. Nielsen, I. Dimitrov, S. Takamuku, P. Jannasch, K. Jankova, S. Hvilsted, *Submitted.*

27. T. Weissbach, E. M. W. Tsang, A. C. C. Yang, R. Narimani, B. J. Frisken, S. Holdcroft, *J. Mater. Chem.* **2012**, 22, 24348–24355

28. A. C. C. Yang, R. Narimani, Z. Zhang, B. J. Frisken, S. Holdcroft, *Submitted.*

29. E. M. W. Tsang, Z. Shi, S. Holdcroft, *Macromolecules* **2011**, 44, 8845–8857.

30. E. M. W. Tsang, Z. Zhang, Z. Shi, T. Soboleva, S. Holdcroft, *J. Am. Chem. Soc.* **2007**, 129, 15106–15107.

31. R. Narimani, Morphological Studies of Ionic Random Graft Copolymers Based on Scattering Techniques. Ph.D. Thesis, Simon Fraser University, Burnaby, BC, Fall 2012.

32. R. N. Kelly, H. D. Wycoff, *Inorg. Synth.* **1946**, 2, 1–3.

33. Z. Xie, C. Song, B. Andreaus, T. Navessin, Z. Shi, J. Zhang, S. Holdcroft, *J. Electrochem. Soc.* **2006**, 153, E173.

34. M. J. Park, N. P. Balsara, *ECS Trans.* **2008**, 16, 1357–1363.

35. T. J. Peckham, J. Schmeisser, M. Rodgers, S. Holdcroft, *J. Mater. Chem.* **2007**, 17, 3255–3268.

36. F. S. Bates, G. H. Fredrickson, *Phys. Today* **1999**, 52(2), 32-38.

37. P. Atkins, J. de Paula, Atkins' Physical Chemistry, Oxford University Press, New York, 2002, p 836.

38. C. Gavach, G. Pemboutoglou, M. Nedyalkov, G. Pourcelly, *J. Membr. Sci.* **1989**, 45, 37–53.

Enhancing the Ionic Purity of Hydrophilic Channels by Blending Fully Sulfonated Graft Copolymers with PVDF Homopolymer

Mads Møller Nielsen, Ami Ching-Ching Yang, Katja Jankova, Søren Hvilsted, Steven Holdcroft

[1]Department of Chemistry, Simon Fraser University, 888 University Drive, Burnaby, British Columbia, Canada V5A 1S6
[2]Department of Chemical and Biochemical Engineering, Danish Polymer Centre, Technical University of Denmark, Søltofts Plads 227, DK-2800 Kgs. Lyngby, Denmark.

Correspondence to: Steven Holdcroft (E-mail: *holdcrof@sfu.ca*)

Additional Supporting Information may be found in the online version of this article.

SYNTHESIS

Materials

The chemicals were purchased from Aldrich and used as received unless otherwise stated: vinylidene fluoride (VDF, +99%), chlorotrifluoroethylene (CTFE, 98%), pentadecafluorooctanoic acid (96%), 2,2-bipyridyl (bpy, +99%), Acetic anhydride (Aldrich, 99.5%), potassium persulfate (KPS, Allied Chemical, reagent grade), sodium metabisulfite ($Na_2S_2O_5$, Anachemia, anhydrous, reagent grade), 1,2-dichloroethane (DCE, Caledon, reagent grade), N-methyl-2-pyrrolidone (NMP, anhydrous, 99.5%), sulfuric acid (Anachemia, 95-98%, ACS reagent). Copper(I) chloride (CuCl, 99%), copper(II) chloride ($CuCl_2$, 99.999%) were purified according to literature[31]. Styrene (St, +99%) was washed twice with 5% aqueous NaOH and twice with water, dried overnight with $MgSO_4$, distilled over CaH_2 under reduced pressure, and stored under N_2 at -20 $^\circ$C.

Synthesis of fluorous macroinitiators

The macroinitiator P(VDF-*co*-CTFE) was previously prepared by emulsion copolymerization of VDF and CTFE. In brief, the polymerization procedure is: To a 160 mL pressure vessel (Parr Instruments) equipped with a 4.14 MPa (600 psi) pressure relief valve and a magnetic stir bar was added a mixture of 100 mL water, 0.40 g KPS, 0.29 g $Na_2S_2O_5$ and 0.04 g pentadecafluorooctanoic acid. A mixture of VDF and CTFE of predetermined composition was then introduced to the reactor, thereby reaching a constant pressure of 2.07 MPa (300 psi) at 60 °C. The polymerization was carried out for 60 to 90 minutes. Freezing, followed by washing with water and ethanol, coagulated the resulting polymer latex. The crude polymer was purified by repeated dissolution in THF and re-precipitation in ethanol, followed by drying at 80 °C under vacuum for 24 hours.

ATRP-grafting of styrene

P(VDF-*co*-CTFE)-*g*-PS was synthesized by ATRP, with the chlorines of the macroinitiator serving as

initiating sites for the monomer. P(VDF-*co*-CTFE)-*g*-PS with 1.1 mol % CTFE was synthesized as follows. 0.9996 g P(VDF-*co*-CTFE) was dissolved in 40 mL NMP in a predried round bottom flask, then 3.0009 g bpy, 40 mL styrene, 0.6406 g CuCl, and 0.0887 g $CuCl_2$ were added. The flask was sealed tight with a septum and degassed over three freeze-pump-thaw cycles to remove oxygen and water from the reactor. The reaction mixture was heated in oil bath under a blanket of nitrogen at 110 °C for a total reaction time of 45 hours. The resulting brown polymer mixture was precipitated in methanol to yield solid polymers. Soxhlet extraction with cyclohexane was performed to remove PS homopolymer. Hereafter followed a final precipitation from methanol.
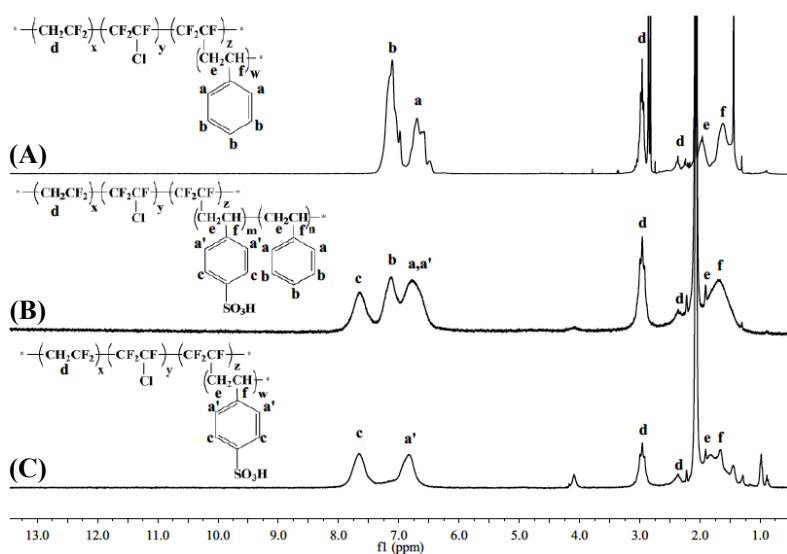

FIGURE S1 ^{1}H NMR spectra of graft polystyrene of (A) pristine Graft$_{2.6-L}$ (B) partially sulfonated Graft$_{2.6-L}$ (DS = 56%) and (C) fully sulfonated Graft$_{2.6-L}$.

MEMBRANE PROPERTIES

TABLE S1 Properties of Graft$_{1.1}$ and blend membranes.

Sample	IEC (mmol g^{-1})	Water uptake (wt%)	[H2O]/[SO$_3$]	Conductivity (mS cm^{-1})	[-SO$_3$H] (M)	$\mu_{estx1000}$ (cm^2 sV^{-1})
Graft$_{1.1}$	1.10±0.07	192±28	62±	46±3	0.77±0.04	0.63
SB40-60	1.22±0.18	66±2	30±	63±3	0.71±0.02	0.92
MB40-60	1.31±0.10	98±3	41±	62±1	0.68±0.08	0.95
LB40-60	1.15±0.09	91±9	44±	62±4	0.72±0.01	0.89
SB25-75	0.60±0.02	32±10	29±	48±6	0.97±	0.51
MB25-75	0.75±0.09	40±3	30±	49±5	0.90±	0.57
LB25-75	0.64±0.02	25±3	21±	51±6	0.90±	0.59

TABLE S2 Properties of partially and fully sulfonated Graft$_{2.6}$. Data has previously been reported.[28]

Sample	IEC[a] (mmol g^{-1})	DS (%)	Water uptake[b] (wt%)	Water content[b] (wt%)	[H2O]/[SO$_3$]	Conductivity[c] (mS cm^{-1})	[-SO$_3$H] (M)	X$_V$ (vol%)	μ$_{estx1000}$ (cm^2 sV^{-1})
	1.12±0.01	18	18±1	15±1	9±1	8±1	1.07±0.01	0.15±0.03	0.07±0.01
	1.72±0.04	31	47±6	32±1	15±1	47±2	1.34±0.04	0.35±0.02	0.37±0.03
	2.27±0.07	53	155±8	61±1	38±2	72±2	1.04±0.07	0.67±0.03	0.77±0.09
P(VDF-*co*-CTFE)-*g*-SPS$_{39}$	2.66±0.06	60	211±6	67±1	45±2	84±11	0.89±0.02	0.76±0.01	0.96±0.04
	3.02±0.05	70	278±25	73±1	53±4	77±9	0.77±0.02	0.80±0.01	1.03±0.03
	3.33±0.08	85	788±33	89±1	136±7	44±2	0.39±0.02	0.96±0.04	1.12±0.09
	3.52$_{theoretical}$	99	1790±55	96±1	283	41±3	0.30±0.08	-	1.42±0.03
	1.23±0.04	19	15±1	13±1	7±1	1±0.1	0.82±0.01	0.10±0.01	0.01±0.00
	1.79±0.04	23	36±1	26±1	11±1	21±1	1.21±0.07	0.25±0.02	0.18±0.02
P(VDF-*co*-CTFE)-*g*-SPS$_{62}$	2.00±0.05	28	48±2	32±1	13±1	34±2	1.38±0.05	0.36±0.03	0.26±0.03
	2.74±0.04	49	298±11	75±1	62±3	68±4	0.66±0.02	0.76±0.03	1.01±0.04
	3.07±0.05	58	835±66	89±1	158±8	33±1	0.33±0.01	0.96±0.02	1.04±0.06
	4.05$_{theoretical}$	99	Partially dissolve in water	-	-	-	-	-	-
	0.74±0.03	12	11±1	10±1	9±2	3±2	0.45±0.07	0.07±0.01	0.06±0.04
	1.35±0.02	23	29±3	22±2	12±1	15±2	1.07±0.05	0.22±0.01	0.14±0.02
	1.48±0.04	27	38±2	27±1	14±1	23±1	1.11±0.03	0.29±0.01	0.24±0.02
P(VDF-*co*-CTFE)-*g*-SPS$_{79}$		30		39±2				0.44±0.02	
	1.81±0.04		65±4		20±1	45±1	1.19±0.03		0.37±0.02
	2.05±0.09	33	128±12	56±2	33±2	69±4	0.91±0.08	0.56±0.05	0.80±0.08
	2.35±0.02	48	815±63	89±1	199±14	33±9	0.34±0.03	1.00±0.01	1.02±0.05
	2.91±0.04	56	1060±94	92±1	211±10	36±7	0.28±0.06	1.00±0.01	1.23±0.08
	4.29$_{theoretical}$	99	Partially dissolve in water	-	-	-	-	-	-

[a] By titration. [b] Room temperature. [c] Soaked in H$_2$O overnight and dabbed with tissue prior to measurements at room temperature. * Errors were calculated as standard deviations over multiple measurements.